EPFL

Thèse n° 10 927

Functional and structural characterization of polyphosphate-accumulating organisms in aerobic granular biofilms

Présentée le 7 juillet 2023

Faculté de l'environnement naturel, architectural et construit
Laboratoire de biotechnologie environnementale
Programme doctoral en génie civil et environnement

pour l'obtention du grade de Docteur ès Sciences

par

Arnaud Michel GELB

Acceptée sur proposition du jury

Prof. T. Kohn, présidente du jury
Prof. C. Holliger, directeur de thèse
Dr N. Derlon, rapporteur
Prof. B.-M. Wilen, rapporteuse
Prof. A. Meibom, rapporteur

École polytechnique fédérale de Lausanne

2023

Acknowledgements

The achievement of this research project is the fruit of a team effort of present and former members of the LBE. I'm looking forward to celebrating this together soon.

I'm grateful to Christof Holliger for giving me the opportunity to join the Laboratory for Environmental Biotechnology (LBE) in 2014 as an intern and later offer a Ph.D. candidate position.
This research project was funded by the Swiss National Science Foundation (SNSF) with collaboration between Christof Holliger, Laboratory for Environmental Biotechnology (LBE)-EPFL together with Nicolas Derlon and Eberhard Morgenroth and, Process Engineering at Eawag-ETHZ.
I want to thank the jury of this thesis: Tamar Kohn, Christof Holliger, Nicolas Derlon, Britt-Marie Wilen, and Anders Meibom, for reviewing this document and providing helpful comments to improve the quality of this manuscript.
I would also like to thank the jury of the research plan validation in 2015: Christof Holliger, Pilar Junier, Eberhard Morgenroth, and Tom Battin for the valuable discussions.
During those years of research, I had the chance to meet and collaborate with several inspiring scientists at EPFL, Eawag, UNIL, DOME - University of Vienna, Environmental Biotechnology - TU Delft, Center for Microbial Communities - Aalborg University, and ETHZ.

This manuscript symbolizes the completion of several challenging years, which I couldn't go through without the valuable support of a long list of amazing people I met on campus, with the Rushteam, and with the flatshares.

Abstract

The Aerobic Granular Sludge (AGS) technology for wastewater treatment is based on dense microbial biofilms in the form of granular aggregates with an excellent settling property allowing high biomass concentrations in bioreactors. This promising biological wastewater treatment is a cost-effective and land-saving alternative to the conventional flocculent activated-sludge technology.
A complex microbial community is intertwined in the dense biofilm structure of AGS, and little is known about the roles and interactions between microorganisms within this matrix. Moreover, there is a need to understand the fundamental microbiology of the AGS to control its stability and performance.
In this context, the physiology and the structural organization of the AGS microbial populations involved in biological phosphorus removal from the influent are investigated in lab-scale conditions.
The experimental identification of the organisms involved in the biological phosphorus removal of the wastewater revealed *Ca.* Accumulibacter phosphatis as the primary organism responsible for phosphorus treatment performance. Regarding the use of acetate and glucose present in the influent, microorganisms belonging to *Ca.* Accumulibacter phosphatis and an unknown genus of *Propionibacteriaceae* are likely the primary consumers of those organic carbon sources, respectively. The spatial organization of the microorganisms in the AGS biofilm showed clusters of microcolonies rather than an organization in concentric layers. Finally, in the experimental conditions used here, and a microbial community dominated by the genus *Ca.* Accumulibacter phosphatis, acetate, propionate, and probably some amino acids (like aspartate or glutamate) could support the biological phosphorus removal from the influent. Glycine was shown to interfere with this metabolism with an effect proportional to its concentration.

Keywords:
- AGS (Aerobic Granular Sludge)
- Complex microbial community
- Wastewater biological phosphorus removal
- SIP (Stable Isotope Probing)
- FACS (Fluorescence Activated Cell Sorting)
- Biofilm structure

Résumé

La technologie des *Aerobic Granular Sludge* (AGS) pour le traitement des eaux usées est basée sur des biofilms microbien denses sous forme d'agrégats granulaires qui ont une excellente propriété de décantation permettant d'obtenir des bioréacteurs contenant des concentrations élevées de biomasse. Ce traitement biologique des eaux usées constitue une alternative rentable et compacte à la technologie conventionnelle des boues activées. Une communauté microbienne complexe est structurée dans les biofilm des AGS, et on sait peu de choses sur les rôles et les interactions entre les microorganismes au sein de cette matrice. En outre, il est nécessaire de développer des connaissances fondamentales sur la microbiologie des AGS afin de contrôler la stabilité et les performances des stations d'épuration des eaux usées à AGS. Dans ce contexte, la physiologie et l'organisation structurelle des populations microbiennes d'AGS impliquées dans l'élimination biologique du phosphate de l'influent sont étudiées dans des conditions de laboratoire. L'identification expérimentale des organismes impliqués dans la déphosphatation biologique des eaux usées a permis de mettre en évidence *Ca.* Accumulibacter phosphatis comme l'organisme principalement responsable de la performance du traitement du phosphate. Concernant l'utilisation de l'acétate et du glucose présents dans l'influent, les micro-organismes appartenant à *Ca.* Accumulibacter phosphatis et un genre inconnu de *Propionibacteriaceae* sont probablement les principaux consommateurs respectifs de ces sources de carbone organique. L'organisation spatiale des microorganismes dans les biofilms d'AGS a montré des grappes de microcolonies plutôt qu'une organisation en couches concentriques. Enfin, dans les conditions expérimentales utilisées ici, et une communauté microbienne dominée par le genre *Ca.* Accumulibacter phosphatis, l'acétate, le propionate, et probablement certains acides aminés (comme l'aspartate ou le glutamate) pourraient favoriser l'élimination biologique du phosphate de l'influent. Il a été également démontré que la glycine interfère avec ce métabolisme avec un effet proportionnel à sa concentration.

Contents

Acknowledgements **iii**

Acknowledgements **iii**

Abstract **v**

Résumé **vii**

List of figures **xiii**

List of acronyms **xv**

1 Introduction **1**
1.1 Wastewater treatment . . . 1
1.1.1 Context . . . 1
1.1.2 Biological wastewater organic carbon, nitrogen, and phosphorus removal . . . 2
1.1.3 Phosphorus in wastewater is a resource to recover . . . 2
1.1.4 The PAOs and GAOs misconceptions . . . 3
1.1.5 Aerobic Granular Sludge . . . 5
1.2 State of research, knowledge gap, and thesis targets . . . 6
1.2.1 AGS biofilm formation . . . 6
1.2.2 AGS biofilm composition . . . 7
1.2.3 Structural organization of AGS biofilm . . . 7
1.2.4 Microbial population interactions in AGS . . . 9
1.2.5 AGS microbial community composition . . . 10
1.2.6 Linking genetic identity and function in communities of uncultured bacteria . . . 10
1.2.7 Analytical methods to study PAOs . . . 11
1.3 Objectives and approach of the thesis . . . 12
1.3.1 Knowledge gaps and research questions . . . 12
1.3.2 Thesis outline . . . 13

2 Production and maintenance of acetate-glucose fed AGS **15**
2.1 Introduction . . . 15
2.2 AGS-EBPR setup . . . 15
2.2.1 AGS-EBPR design . . . 15
2.2.2 AGS-EBPR start-up conditions . . . 17

2.3 SBR phases . . . 17
2.3.1 Anaerobic feeding . . . 17
2.3.2 Aeration . . . 18
2.3.3 Settling of the biomass and withdrawal of the treated effluent . . 18
2.4 AGS-EBPR performances measurements . . . 19
2.4.1 Nutrients removal . . . 19
2.4.2 Sludge monitoring . . . 21
2.5 Bacterial community members detected by 16S rRNA gene amplicon sequencing . . . 21
2.6 Supplementary material . . . 22
2.6.1 Computer AGS-EBPR interface . . . 22
2.6.2 Influent / effluent interface . . . 23
2.6.3 pH control interface . . . 24
2.6.4 Aeration control interface . . . 25
2.6.5 Signal acquisition interface . . . 26
2.6.6 PID controlling the dissolved oxygen . . . 27
2.6.7 PID controlling the pH . . . 27
2.6.8 Data acquisition . . . 28
2.6.9 Structure of the code used for the AGS-EBPR operation . . . 28

3 Identification of polyphosphate-containing cells present in AGS 29
3.1 Introduction . . . 29
3.2 Material and methods . . . 32
3.2.1 Sample preparation . . . 32
3.2.2 Sample fixation . . . 33
3.2.3 Dye titration . . . 33
3.2.4 Gating strategy . . . 34
3.2.5 Voltage optimization . . . 34
3.2.6 Performance tracking . . . 35
3.2.7 Sorting . . . 36
3.2.8 DNA extraction . . . 36
3.2.9 Amplicon sequencing . . . 36
3.2.10 Analysis of the sequencing reads . . . 38
3.2.11 Material and reagents . . . 40
3.3 Results and discussion . . . 41
3.3.1 Experimental strategy and challenges . . . 41
3.3.2 PolyP positive cells detection in an AGS-EBPR bioreactor operated with a glucose-acetate influent . . . 43
3.3.3 PolyP positive cells detection in an AGS-EBPR bioreactor operated with an influent containing VFAs and fermentable mono- and polymeric substrates . . . 45
3.4 General conclusions and perspectives . . . 46
3.5 Supplementary figures . . . 47

4 Investigation of the AGS metabolic network using ^{13}C-enriched substrates 53
4.1 Introduction . . . 53
4.2 Material and methods . . . 56

4.2.1 Sample preparation . . . 56
4.2.2 DNA extraction and purification . . . 56
4.2.3 Amplicon sequencing . . . 56
4.2.4 PHA analysis . . . 56
4.2.5 DNA-SIP . . . 57
4.2.6 Nucleoside analysis . . . 59
4.3 Results and discussion . . . 60
4.4 General conclusions and perspectives . . . 66

5 Localization of polyphosphate-containing cells in the granular biofilm 67
5.1 Introduction . . . 67
5.2 Material and methods . . . 69
5.2.1 X-ray micro-computed tomography . . . 69
5.2.2 PolyP labeling on thin cross-sections . . . 69
5.2.3 Light-Sheet Fluorescence Microscopy analysis . . . 70
5.3 Results and discussion . . . 74
5.3.1 Macro-scale properties of aerobic granular biofilm aggregates . . 74
5.3.2 Micro-scale properties of granular biofilm aggregates and PAOs microcolonies . . . 76
5.3.3 Micro-scale 3D structure of granular biofilm aggregates and PAOs distribution observed by LSFM . . . 78
5.4 General conclusions and perspectives . . . 82
5.5 Supplementary figures . . . 83

6 Identification of substrates triggering anaerobic polyphosphate hydrolysis in AGS 85
6.1 Introduction . . . 85
6.2 Material and methods . . . 88
6.2.1 AGS-EBPR operation and influent composition . . . 88
6.2.2 DNA extraction and amplicon sequencing . . . 88
6.2.3 PHA analysis . . . 88
6.2.4 Glycine analysis . . . 88
6.2.5 Raman-FISH . . . 89
6.3 Results and discussion . . . 90
6.3.1 Influence of different carbon sources on both AGS-EBPR bioreactors 90
6.3.2 Influence of different amino acids on the performances of bioreactor RA . . . 94
6.3.3 Dose-dependent response of the glycine on the anaerobic phosphorus release in bioreactor RA . . . 96
6.3.4 Addition of glycine in bioreactor RA at different SBR cycle phases 99
6.3.5 Aerobic uptake of phosphorus in bioreactor RA after anaerobic exposure to glycine . . . 101
6.3.6 Following dynamics of intracellular storage polymers with Raman-FISH . . . 103
6.4 General conclusions and perspectives . . . 105
6.5 Supplementary figures . . . 105

7 Concluding remarks 107

Bibliography **132**

Curriculum Vitae **133**

List of Figures

1.1 Four different phases of an SBR operation 5
1.2 Two different possible mechanisms to explain AGS formation 7
1.3 Example of discrepancy in the AGS microbial structure between *in-situ* labeling and model 8
1.4 Representation of the functional relationships occurring in AGS 9

2.1 Picture of the bioreactor setup used for the Stable Isotope Probing 16
2.2 Effect of an operational failure on the nutrient removal 20

3.1 Gating strategy of the AGS cell suspension analyzed by flow cytometry leading to the selection of polyP positive cells 42
3.2 Control of the gating strategy with an N by N bivariate plot of the sample's fluorescence signal 42
3.3 Assessment of the microbial community throughout the experimental procedure leading to the sorting of the PAOs fraction 44

4.1 Biofilm components (bacteria and EPS) as a source of nutrients for other bacteria not consuming VFAs during the anaerobic phase 55
4.2 Nucleosides labeling with ^{13}C-glucose 60
4.3 Assessment of the microbial community before and after the DNA-SIP . 61
4.4 ^{13}C incorporation in PHA monomers 62
4.5 ^{13}C incorporation in PHA monomers 63
4.6 ^{13}C incorporation in the DNA of the microbial community 65
4.7 DNA-SIP profiles of an unknown *Propionibacteriaceae* genus and *Ca.* Accumulibacter 65

5.1 Confocal fluorescence microscopy versus Light-Sheet Fluorescence Microscopy 70
5.2 AGS macroscopic properties 74
5.3 X-ray micro-computed tomography 76
5.4 2D AGS structure observation 77
5.5 3D AGS structure LSFM observation 78
5.6 Multi-view 3D reconstruction of an AGS biofilm aggregate 79
5.7 Image analysis workflow 81

6.1 Schematic diagram of metabolic cross-feeding in EBPR processes 86
6.2 Effect of different carbon sources on bioreactor RB 90

6.3 Effect of different carbon sources on bioreactor RA 91
6.4 Effect of individual amino acids on bioreactor RA 95
6.5 Dose-dependent effect of glycine on bioreactor RA 97
6.6 COD and PO_4-P concentration during SBR cycles in bioreactor RA treating influents with different glycine concentrations 98
6.7 Effect of a glycine addition in the anaerobic and aerobic phases during different SBR cycles of bioreactor RA 100
6.8 Comparison between SBR cycles performed with the reference influent with an influent containing glycine as sole organic carbon source on bioreactor RA 102
6.9 FISH and Raman microspectroscopy 104

List of acronyms

3-HB: 3-HydroxyButyrate
3-HV: 3-HydroxyValerate
AGS: Aerobic Granular Sludge
ATP: Adenosine TriPhosphate
BOD: Biological Oxygen Demand
COD: Chemical Oxygen Demand
CV: Coefficient of Variation
DAPI: 4’,6-DiAmidino-2-PhenylIndole
EBPR: Enhance Biological Phosphorus Removal
EDM: Euclidean Distance Matrice
EDTA: EthyleneDiamineTetraAcetic acid
EPS: Extracellular Polymeric Substances
FACS: Fluorescence Activated Cell Sorting
FCM: Flow CytoMetry
FISH: Fluorescence In Situ Hybridization
FSC: Forward Scatter
GAO: Glycogen Accumulating Organisms
LSFM: Light Sheet Fluorescence Microscopy
LUT: LookUp Table
MAR-FISH: MicroAutoradiography-coupled FISH
MFI: Mean Fluorescent Intensity
NADH: reduced form of Nicotinamide Adenine Dinucleotide (H for hydrogen)
NanoSIMS: Nanoscale Secondary ion Mass Spectrometry
OTU: Operational Taxonomic Unit
PAO: Polyphosphate Accumulating Organisms
PHA: PolyHydroxyAlkanoate
PI: Propidium Iodide
PID: Proportional Integral Derivative
PMT: Photomultiplier Tube
PolyP: PolyPhosphate
PSF: Point Spread Function
PTFE: PolyTetraFluoroEthylene
RA: AGS bioReactor A
RB: AGS bioReactor A
RCF: Relative Centrifugal Force
RI: Refractive Index
SBR: Sequencing Batch Reactor

SD: Staining Index
SIP: Stable Isotope Probing
SSC: Side Scatter
SVI: Sludge Volume Index
SRT: Sludge Retention Time
TSS: Total Suspended Solids
VFA: Volatile Fatty Acid
VI: Voltration Index
VSS: Volatile Suspended Solids

1 Introduction

1.1 Wastewater treatment

1.1.1 Context

Pollutants in wastewater can be produced by domestic, industrial, and agricultural activities. Each Swiss inhabitant consumes, on average, approximately 300 liters of tap water daily (Société Suisse de l'Industrie du Gaz et des Eaux , 2019), which must be treated after use to minimize environmental and human health issues. Untreated wastewater may carry toxic compounds, threaten aquatic life and induce eutrophication of surface water. Eutrophication is an adverse ecological effect due to increased water nutrient concentrations, mainly phosphorus and nitrogen, two limiting nutrients for algal growth in many freshwater ecosystems (Gleisberg et al., 1976). Eutrophication can lead to the depletion of oxygen in the water body and the production of microbial toxins, which strongly impacts aquatic biodiversity (Schindler, 1974).
In Switzerland, 98% of the population lives connected to a wastewater treatment plant (Office fédéral de la statistique, 2021). Processes used to treat wastewater depend on the treatment requirements defined by the receiving environment and the wastewater load (Exigences relatives à la qualité des eaux, OEeaux 1998). Traditionally, three steps of wastewater treatment are distinguished. The primary treatment aims to remove suspended solids from wastewater. The secondary treatment can treat by biological processes, dissolved and suspended organic material, nitrogen, and phosphorus. The tertiary treatment includes water disinfection and micro-pollutant removal (Loi fédérale sur la protection des eaux, LEaux 1991).

1.1.2 Biological wastewater organic carbon, nitrogen, and phosphorus removal

Organic carbon, nitrogen, and phosphorus concentrations in wastewater depend on water usage. For example, over the period 2015-2020, the wastewater treated by the wastewater treatment plant in the Swiss city of Thun had an average of 500 mg_{COD}/L, 50 mg_{Ntot}/L, and 8 mg_{Ptot}/L (http://www.arathunersee.ch). The removal of the different pollutants from wastewater requires distinct microbial metabolisms. Some microbial activities are performed in the presence of oxygen (aerobic conditions), and some in the absence of oxygen (anaerobic conditions). Two approaches can combine aerobic and anaerobic conditions in wastewater treatment plants; one is to separate the two conditions spatially (e.g., in different tanks); the other is to have a temporal switch of conditions (e.g., by intermittent aeration).
The organic carbon in the wastewater is classically characterized by the biodegradability fraction measured after a 5 days incubation in aerobic conditions (biological oxygen demand, BOD_5). Heterotrophic bacteria can biodegrade organic carbon in aerobic or anaerobic conditions (respiration or fermentation). Biological nitrogen removal from wastewater can be accomplished by converting ammonium to nitrogen gas. This transformation is classically performed sequentially by two different microorganisms. First, nitrifying microorganisms use ammonium as an electron donor in the presence of oxygen, which catalyzes ammonium oxidation into nitrite. Some nitrifiers catalyze nitrite oxidation to nitrate (Warington, 1878). Denitrifying microorganisms can then respire nitrite and nitrate (Gayon and G. Dupetit, 1886). Denitrifiers are often facultative aerobic heterotrophic bacteria able to use an oxidized form of nitrogen in the absence of oxygen causing the formation of nitrogen gas and leading to nitrogen removal from wastewater (Ferguson, 1994).
The biological phosphorus removal from the wastewater process uses the ability of certain heterotrophic microorganisms to immobilize phosphorus intracellularly in the form of polyphosphate (polyP). Those bacteria are called Polyphosphate-Accumulating Organisms (PAOs). It has also been shown that some PAOs are involved in nitrogen removal from wastewater by denitrifying nitrite and nitrate in the absence of oxygen (Kuba et al., 1993).

1.1.3 Phosphorus in wastewater is a resource to recover

Phosphorus is widely used as a fertilizer and is a limited nonrenewable resource mined in only a few countries (Heffer et al., 2006). In Switzerland, 100 % of the phosphorus fertilizer is imported, corresponding to approximately 6’000 tons/year (Stefan Hartmann, 2019). Around 5800 tons/year of phosphorus is lost through the wastewater due to the lack of recycling (Claudia R. Binder et al., 2019). In 2026 the phosphorus in the Swiss municipal wastewater will have to be recycled to at least 45% (OLED 2016, Art. 15). In this context, the "Enhanced Biological Phosphorus Removal" (EBPR) supported by PAOs is getting increasing attention as a sustainable, effective, and economical process to recover phosphorus (James Barnard, 1976, Oehmen et al., 2007, R. J. Seviour et al., 2003, Welles et al., 2015, N. Gilbert, 2009). The phosphorus immobilized in the PAO cells can, for example, be recovered through the release of orthophosphate and its precipitation as struvite, a magnesium ammonium phosphate

mineral, (Yuan et al., 2012) or by the thermal treatment of the sewage sludge enriched in polyP (Kwapinski et al., 2021).

1.1.4 The PAOs and GAOs misconceptions

The definition of PAOs used here is microorganisms accumulating polyP in a wastewater treatment plant environment using the dissolved phosphorus present in the wastewater. GAOs are here defined as heterotrophic microorganisms specifically selected by the EBPR process but not able in these conditions to accumulate polyP using the dissolved phosphorus present in the wastewater. PAO and GAO are positively selected in EBPRs by the alternating anaerobic carbon-feast and aerobic carbon-starvation periods (Comeau et al., 1986, Kuba et al., 1993, Satoh et al., 1992, M. C. M. van Loosdrecht, Hooijmans, et al., 1997, Lemos et al., 1998, Mino et al., 1998, Y. Zhou et al., 2010). In lab scale EBPRs feed with volatile fatty acids (VFAs) such as acetate and propionate, the PAO *Candidatus* Accumulibacter phosphatis, present in full-scale EBPR systems (He et al., 2008), is often enriched from activated sludge. The abundance of this genus in numerous lab-scale EBPRs explains the numerous studies on this PAO despite its absence of isolation in pure culture up to now (Murray and Stackebrandt, 1995, Lu et al., 2006, McMahon et al., 2007). The knowledge obtained from those lab scale models was used to define the canonical PAO metabolism in EBPR regardless that full-scale EBPR systems have a more complex substrate composition and diverse physicochemical conditions.
The described canonical PAOs metabolism is as follows: During the anaerobic feast phase, VFAs are taken up by PAOs and stored into poly-β-hydroxyalcanoate (PHA) polymers. The energy in the form of adenosine triphosphate (ATP) required for the VFAs uptake is provided by the hydrolysis of polyP into orthophosphate monomers which are excreted, and by the hydrolysis of intracellular glycogen. Nicotinamide adenine dinucleotide (NADH) is used as reducing power for PHA synthesis. During the subsequent carbon-starvation period under aerobic conditions, PAOs use intracellular PHA as an electron-donor and carbon source for cell maintenance, growth, and the synthesis of intracellular glycogen and polyP (Comeau et al., 1986). The EBPR process accomplishes the phosphorus removal from the wastewater by PAOs having a net aerobic uptake of orthophosphate from the wastewater exceeding the predeceasing orthophosphate release during the anaerobic phase (Mino et al., 1998, Oehmen et al., 2007).
GAOs, formerly called G-bacteria (Cech and Hartman, 1993), are described to have similar metabolism as the canonical PAO metabolism but without storage of polyP in EBPR conditions. GAOs are using glycogen for energy and reducing equivalents under anaerobic conditions. Interestingly, depending on the environmental conditions PAOs can present a phenotype similar to GAOs (Acevedo et al., 2012). Supposedly GAOs compete with PAOs for the uptake of VFAs under anaerobic conditions. Since GAOs do not remove phosphorus from wastewater, it is believed that these organisms are not desired in EBPR systems. The suggested name for a γ-*Proteobacteria* cluster presenting a GAO phenotype in a lab-scale bioreactor was *Candidatus* Competibacter phosphatis (Crocetti et al., 2002).
The effect of the organic carbon/phosphorus ratio, VFA carbon source, pH, and temperature on the PAO and GAO has been extensively studied (G. J. F. Smolders et al.,

1994a, G. J. F. Smolders et al., 1994b, Brdjanovic et al., 1998, Mino et al., 1998, Mino, 2000, Zeng, Lemaire, et al., 2003, Oehmen et al., 2006, Oehmen et al., 2007, Lopez-Vazquez et al., 2009). It was also suggested that if PAOs have sufficient polyP storage, they will keep their competitive advantage over GAO on the uptake of organic carbon (Qiu et al., 2019, Stokholm-bjerregaard et al., 2017). The *Ca.* Accumulibacter phosphatis vs *Ca.* Competibacter phosphatis bacteria species concept is seducing by its simplicity and has been widely adopted in the wastewater treatment field, despite the inappropriate association of a phenotype with a phylogenetic affiliation. This misconception does not dismiss the necessity to characterize the microbial community to understand how to promote polyP accumulation in full-scale EBPR processes. As the composition of bacterial communities is influenced by the type of wastewater treated, the information gathered on one sample might not apply to another time period or EBPR facility (Coats et al., 2017). Another common error is to use only the data of the abundance of a microorganism to predict EBPR biological phosphorus removal performances. The misunderstanding of the relationship between phylogeny, phenotype, abundance in the microbial community, and phosphorus removal had and is still affecting the quality of the knowledge generated by the research in the field of wastewater treatment.

From the seventies to the early nineties, the genus *Acinetobacter*, isolated from activated sludge, has been studied as a model EBPR bacterium (Deinema et al., 1985, Ohtake et al., 1985, van Groenestijn et al., 1989, Bark et al., 1992). The use of Fluorescence *In situ* Hybridization (FISH) probes targeting the genus *Acinetobacter* on samples from full-scale EBPR plants showed that this organism was present in low abundance and was therefore considered as not relevant for the biological phosphorus removal from the wastewater (Kortstee et al., 1994, Wagner et al., 1994, Kämpfer et al., 1996, M. C. M. van Loosdrecht, Smolders, et al., 1997, Blackall et al., 1998, Helmer and Kunst, 1998, Mudaly et al., 2001). Detecting intracellular polyP in microorganisms affiliated to *Acinetobacter* in lab-scale or some full-scale EBPRs does not mean that this organism will have a PAO phenotype in every full-scale EBPR plant. The low proportion of an organism measured in a full-scale EBPR (if the measurement reflects the real abundance) does not mean this organism might not have a significant role in phosphorus removal through the intracellular accumulation of large quantities of polyP. This reasoning is valid for all PAO candidates, including the genus *Tetrasphaera*, an organism growing in popularity (Maszenan et al., 2000, W.-T. Liu et al., 2001, Hanada et al., 2002, Eschenhagen et al., 2003, Kong et al., 2005, Günther et al., 2009, Wang et al., 2009, Nguyen et al., 2011). Organisms belonging to the *Tetrasphaera* genus were detected as PAO in EBPR wastewater treatment plants (Hanada et al., 2002, Muszynski and Miłobedzka, 2015, J. L. Nielsen et al., 2012, Stokholm-bjerregaard et al., 2017). Several *Tetrasphaera* species have been cultivated in pure culture, and the formation of intracellular polyP was observed for some of them (Barnard et al., 2017, Kristiansen et al., 2013). The studied *Tetrasphaera* does not produce PHA with anaerobic uptake of sugars and amino acids (Barnard et al., 2017, P. H. Nielsen et al., 2019). Some other PAO affiliated to *Ca.* Halomonas phosphatis (Nguyen et al., 2012), *Gemmatimonas aurantiaca* (H. Zhang et al., 2003), *Ca.* Obscuribacter (Soo et al., 2014) and *Dechloromonas* (Kim et al., 2013, Zeng, Yuan, et al., 2003) have been identified and should be further studied to understand their PAO metabolism.

1.1.5 Aerobic Granular Sludge

The activated-sludge process has been used for more than 100 years worldwide in many wastewater treatment plants (Ardern and Lockett, 1914). This biotechnological process is based on microorganisms in the form of flocculent aggregates with a size ranging from 0.05 to 0.20 mm (Ivanov et al., 2006). An alternative to this well-established process is the Aerobic Granular Sludge (AGS) technology based on dense microbial biofilms in the form of granular aggregates. A biofilm is an aggregate of microorganisms in which cells are frequently embedded within a self-produced matrix of "Extracellular Polymeric Substances" (EPS) composed of a conglomeration of various extracellular polymers (polysaccharides, proteins, and extracellular DNA) (Flemming and Wingender, 2010). The AGS definition stipulates that AGS are aggregates of microbial origin, which do not aggregate under reduced hydrodynamic shear and settle significantly faster than activated sludge flocs (de Kreuk, Kishida, et al., 2007). Over the past years, different patents have been registered on the AGS technology. In 2021, over 90 wastewater treatment plants are in operation or under construction with this technology worldwide. The strengths of the AGS system are the operation with a high biomass concentration, and a fast solid-liquid separation to recover the treated water due to the dense and fast settling proprieties of the AGS biofilm aggregates (Morgenroth et al., 1997). Those features make this process particularly adapted to the "Sequencing Batch Reactor" (SBR) configuration, which consists of a bioreactor separating temporally the anaerobic, aerobic conditions and the sedimentation of microorganisms rather than by spatial separation (Ardern, 1927, Irvine and Arthur W. Busch, 1979). The different phases of the SBR operation are presented in Figure 1.1.

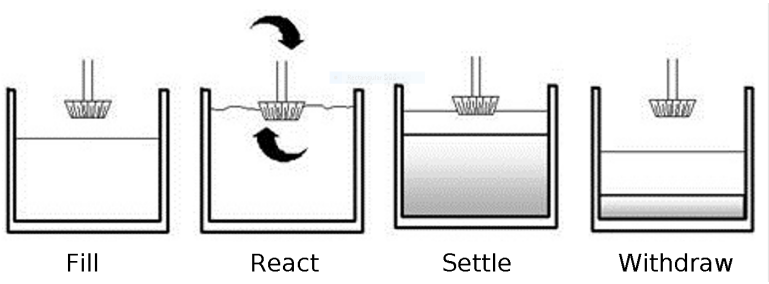

Figure 1.1: **Four different phases of an SBR operation**
Filling phase: The tank is filled with wastewater.
Mixing phase: The reactor is aerated and mixed to provide oxygen to the microbial aerobic metabolisms.
Settling phase: The aeration and mixing are stopped to separate the microorganisms from the treated water by gravitational sedimentation.
Discharging phase: Before a new wastewater injection, the treated water in the upper part of the tank is discharged.

The AGS operated in SBR are cost-effective and land-saving compared to conventional flocculent activated sludge technology (de Bruin et al., 2004). The AGS, composed of millimeter scale biofilm aggregates, creates a spatial separation of oxic and anoxic environments. The contact zone between the AGS biofilm and the aerated

wastewater creates an aerobic zone in the biofilm. The anoxic zone is situated deeper in granular biofilm and is formed by the depletion of oxygen consumed by aerobic microorganisms. The variety of metabolisms occurring within AGS biofilm is due to different microenvironments with different physicochemical conditions. AGS biofilm can be seen as a micro-scale ecosystem composed of a network of microbial populations interacting with each other and with their environment involving nutrient and energy flows. The wastewater is commonly injected in AGS-EBPR systems from the bottom into the settled AGS in a plug-flow mode (Derlon et al., 2016). The feeding is performed in anaerobic conditions to promote the anaerobic carbon storage by PAOs and GAOs. The goal is to remove the organic carbon from the wastewater during the anaerobic phase, and therefore prevent the use of organic carbon in the subsequent aerobic conditions by heterotrophic aerobic organisms having a faster growth rate than PAOs and GAOs in those conditions. Promoting slow-growing PAO and GAO is important for the stability of the AGS-EBPR process (McSwain et al., 2004, de Kreuk and van Loosdrecht, 2004, Winkler et al., 2018). The aerobic mixing phase is necessary to perform the nitrification and the oxidation of the stored carbon source by PAOs and GAOs.

1.2 State of research, knowledge gap, and thesis targets

AGS technology's potential has led to intensive research worldwide on different aspects of this system. The AGS technology has been successfully applied to different types of wastewater, ranging from diluted municipal wastewater (de Kreuk and van Loosdrecht, 2006) to concentrated industrial wastewater (Arrojo et al., 2004). The following sections detail some specific areas of research on AGS.

1.2.1 AGS biofilm formation

AGS are formed in SBR by selecting microorganisms that can aggregate into dense biofilm using short settling times (Morgenroth et al., 1997), sufficient hydraulic retention times (Beun et al., 1999), adequate shear forces (Tay et al., 2001), and by removing excess sludge selectively (Lochmatter and Holliger, 2014 Bassin et al., 2019, Campo et al., 2020). Under such conditions, slow-settling microbial aggregates are washed out from the reactor; therefore, microorganisms producing a dense biofilm matrix are positively selected. The formation of AGS from activated sludge flocs takes several weeks (Lochmatter et al., 2013). The exact mechanisms leading to the formation of AGS are not yet characterized; two hypotheses for the aerobic granulation process are presented in Figure 1.2. The time to form AGS can be reduced by adding compounds promoting the aggregation of microorganisms, such as calcium and magnesium (Morgenroth et al., 1997), iron (Tsuneda et al., 2004), or activated carbon (J.-h. Zhou et al., 2015). Granulation can also be enhanced with bio-augmentation with microorganisms showing high aggregation ability (Ivanov et al., 2006, Coma et al., 2012).

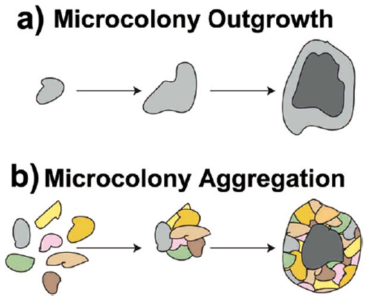

Figure 1.2: **Two different possible mechanisms to explain AGS formation**
From Barr et al., 2010, courtesy of Frances Slater.
a) Microcolony outgrowth: a small microcolony composed of one bacterial type is forming its own dense granule.
b) Microcolony aggregation: numerous small microcolonies of different bacterial types aggregate and grow as an entity.

1.2.2 AGS biofilm composition

The properties of AGS have been reviewed in detail previously (Li et al., 2006). The biofilm matrix has been the subject of particular attention to understanding its composition and mechanical stability. AGS have been described as a protein-polysaccharide hydrogel (T. W. Seviour et al., 2009). *Ca.* Competibacter phosphatis might produce a specific exopolysaccharide named granulan (T. W. Seviour et al., 2011). However, in AGS not dominated by *Ca.* Competibacter phosphatis, other exopolysaccharides (e.g., alginate, Lin et al., 2010) or proteins (e.g., amyloid fibers, Romero et al., 2010) have been proposed to compose the AGS matrix (T. W. Seviour et al., 2012). Labeling different glycoconjugates with lectins on sections of AGS biofilm has revealed that the EPS matrix of AGS can contain diverse structural molecules (Weissbrodt et al., 2013a). The EPS composition depends on the compounds formed by the microorganisms present in the community in response to the operational conditions. For this reason, the EPS structure of AGS can be heterogeneous and is expected to vary in composition in-between aggregates and different bioreactors (Leventhal et al., 2018).

1.2.3 Structural organization of AGS biofilm

The lasting presence of an organism in AGS implies that this organism is producing a dense biofilm matrix or is colonizing the biofilm produced by other members of the microbial community. Some PAOs and GAOs have been associated with EPS production and stable granulation (de Kreuk and van Loosdrecht, 2004). The structural organization in AGS biofilm of different microorganisms displaying key activities for wastewater treatment has been represented with different models (Winkler, Bassin, et al., 2012, Winkler, Kleerebezem, Khunjar, et al., 2012, Winkler, Kleerebezem, de Bruin, et al., 2013) (Figure 1.3). However, the validity of those models has been questioned by independent experimental observation of the organization of microbial guilds using thin sections of AGS biofilm (de Kreuk et al., 2005, Lemaire et al., 2008).

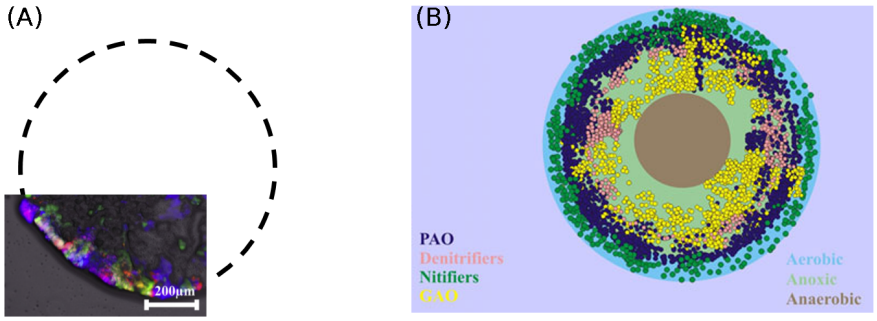

Figure 1.3: **Example of discrepancy in the AGS microbial structure between *in-situ* labeling and model**
From Winkler, Kleerebezem, Khunjar, et al., 2012.
(A) *in-situ* labeling using probes targeting the 16S rRNA.
PAO (blue staining), Nitrifiers (red staining), and GAO (green staining).
(B) Predicted model.
Nitrifiers are localized in the oxic outer layer. Denitrifiers and PAO are localized in the inner anoxic layer (absence of oxygen and presence of nitrite and nitrate).

Studies of AGS biofilm structure in our laboratory have revealed large internal voids and channels irrigating the biofilm showing a cauliflower-like structure (Gonzalez-Gil and Holliger, 2014). These observations question the organization of microorganisms in concentric layers. Channels in the AGS biofilm would allow nutrients and products of microbial metabolisms to be transferred. This consideration involves a more complex diffusion of carbon sources, electron donors, and acceptors in the biofilm. The heterogeneity of the organization of microbial populations observed between different AGS-EBPR and between different AGS biofilm aggregates originating from the same AGS-EBPR does not support the existence of a general model representing the microbial structural organization (Lemaire et al., 2008, Barr et al., 2010). Variations in AGS biofilm thickness likely lead to a different ratio of oxic/anoxic zones. They might increase the number of micro-environments in granular biofilm and, therefore, the diversity of niches hosting different microbial populations.

1.2.4 Microbial population interactions in AGS

The investigation of the AGS microbial community has revealed a substantial diversity (Yi et al., 2003). The cohabitation of different bacterial populations in AGS suggests many microbial interactions. Predominant bacterial populations detected in an AGS-EBPR have been combined in the conceptual model Figure 1.4 according to their predicted metabolisms (Weissbrodt et al., 2014). This representation emphasizes a co-occurrence of different nutrients and energy flows in the AGS ecosystem.

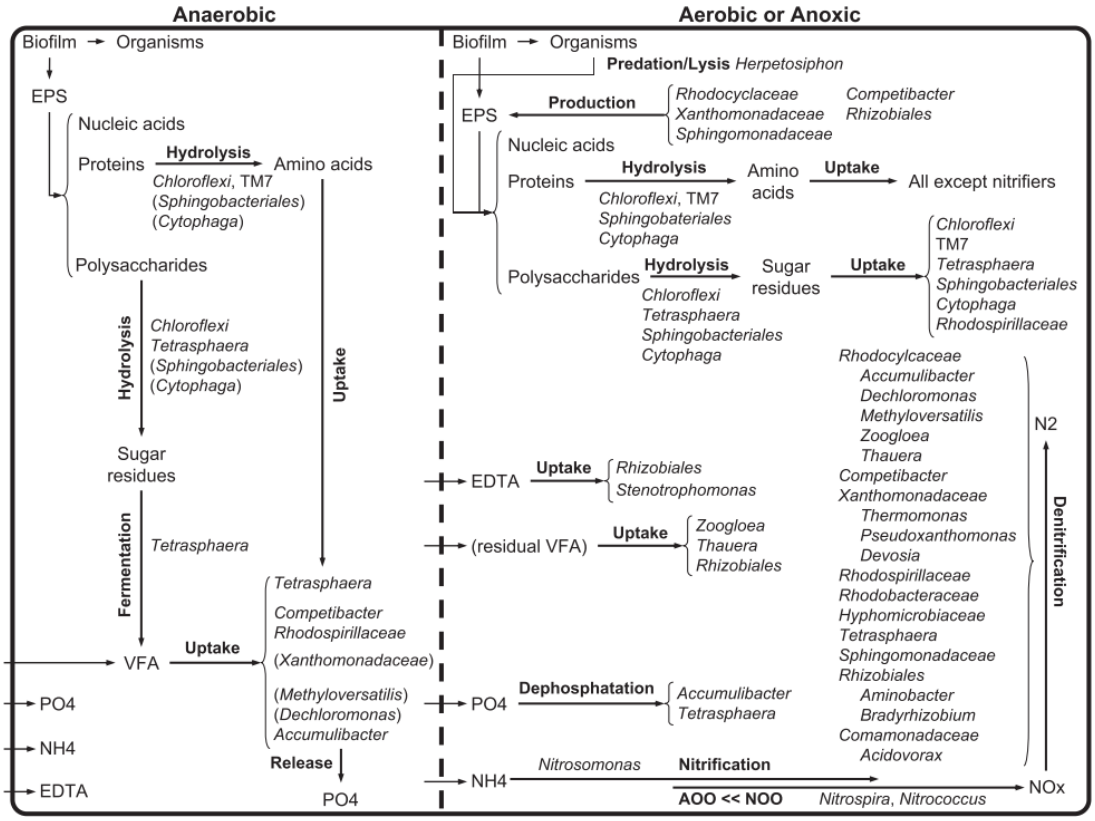

Figure 1.4: **Representation of the functional relationships occurring in AGS** From Weissbrodt et al., 2014
Bacterial processes are displayed with thick arrows. Physiological investigations should confirm the function of the bacteria indicated in parentheses. Phosphorus and nitrogen uptake for anabolic requirements are not represented.
Legend: Extracellular polymeric substances (EPS), volatile fatty acids (VFA), orthophosphate (PO_4^{3-}), ammonium (NH_4^+), sulfate (SO_4^{2-}), ethylenediaminetetraacetic acid (EDTA), nitrite and nitrate (NO_x), nitrogen gas (N_2)

Multi-species microbial communities involve stable and transient interactions between their members. Exchanges of soluble organic compounds and predation have been revealed between bacterial populations of microbial biofilms (Dolinšek et al., 2013). Positive, neutral, or negative interactions can be correlated with the 3D organization of bacterial populations in biofilms (Maixner et al., 2006). Studies of the microbial structure of AGS biofilm should not be limited to measuring the presence

and abundance of microbial populations. However, they should also include the assessment of the functional role of microorganisms. The functional importance of some microbial populations in AGS might vary based on the type of inoculum used and bioreactor operations (e.g., wastewater composition, temperature, pH, and aeration). It is known that different microorganisms can have redundant functionalities and that some microorganisms are metabolically versatile.

1.2.5 AGS microbial community composition

The correlation between the microbial community composition in AGS and wastewater treatment performances is the subject of numerous studies (Lochmatter et al., 2013, Tan et al., 2014, Weissbrodt et al., 2014). Functional groups of microorganisms involved in the wastewater treatment were identified (e.g., COD removal, nitrogen removal, phosphate removal) (P. H. Nielsen et al., 2010). A significant difference in the microbial community was observed between lab-scale AGS-EBPR treating an influent containing volatile fatty acids as the main organic carbon source and AGS-EBPR treating real wastewater (Layer et al., 2019). Because the composition of the bacterial community between bioreactors is variable (Coats et al., 2017, Mielczarek et al., 2013), it is essential to aggregate data from multiple wastewater treatment plants at different times of the year before drawing a general conclusion (Wu et al., 2019).

1.2.6 Linking genetic identity and function in communities of uncultured bacteria

Traditionally the phenotype of microorganisms cultivated in pure culture is performed by screening different conditions in microplates or microarrays (Bochner, 2009). This culture-dependent approach cannot be used to test the metabolic capabilities of most microorganisms in the environment, which are unavailable in pure culture yet.
The identity of a bacteria is classically revealed *in situ* with Fluorescence *In situ* Hybridization (FISH) using probes targeting specific phylogenic groups or *ex situ* with 16S rRNA gene amplicon sequencing.
If the phenotype of a cell cannot be cytochemically or immunohistochemically stained, several techniques have been developed to reveal specific metabolic activity in complex communities.
The MicroAutoRadiography-Fluorescence *In situ* Hybridization (MAR-FISH) (Lee et al., 1999) detects the uptake of a radiolabeled substrate by individual cells.
Stable Isotope Probing (SIP) is an *ex situ* approach using stable isotope tracers to determine metabolically active cells in a microbial community by analyzing informative phylogenetic biomarkers, namely lipids (Boschker et al., 1998), DNA (Radajewski et al., 2000), and RNA (Zarlenga and Gamble, 1987).
Raman spectroscopy and mass spectrometry (Nanoscale Secondary-Ion Mass Spectrometry, NanoSIMS) combined with stable isotope substrates or deuterated water will identify *in situ* the cells metabolically active in a bacterial community (Behrens et al., 2008).
BromodeoxyUridine (BrdU) incorporation is used to detect growing cells by incorpo-

rating this thymidine analog revealed by immunofluorescence or immunocapture techniques (Urbach et al., 1999).
IodoNitroTetrazolium violet (INT) detects cells with active respiratory activity with the formation of intracellular insoluble formazan crystals allowing the separation of the labeled cells on a density gradient (Whiteley et al., 2000).
The recent development of flow cytometry and microfluidics platforms offers new possibilities for studying metabolism in microbial communities (e.g., single-cell secretomics with droplet mass spectrometry (Terekhov et al., 2017, Nakamura et al., 2016).

1.2.7 Analytical methods to study PAOs

Different approaches can be applied to detect or quantify PAOs using their presence of intracellular polyP and have been the subject of different reviews (Eixler et al., 2005, Serafim et al., 2002, Hupfer et al., 2008, Rao et al., 2009, Majed et al., 2012). A selection of those methods is listed in Table 1.1.
Those methods detect the PAO phenotype but do not provide phylogenetic information. The link between the phenotype and the phylogeny of the PAOs can be obtained with "Fluorescence *In Situ* Hybridization" (FISH) and the detection of intracellular polyP, for example, by fluorescent staining (W.-T. Liu et al., 2001), radiolabeling (Schroeder et al., 2008) or Raman spectroscopy (Fernando et al., 2019). FISH limitations of the identification of PAOs are the requirement of previous knowledge of the 16S rRNA gene sequence of the target microorganism and that the cells of interest should have sufficient permeability to the FISH probes. This limitation can be overcome using the untargeted approach composed of fluorescent staining followed by cell sorting with flow cytometry and metagenomic identification of the PAOs (Miyauchi et al., 2007).

Technique	Reference
Neisser polyP staining for light microscopy	Richards and Gurr, 1966
PolyP fluorescent staining for fluorescent microscopy or flow cytometry	Tijssen et al., 1982 (DAPI), Tatsuhiro et al., 2001 (Neutral red), Günther et al., 2009 (Tetracycline), Lorenz et al., 1997 (Fura-2)
Electron microscopy	Sicko-Goad and Lazinsky, 1986, Baxter and Jensen, 1980, Buchan, 1983
Cryoelectron tomography and spectroscopic imaging	Comolli et al., 2006
X-ray analysis	Alvarez and Jerez, 2004
Nuclear Magnetic Resonance Spectroscopy	Florentz et al., 1984, Uhlmann et al., 1990, Jing et al., 1992. Röske and Schönborn, 1994
RAMAN spectroscopy	Majed and Gu, 2010
Mass spectrometry	Rao et al., 2009
NanoSIMS	Langer et al., 2018
Enzyme assays	Hupfer et al., 2008
Protein affinity	Saito et al., 2005

Table 1.1: **Inventory of techniques applied to the detection of polyP**

1.3 Objectives and approach of the thesis

1.3.1 Knowledge gaps and research questions

The main objective of this thesis was to create knowledge on the physiology and structural organization of the AGS microbial populations involved in biological phosphorus removal from wastewater. The knowledge gaps and respective research questions are:
(1) The metagenomic approach is valuable in characterizing the microbial community composition of AGS. However, identifying the active PAOs requires the detection of the microorganisms based on their intracellular polyP. A Flow cytometry Activated Cell Sorting (FACS) based on polyP labeling was developed to overcome the limitations of the targeted methods or the methods based on cultivation and addresses the research question: Is *Ca.* Accumulibacter phosphatis the only PAO in a lab-scale AGS-EBPR treating artificial wastewater containing acetate and glucose as organic carbon sources, and are there other AGS bacterial populations containing polyP at the end of the aeration phase?
(2) The AGS microbial community diversity obtained in an AGS-EBPR treating artificial wastewater containing acetate and glucose as organic carbon sources is more complex than expected. Can a carbon food chain involving primary consumer and cross-feeding interactions explain this coexistence of numerous bacterial populations? To investigate this, the carbon flow in the AGS microbial community was followed using the two carbons sources acetate and glucose present in the influent labeled with ^{13}C heavy carbon isotope and analyzing the "heavy" DNA formed.
(3) Due to the controversy over the structural organization of the granular biofilm, a method was developed to microscopically assess the 3D structure of the granular biofilm to address the research question: Is the granular biofilm formed by microorganisms functionally arranged in concentric layers?
(4) The organic carbon sources supporting the PAO metabolism in a specific experimental condition cannot be deduced from previous results on AGS-EBPR using different operational conditions and harboring different AGS microbial communities. The question was, which carbon sources in a lab-scale AGS-EBPR, performing stable complete anaerobic phosphorus and COD removal over time, support the PAO metabolism? Two lab-scale AGS-EBPR treating different artificial wastewaters were used to test the effect of individual carbon sources on phosphate release during the anaerobic phase.

The relevance of this work was to focus on PAOs using different approaches, some of them being applied for the first time in this field of research. The protocols and results generated in this thesis aim to be useful for the research community to build further knowledge on the AGS and EBPR process. The ultimate objective is to improve the design and operation of those systems to increase their efficiency and reliability to face the current and future challenges of wastewater treatment.

1.3.2 Thesis outline

The thesis was structured as a cumulative dissertation divided into seven chapters. Chapter 1 contains the introduction and the presentation of the Ph.D. thesis objectives and outline. Chapter 2 presents the set-up and operation of the lab-scale AGS-EBPR used in Chapters 3 to 5. Chapter 3 focuses on identifying polyP-containing cells of the microbial community using fluorescent labeling of the polyP and cell sorting by a flow cytometer. In Chapter 4, a stable isotope probing approach was applied by feeding the two organic carbon sources acetate and glucose labeled with the ^{13}C heavy carbon isotope. The populations of microorganisms consuming them were identified by analyzing the heavy DNA by 16S rRNA gene amplicon sequencing. Chapter 5 presents studies on the structure of the granular biofilm using X-ray micro-computed tomography and on the organization of the PAO organisms within the granular biofilm using confocal and light-sheet fluorescence microscopy. Chapter 6 aimed to identify the organic carbon sources in the influent supporting the biological phosphorus removal in lab-scale AGS-EBPR. Finally, Chapter 7 presents some concluding remarks and a brief outlook on the Ph.D. thesis.

2 Production and maintenance of acetate-glucose fed AGS

Author Contributions:
The conceptualization, methodology, and writing the original draft of this chapter were performed by Arnaud Gelb with the supervision of Christof Holliger.
The other individual contributions are listed below:
- Funding acquisition: Christof Holliger, Nicolas Derlon, and Eberhard Morgenroth.
- Methodology: Jean-Pierre Kradolfer and Samuel Lochmatter (AGS-EBPR bioreactors operation)
- Writing review: Julien Maillard and Laetitia Cardona.

2.1 Introduction

Sequencing Batch Reactors (SBRs) are well adapted to promote and maintain Aerobic Granular Sludge (Beun et al., 1999). The selective pressure applied on the settling velocity with a short settling time before the withdrawal of the clarified treated water favors the formation of fast settling granular biofilm aggregates. This chapter presents the lab-scale AGS bioreactor setup with Enhanced Biological Phosphorus Removal (EBPR) used in Chapters 3 to 5.

2.2 AGS-EBPR setup

2.2.1 AGS-EBPR design

The conception of the lab-scale AGS-EBPR presented in this chapter was inspired by the design of Morgenroth et al., 1997 and Beun et al., 1999 and is similar to the AGS-EBPRs used in Lochmatter et al., 2013 and Weissbrodt et al., 2014. The AGS-EBPR used here consists of a column with a working volume of 2.4 L and a 50% exchange ratio. The up-flow velocity was 0,42 m/h with a feeding of the influent from the bottom of the AGS-EBPR for 1 h. The internal diameter of the column is 60 mm which gives a height-to-diameter ratio of approximately 15. The mid-height of the SBR column is at approximately 42 cm, leading to a critical settling velocity

of 5,1 m/h with a 5 min settling time. The AGS-EBPR comprises double-walled glass sections containing water maintained at 18°C to keep the temperature between 18°C and 20°C inside the AGS-EBPR throughout the year.
A PVC module was placed between two glass sections to insert the probes, the pH regulation inlets, and the effluent outlet at the half-height of the column working volume. Once filled, the SBR headspace volume was about 1L. With this reactor design, the mixing is performed by injecting gas through the port located at the lowest part of the bioreactor.
The pH was regulated at 7.5±0.1 by adding 0.5%(w/w) HCl or NaOH aqueous solution. To monitor if the effluent contains biomass, the treated water, before being discharged, transitions into a clarifier.
In Chapter 4, a bioreactor with a working volume of 0.4 L was used for the labeling with ^{13}C organic carbon substrates (Figure 2.1). This bioreactor had the same setup and operating conditions as the bioreactor with a working volume of 2.4 L mentioned above, except for the working and headspace volume and an insertion of the probes, the pH regulation inlets, and the effluent outlet from the top PVC cap.

Figure 2.1: **Picture of the bioreactor setup used for the Stable Isotope Probing**
AGS mixed during the SBR aerobic phase.
Coin diameter: 17.15 mm

2.2.2 AGS-EBPR start-up conditions

The SBR was inoculated with activated sludge from the aerated zone of the wastewater treatment plant of Thun (46°46’51.6 "N 7°35’50.7 "E, 11/03/2014), which includes a biological phosphorus removal of the wastewater in a continuous anaerobic-anoxic-aerobic process. The average load in the wastewater treated in Thun from 2015 to 2020 is approximately 500 mg_{COD}/L, 50 mg_{Ntot}/L, and 8 mg_{Ptot}/L (http://www.arathunersee.ch). Mature AGS meeting the criteria defined in de Kreuk, Kishida, et al., 2007 were formed following the start-up strategy developed by Lochmatter and Holliger, 2014. Shortly: the selective pressure on the settling velocity of the biomass was gradually increased by lowering the settling time from 45 min to 5 min over a month. This promotes the formation of dense biomass aggregates while ensuring that all the influent’s organic carbon (measured with the COD) is consumed before the beginning of the aeration phase. The gradual washout of the slow settling biomass did not compromise the nitrogen and phosphorus treatment performances.

2.3 SBR phases

The succession of an anaerobic feeding followed by an aerobic condition is obtained in the same reactor thanks to the SBR temporal separation capability. The operation of the SBR is adapted from de Kreuk and van Loosdrecht, 2004. A hydraulic retention time (HRT) of 7 h was obtained with a 3 h 30 min cycle consisting of 3 phases: 1 h 20 min of anaerobic feeding, 2 h of aeration, and 10 min of settling of the AGS and withdrawal of the treated effluent. Solids Retention Time (SRT) or Sludge age corresponds to the average residence time of the microorganisms in the bioreactor linked to the removed sludge mass. Here every two days, 10% of the total mixed volume of the bioreactor was sampled at the middle height of the bioreactor and wasted 10 min before the end of the aerobic phase. The SRT represents the average growth rate imposed on the microbial community. As the AGS-EBPR is not a homogeneous system, the individual cell growth rate a the biofilm micro-scale varies with the availability of the nutrients.
The different SBR phases were programmed with the DaQFactory software in distinct code sequences. The details of the code used for the control and data acquisition are presented in the following GitHub repository:
https://github.com/ArnaudGelb/EPFL.

2.3.1 Anaerobic feeding

The anaerobic phase starts after an N_2 flushing to strip the oxygen remaining from the previous aeration phase. It is also possible to replace this N_2 flushing with an idle phase to rely on the biological oxygen consumption of the biomass to create an anaerobic environment before the influent injection. The influent composition is based on the book’s guidelines "Experimental Methods in Wastewater Treatment" section 2.2.2.4 (M. C. M. van Loosdrecht et al., 2016). The influent was prepared as described later to reach the following final concentrations: 3.57 mM Na-Acetate, 1.04 mM D-Glucose, 2.00 mM NH_4Cl, 0.64 mM K_2HPO_4, 0.37 mM $MgSO_4$, 0.48 mM KCl,

0.10 mM $CaCl_2$, 1 mg/L yeast extract, 0.3 mL/L trace elements solution (Vishniac and Santer, 1957). The obtained osmolarity is around 21 mOsm. This artificial wastewater has a COD/NH_4-N/PO_4-P ratio of 400/28/20 mg/L, leading to a substrate load of 1.4 kg COD/m^3/day (the COD contribution of the yeast extract and the trace element solution are neglected).
The influent used has a high phosphorus concentration compared to Swiss municipal wastewater (Gujer, 2006). The aim was to favor the polyphosphate-accumulating organisms (PAOs) responsible for the biological phosphorus removal of the wastewater. The phosphorus concentration in the influent and the sludge age are two parameters used to ensure that the PAOs will have sufficient polyphosphate (polyP) storage to provide the energy for the complete anaerobic uptake of the influent's soluble organic carbon. Wentzel et al., 1985 have reported that the anaerobic storage of 2 mg_{COD} by PAOs requires the hydrolysis of polyP and the extracellular release of 1 mg_{PO_4}. Therefore, a low phosphorus concentration in the influent and a sludge age allowing a sufficient polyP pool will successfully promote the PAO over aerobic heterotrophs lacking the selective advantage of storing organic carbon during the anaerobic phase.
The influent was prepared by mixing two autoclaved mediums concentrated 24 times with sterile filtered distilled water at 0.2 µm. One concentrated medium contains all the components except phosphorus to avoid the formation of precipitates. The Glucose was dissolved at 5%(w/v), autoclaved separately, and then added to the medium under a laminar flow. The second concentrated medium contains only dihydrogen phosphate. Having the phosphorus source autoclaved separately might prevent the formation of hydrogen peroxide (Tanaka et al., 2014).

2.3.2 Aeration

The dissolved oxygen regulation at 2 mg/L during the aeration phase was achieved with the headspace gas recirculation as Mosqueracorral et al., 2005 proposed and adjusted when required by adding air or N_2. The gas pump delivers a flow rate of 1 L/min, leading to an up-flow superficial gas velocity ranging between 0.006 and 0.012 m/s.

2.3.3 Settling of the biomass and withdrawal of the treated effluent

All gas injections into the reactor are stopped to interrupt the mixing for the biomass to settle before the treated water is withdrawn from the upper half of the SBR. The pH regulation is inactivated during this phase due to the absence of mixing. According to Tay et al., 2002, typical SVI values range between 50 mL/g and 80 mL/g. As the AGS density is comparable to activated sludge density, the settling velocity of AGS is mainly influenced by the size of the particles (Etterer and Wilderer, 2001).

2.4 AGS-EBPR performances measurements

2.4.1 Nutrients removal

The acetate and glucose uptake during the anaerobic feeding were indirectly measured with the chemical oxygen demand (COD). The phosphorus release during the anaerobic feeding and the subsequent phosphorus uptake during the aerobic phase was followed by orthophosphate measurement. The nitrification and denitrification were followed by the ammonium, nitrite, and nitrate measurements during the aerobic phase. Here the NO_2 emission was not monitored. Still, as a greenhouse gas and a significant cause of stratospheric ozone destruction (Ravishankara et al., 2009) undesirably produced with nitrification and denitrification (Colls, 1990); one could measure NO_2 using the approach used by Lochmatter et al., 2014.
The liquid samples were processed according to the manufacturer's instructions after filtration at 0.45 µm (LCK514 and LCK 314, Hach®, 14752, 14773, 14776, and 14848, Merck-Millipore®) to obtain a colorimetric readout of the concentration of the nutrients. This type of measure was chosen for its ease of application and fast readout. The measures of standard curves prepared using influent or effluent as solvent did not detect interference on these colorimetric assays (this is not the case with influents containing amino acids). The concentrations of the wastewater components in the influent were measured after appropriate dilution in distilled water to compare the experimental values to the targeted theoretical values. The concentrations of the wastewater components in the effluent were measured every two weeks at the same time as the cleaning of the bioreactor probes. The limits of detection of the colorimetric tests used allow measuring concentrations of COD > 15 mg_{O_2}/L, NH_4^+ > 0.05 mg_{NH_4-N}/L, NO_2^- > 0.02 mg_{NO_2-N}/L, NO_3^- > 0.5 mg_{NO_3-N}/L, and PO_4^{3-} > 0.05 mg_{PO_4-P}/L. The concentrations of COD, NH_4^+, NO_3^-, and PO_4^{3-} in the bioreactor effluent were generally below the limits of detection of the colorimetric tests, which translates into very high removal efficiencies of these wastewater pollutants. Exceptions were observed when the bioreactor experienced an operational failure. An example of the effect of an operational failure on nutrient removal is presented in Figure 2.2.

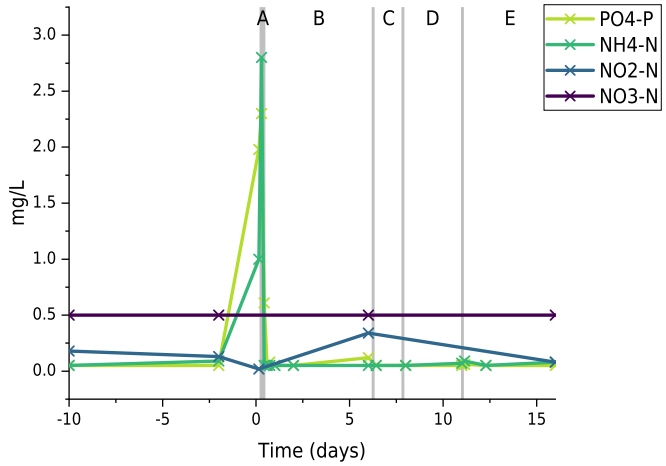

Figure 2.2: **Effect of an operational failure on the nutrient removal**
PO_4^{3-}, NH_4^+, NO_2^-, and NO_3^- were measured in the effluent before and after an operation failure of the bioreactor.
The operation failure, indicated at day 0, was due to a loss of biomass caused by a mixing of the bioreactor not interrupted at the end of the aerobic phase interfering with the settling phase and causing biomass to be withdrawn from the bioreactor.
The theoretical nutrient concentration of the influent is 300 mg_{O_2}/L, 28 mg_{NH_4-N}/L, and 20 mg_{PO_4-P}/L.
The NH_4^+ and PO_4^{3-} measurements were more frequent after the operational failure.
During the time frame A, B, C, D, and E defined by the vertical bars, the volume of influent injected in the bioreactor was adapted to 37.5%, 30%, 37.5%, 45.5%, and 50% of the total working volume of the bioreactor, respectively.

2.4.2 Sludge monitoring

The total suspended solids (TSS) and volatile suspended solids (VSS) were performed according to the methods described in "Standard Methods for the examination of water and wastewater" (2540-D and 2540-E, 2017). A volume of 50 mL of mixed sludge was sampled from the middle of the lab-scale bioreactor 10 min before the end of the aeration phase. The sample was then filtered on a glass fiber filter (10421030, Whatman) using a pressure filter holder, then placed in an aluminum cup to be dried at 105°C for 24h. For the VSS measurement, the dried biomass was calcined at 550°C for 2h. The Sludge Volume Index (SVI) was obtained with the TSS, and the volume occupied by the sludge bed after different settling times up 30 min corresponding to the classical SVI index (Mohlman, 1934). Typical $SVI_{3_{min}}$ were ≈70 mL/g. $SVI_{5_{min}}$, $SVI_{10_{min}}$, and $SVI_{30_{min}}$ were ≈60 mL/g leading to $SVI_{30/5}$ and $SVI_{30/10}$ ratios of > 90%. These values are comparable to SVIs obtained in other laboratory AGS-SBRs (Lochmatter and Holliger, 2014, Layer et al., 2019, Adler, 2019) and show that the AGS of the bioreactor presented here had excellent settling properties.

2.5 Bacterial community members detected by 16S rRNA gene amplicon sequencing

The microbial community composition was assessed with 16S rRNA gene amplicon sequencing in Chapters 3 and 4. Amongst the dominant microbial groups, several were identified in the Metagenome Assembled Genomes (MAG) of Adler, 2019: the PAO *Ca.* Accumulibacter, the nitrite oxidizing bacteria *Nitrospira*, the aerobic heterotrophs *Ferruginibacter*, *Pseudoxanthomonas*, Rhodobacter, *Thiothrix*, and the fermenters *Defluviimonas*, *Flavobacterium*, and *Propioniciclava*.
Some microbial groups were absent from the MAG but detected in the bioreactors operated by Manuel Layer (Layer et al., 2019): the GAOs *Ca.* Competibacter and *Ca.* Contendobacter, the aerobic heterotrophs *Acidovorax*, the fermenters *Anaerolinea*, *Kouleothrix*, and *Runella*.
Some other microbial groups were not reported in Adler, 2019 nor Layer et al., 2019, for example, the aerobic heterotrophs *Hydrogenophaga*, *Leifsonia*, *Lysobacter*, and *Rurimicrobium*, the fermenters *Geothrix*, *Ignavibacterium*, *Rhizorhapis*, and *Rhodoferax*, and some microorganisms with unknown functions such as unknown *Chitinophagales* genus, unknown *Propionibacteriaceae* genus, unknown *Rhodobacteraceae* genus, unknown *Saccharimonadales* genus, unknown *SJA-28* genus, *AAP99*, *Pajaroellobacter*, and *Tahibacter*.
In this lab-scale AGS-EBPR bioreactor, the presence of glucose in the influent did not promote PAO belonging to the genus *Tetrasphaera* even though glucose was shown to support a PAO metabolism by microorganisms belonging to this genus with anaerobic uptake and fermentation of glucose (Kristiansen et al., 2013).

2.6 Supplementary material

2.6.1 Computer AGS-EBPR interface

The global architecture is formed of a host PC running a dedicated SCADA (Supervisory control and data acquisition) software which uses the Input/Output (I/O) channels of WAGO® PLC (Programmable Logical Controller) for all Analogic/Digital conversion for I/O on the bioprocess. One host PC Control Station and one WAGO PLC manage the data acquisition, sequencing control, and regulation of two AGS-EBPRs. In case of a power outage, the computer and the power supply of the Ethernet controller are powered by a UPS (Uninterruptible Power Supply).

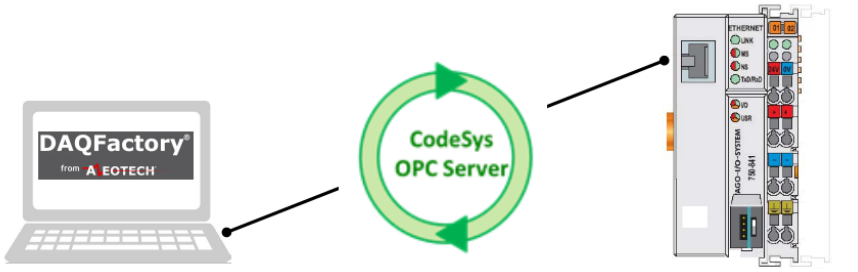

Computer: Intel® Core™ i5-337U CPU 1.80GHz, RAM 4GB, SSD 250GB, Microsoft® Windows® 10 Education
Supervisory Control (SCADA) Software: DAQFactory® Pro (Release 5.90), AzeoTech® Software configuring and programming Tools:
- Wago-I/O-Check (v3.6.1), Wago®
- CoDeSys 2 (v2.3.9.40), CODESYS® Group
- OPConfig (2.3.13.11), CODESYS® Group
- Softing OPC Demo Client (v4.20.00), Softing®

Ethernet Controller: 750-841, Wago®
UPS: SU1400I, APC®

2.6.2 Influent / effluent interface

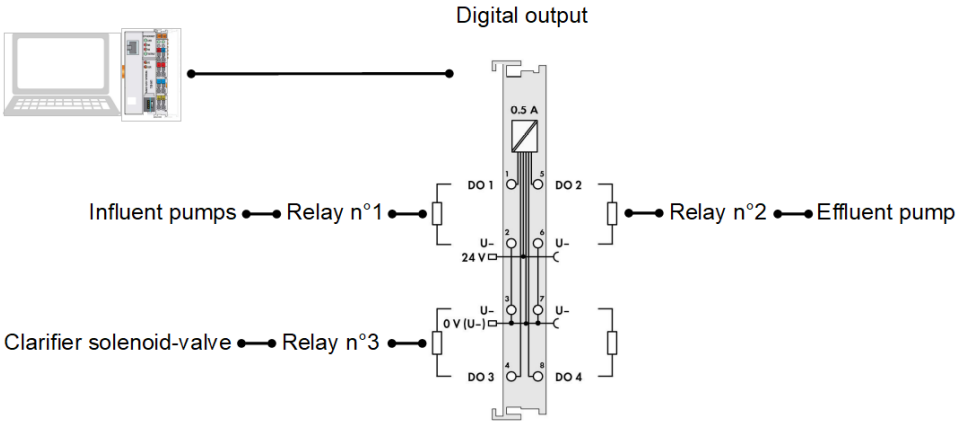

Digital output: 750-531, Wago®
Relay: LZX:PT270024, Siemens®
Influent pumps:
- Medium pump: 77521-57 Masterflex® (7rpm)
- Pump head: 07014-20, Masterflex® (two mounted in series)
- Tubing: 06508-14, Masterflex®
- Water pump: 77521-57, Masterflex® (22rpm)
- Pump head: 07014-20, Masterflex®
- Tubing: 06508-14, Masterflex®

Effluent pump:
- Pump: ISM 444, ISMATEC® (95rpm)
- Pump head: 380AD, ISMATEC®
- Tubing: 06508-18 Masterflex®

Clarifier valve: SCE210C094, ASCO™

2.6.3 pH control interface

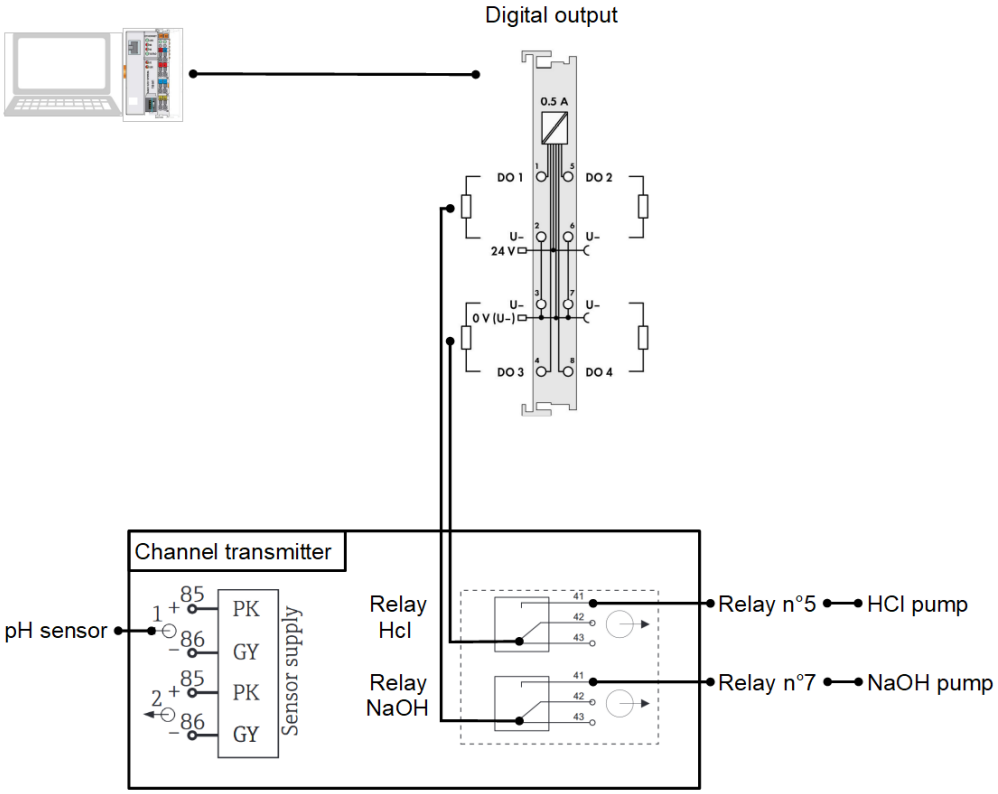

Digital output: 750-531, Wago®
Channel transmitter: Liquiline CM442-19W0/0, Endress+Hauser®
pH sensor: CPS471D, Endress+Hauser®
Relay: LZX:PT270024, Siemens®
HCl and NaOH pumps:
- Pump: 07542-20, Masterflex® (17rpm)
- Pump head: 07014-20, Masterflex®
- Tubing: 06508-14, Masterflex®

2.6.4 Aeration control interface

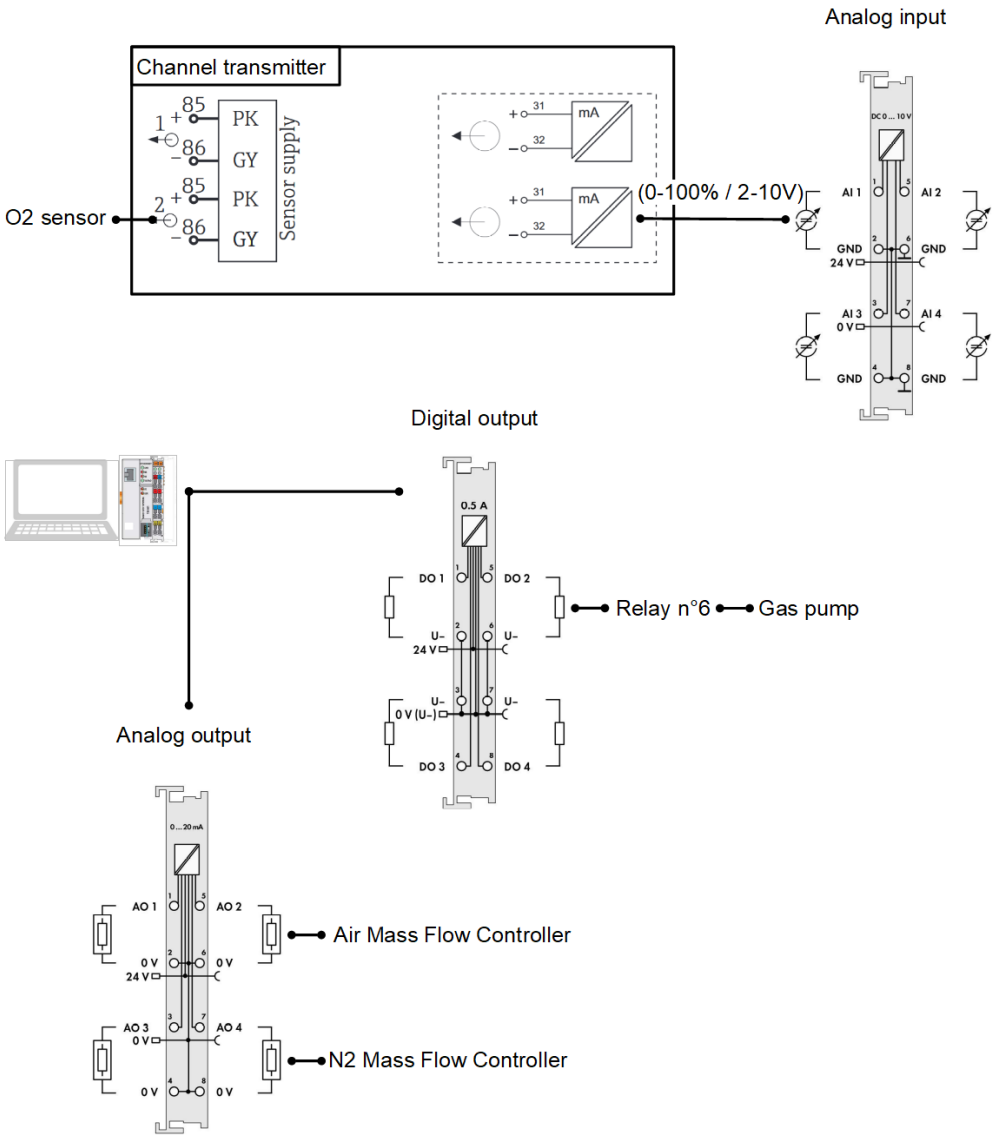

Channel transmitter: Liquiline CM442-19W0/0, Endress+Hauser® with a 500Ω resistance mounted in parallel on the probe signal output
Oxygen sensor: COS22D, Endress+Hauser®
Relay: LZX: PT270024, Siemens®
Digital output: 750-531, Wago®
Analog input: 750-459, Wago®
Analog output: 750-553, Wago®
Gaz pump: N86 KN.18, KNF® Neuberger equipped with a metering valve SS-6L-MM, Swagelok® to reduce the air inflow
Mass flow controller:
- Controller: 5878, Brooks® Instrument
- Air flow controller: 5850E (Air, 0-2 ln/min), Brooks® Instrument
- N_2 flow controller: 5850E (N_2, 0-2 ln/min), Brooks® Instrument

2.6.5 Signal acquisition interface

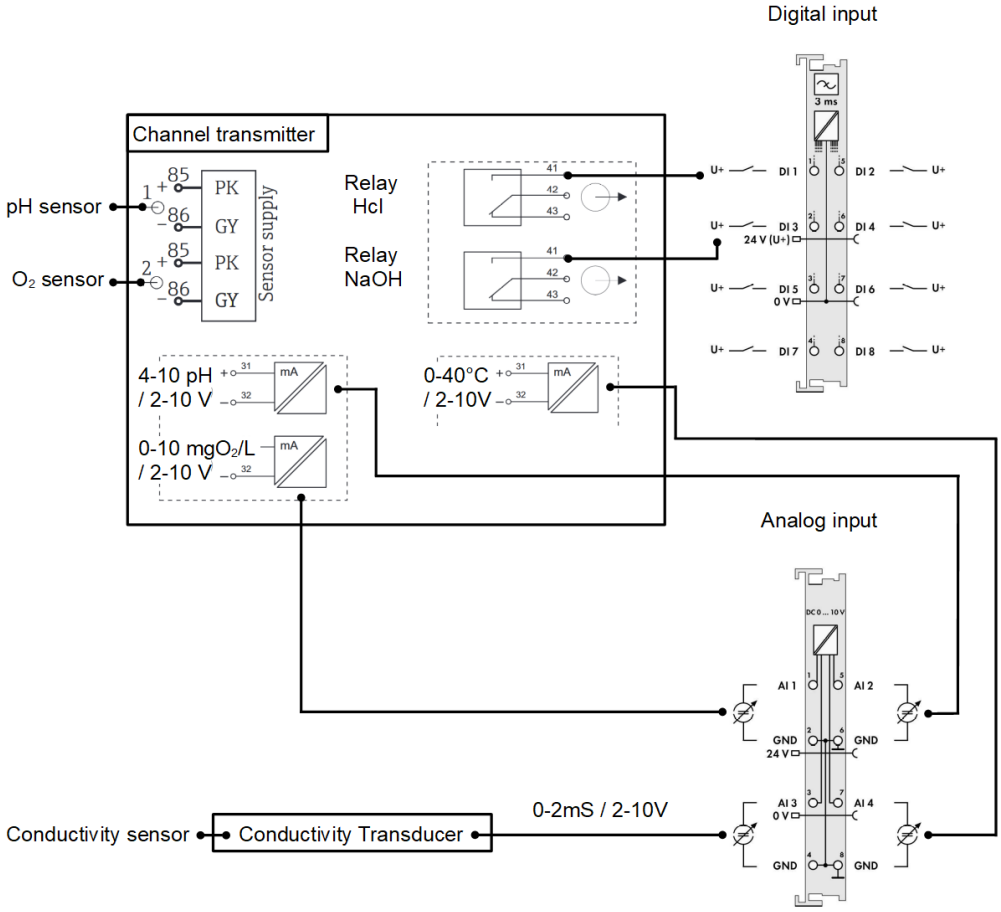

Channel transmitter: Liquiline CM442-19W0/0, Endress+Hauser® with a 500Ω resistance mounted in parallel on the probe signal outputs
Analog input: 750-459, Wago®
Digital input: 750-430, Wago®
pH sensor: CPS471D, Endress+Hauser®
Oxygen sensor: COS22D, Endress+Hauser®
Conductivity Transducer: 202732, Jumo®
Conductivity sensor: 202922/10-0100, Jumo®

2.6.6 PID controlling the dissolved oxygen

DAQFactory PID loop:
- Loop Interval: 1sec
- PID algorithms: Out = P * (e + i/I - D*dPV)

	Air Mass Flow Controller	N_2 Mass Flow Controller
Set point	1.9 mg/L	2.0 mg/L
Proportion (P)	2	1
Integral (I)	10	0
Derivative (D)	0	0
Reverse acting	No	Yes
Out range	0-1 L/min	0-0.1 L/min
Integral Limit	0	0
Reset on start	Yes	Yes

2.6.7 PID controlling the pH

Liquiline pH PID controller:
- Process type: Batch
- Controller type: PID 1-side
- Relay maximum frequency: 60 min^{-1}

Only the proportional of the PID controller was used to avoid the accumulation during the period in which pH regulation is inactivated by turning the pH pumps off.

	HCl pump	NaOH pump
Set point	7.5pH	7.5pH
Integral action time (Tn)	0sec	0sec
Derivative action time (Tv)	0sec	0sec
Proportional band (Xp)	1pH	1pH
Tolerance range (Xn)	0.1	0.1
Max Y change rate/s	0.01	0.01
Effective direction	Direct	Reverse

2.6.8 Data acquisition

Averages of the acquired values are exported every 5 min in a .xls file.

Input	Acquisition timing
Dissolved oxygen	2 sec
pH	30 sec
Conductivity	30 sec
Temperature	30 sec
HCl pump activation	Asynchronous read
NaOH pump activation	Asynchronous read

2.6.9 Structure of the code used for the AGS-EBPR operation

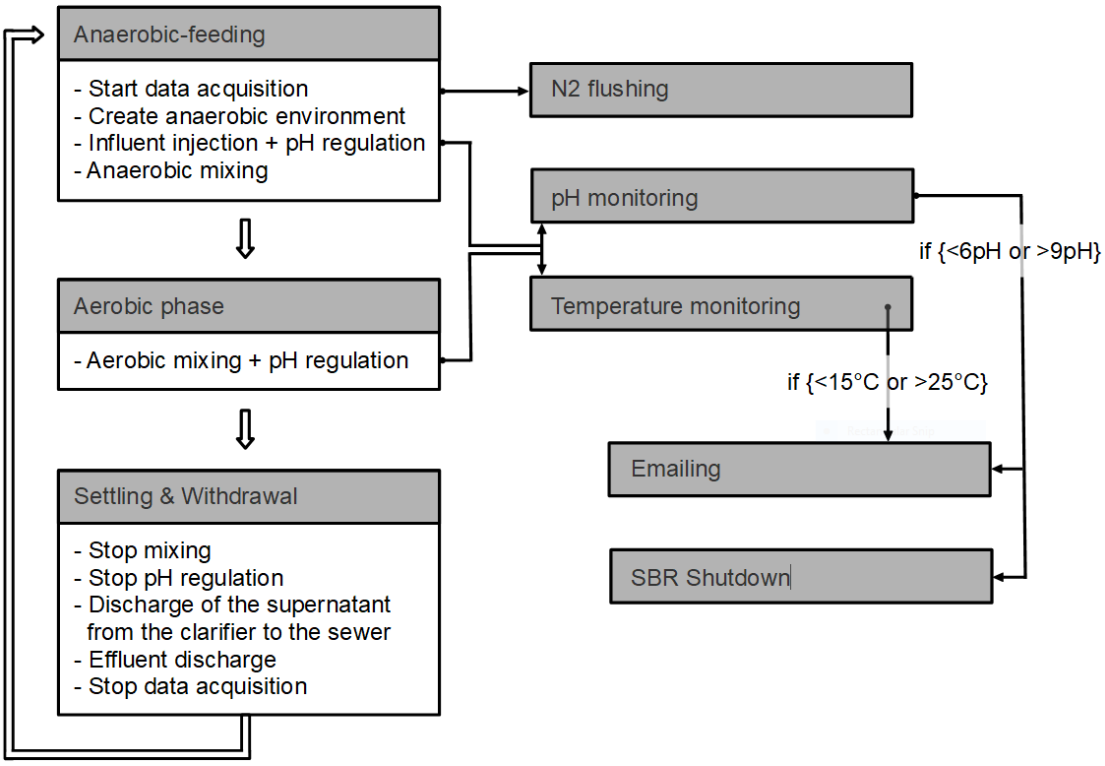

3 Identification of polyphosphate-containing cells present in AGS

Author Contributions:
The conceptualization, methodology, and writing the original draft of this chapter were performed by Arnaud Gelb with the supervision of Christof Holliger.
The other individual contributions are listed below:
- Funding acquisition: Christof Holliger, Nicolas Derlon, and Eberhard Morgenroth.
- Investigation: Emmanuelle Rohrbach and Xenia Bender (16S rRNA gene sequencing library).
- Methodology: Loïc Tauzin and Vladimir Sentchilo (FACS)
- Resources: "Genomics Technologies Facility" led by Julien Marquis at UNIL Lausanne (amplicon sequencing reads), "Department of Fundamental Microbiology" led by Jan Roelof van der Meer at UNIL Lausanne (FACS).
- Writing review: Julien Maillard and Laetitia Cardona.

3.1 Introduction

The bioprocesses used in environmental engineering have been, for decades, operated successfully, relying mainly on empirical knowledge. The advances in molecular biology techniques now allow a deeper understanding of these biological systems. A rational bioprocess optimization and diagnosis require characterizing the microbial populations involved. On the other hand, the characterization of the physiology of many microorganisms involved in wastewater treatment is challenging because of the lack of pure cultures (Mino et al., 1998). Another layer of complexity comes from the dynamic fluctuations of the microbial populations in response to physicochemical changes and to the interactions occurring within the microbial community. One of the aims of treating domestic and industrial wastewater is to remove phosphorus before the discharge of the water into the environment. The biological phosphorus removal from the wastewater is based on the ability of Polyphosphate-Accumulating Organisms (PAOs) to form large quantities of polyphosphate (polyP) in their cells.
The intracellular polyP structure was first described as "volutin granules" by Schlegel and Zaborosch in 1969 in *Spirillum volutans* (Dreisbach, 1988). In the biological phosphorus removal of the wastewater or Enhanced Biological Phosphorus Removal

(EBPR), the PAO development is promoted, causing the incorporation of phosphorus in the biomass beyond its anabolic requirement. This chapter focused on the active PAOs present in the lab-scale AGS Sequencing Batch Reactors (SBR) described in Chapter 2 of the thesis. The AGS process is based on a complex microbial community intertwined in dense biofilm aggregates. The diverse micro-environments in the AGS biofilm aggregates potentially favor PAOs with different metabolic activities.
The ability to form polyP is widespread in almost all living organisms (Docampo et al., 2005) and is believed to be a regulatory mechanism for stress and survival (Kornberg et al., 1999). This complicates the prediction of PAOs at the genetic level among members of the microbial community involved in the EBPR.
The biological phosphorus removal from the wastewater aims to immobilize the phosphate in the biomass regardless of the type of metabolism leading to the polyP accumulation. Nevertheless, the observation of intracellular polyP in the members of the EBPR microbial community does not imply that the polyP experiences anaerobic hydrolysis to perform anaerobic carbon uptake and aerobic polyP replenishment during the SBR phases (e,g,. Ralstonia eutropha Tumlirsch et al., 2015, Achbergerová and Nahálka, 2011).
P. H. Nielsen et al., 2019 suggested that bacteria from the genera *Tetrasphaera* and *Ca.* Accumulibacter are relevant PAOs in most wastewater treatment plants worldwide. The identification and characterization of PAOs present in EBPR processes are still subject to research and likely depend on the wastewater treatment plant site (different habitat) and colonization history (different community structure legacy).
Using taxonomic characterization to study microbial communities has the limitation that the metabolic properties of the microorganisms are not related to their phylogeny. In contrast, physiological probes seek cells with desired functions without prior knowledge of the studied microbial community composition.
The presence of polyP stored by PAO is commonly observed with light microscopy using cytochemical staining based on cationic dyes binding to the anionic polyP. Methylene blue is the active component of Neisser (Eikelboom and van Buijsen, 1983) and Loeffler's methylene blue (Murray et al., 1994) staining. Toluidine blue, which shares the same properties as methylene blue, can also stain polyP (Bartholomew, 1981).
The most common dye to detect polyP stored by PAO with fluorescence microscopy is the DNA dye 4',6-Diamidino-2-Phenylindole, Dihydrochloride (DAPI). It is considered that a low DAPI concentration (<5 µM) leads to a blue fluorescence related to bacterial DNA only, while an intense yellow fluorescence due to polyP is obtained at higher DAPI concentrations (Streichan et al., 1990, Kawaharasaki et al., 1999, W.-T. Liu et al., 2001).
Other fluorescent dyes were mentioned in some research articles, such as neutral red (accumulates in its protonated form in the presence of the acidic polyP, Ezawa et al., 2001), tetracycline (fluorescence based on the presence of Mg^{2+} and Ca^{2+} associated with polyP, Günther et al., 2009), Fura-2 (fluorescence based on the reduction of Mn^{2+}-induced quenching by polyP, Lorenz et al., 1997), and JC-D7 (cationic fluorescent dye binding to the anionic polyP, Angelova et al., 2014). Another approach for polyP labeling described by Saito et al., 2005 uses the affinity of a recombinant polyphosphate binding domain linked with an epitope tag detected by indirect immunolabeling.
Flow cytometry (FCM) is a powerful culture-independent technique enabling the

detection and characterization of microbial communities using taxonomic probes targeting variable regions of the 16S rRNA genes and probes labeling microbial compounds (e.g., PHA, glycogen, polyP). Although FCM is restricted to analyzing single cells in liquid suspension, communities in a biofilm can be processed after an appropriate extraction of individual cells from the biofilm matrix.
FCM includes the possibility of quantifying bacteria of interest on a large number of cells. The acquisition of such sample size facilitates the collection of statistically relevant data compared to conventional microscopy analysis. The main challenge of FCM is that it is almost too easy to produce data, leading to a number of publications with poor results. Correct instrument setup, controls, compensation, and sorting strategies are, in fact, time demanding (Cossarizza et al., 2017). Correct FCS settings determination is described in detail in the gating strategy, voltage optimization, and performance tracking sections in the Material and methods below.

To optimize the microbial biological phosphorus removal from the wastewater, the microorganisms responsible for this activity need to be identified. This chapter aimed to detect PAOs in a lab-scale bioreactor containing Aerobic Granular Sludge (AGS). The adopted strategy to identify PAOs was to use a culture-independent method without *a priori* knowledge of the microbial community composition. To this end, the intracellular polyP storage was labeled with the fluorescent dye DAPI to perform cell sorting after analysis by flow cytometry. The collected cells were then identified using 16S rRNA gene amplicon sequencing.

3.2 Material and methods

3.2.1 Sample preparation

Since FCM is a single-cell method, AGS biofilm must be processed to prepare a single-cell suspension. The formation of a cell suspension from a biofilm has to be optimized for each sample type. The main methods to dissociate cells are enzymatic digestion, chemical dispersion, and mechanical disintegration. Braun et al., 2011 suggested using different enzymes (amylase, pectinase, cellulase, DNase) to cope with the diverse nature of bacterial EPS. The biofilm disaggregation can be helped with chemical dispersants. Chelating molecules (EDTA, sodium pyrophosphate) are sequestering divalent cations used by some adhesion molecules for cell-cell or cell-matrix interactions. Detergents (e.g., SDS, Tween 20) are amphiphilic molecules preventing macromolecule association. As it is difficult to control and evaluate the effect of enzymatic digestion and chemical dispersants on cell lysis, these two approaches were not applied here. The cell suspension from AGS was solely obtained with mechanical homogenization. First, the sample was disrupted by shearing using a Potter-Elvehjem homogenizer, followed by a finer homogenization with a Dounce homogenizer.
A volume of 50 mL of mixed sludge was collected at the end of the aerobic phase to maximize intracellular polyP storage. All homogenization steps are performed at 4°C to prevent sample decay. First, the sample was disrupted by sheering using a Potter-Elvehjem homogenizer (pestle clearance: 150-250 µm) with a motor-driven PTFE pestle. The tube was pressed upon the pestle rotating at 350 rpm once. Then the supernatant was discarded after centrifugation (5 min at 8'000 RCF, 4°C) and resuspended in 50 mL of ice-cold 10 mM HEPES buffer. This washing step was repeated once to remove the media, and then the biomass concentration was adjusted to 0.1 g of wet pellet per mL in 10 mM HEPES buffer. The sample was homogenized with the Potter-Elvehjem using ten ups and downs of the tube on the pestle rotating at 700 rpm. After pushing the tube up, the down motion was performed slowly. Shearing forces are created as the sample and liquid squeeze up and past the pestle. Then a Dounce homogenizer (pestle clearance: 20-56 µm) was used to obtain a finer homogenization. The Dounce homogenizer also relies on pushing the sample between the sides of the tube and the pestle. The pestle was pressed down and then lifted 20 times. The obtained biofilm suspension contains single cells, particles of the biofilm matrix, and remaining cell clusters, which were not disrupted. Therefore, a filtration step with a pore size of 4-7 µm was performed to obtain a cell suspension. The turbidity measure, obtained with the absorbance value at 600 nm (A_{600nm}), was used to estimate the cell concentration in the obtained suspension. It is worth noticing that this turbidity value varies depending on the spectrophotometer optical setup (Eppendorf AG, 2015).

3.2.2 Sample fixation

The cell suspension obtained from the homogenized AGS was fixed with formaldehyde. The formaldehyde reacts with primary amines of proteins forming reactive complexes that may combine with each other or with hydrogen groups. Formaldehyde can also cross-link nucleotides and unsaturated lipids but tends to be nonreactive with carbohydrates (French and Edsall, 1945). The fixation was done at 4°C to prevent sample degradation. As a result, a decrease in the chemical reaction rate between the fixative and the sample occurs (Thavarajah et al., 2012). The fixative solution was buffered at a neutral pH to allow uncharged amino groups to react with formaldehyde. As the concentration of fixative affects the fixation rate, the degree of sample cross-linking can be defined by the formaldehyde concentration. An under-fixation will not stabilize the sample correctly over time. On the other hand, an over-fixation can limit the accessibility of the dye to the desired structure. Among the different formaldehyde concentrations tested, the polyP positive cells are optimally detected following treatment with 2% formaldehyde at 4°C for 4h. Fixation of the samples using formaldehyde concentration lower than 2% decreases the labeling repeatability. The cell suspension was diluted with ice-cold 10 mM HEPES buffer adjusted to pH 7.4 with KOH to reach an A_{600nm} value of 1 after adding the fixative solution. The fixation reaction was performed for 4 h at 4°C. The fixative solution was discarded after centrifugation (5 min at 6'000 RCF, 4°C). The centrifugal speed has been optimized for cell recovery while avoiding cell clumping due to excessive centrifugal force. The pellet was resuspended in 10 mM HEPES buffer supplemented with 1% BSA (w/v) to quench the formaldehyde excess. Another washing step was performed after centrifugation in 10 mM HEPES buffer, and then the sample was resuspended in 0.5 volume of 10 mM HEPES buffer. The cell permeabilization was performed using a 0.5 volume of absolute ethanol at -20°C was transferred drop by drop into the cell suspension while vortexing at intensity 4 to avoid cell clumping. Then the cells were incubated for 30 min at -20°C.

3.2.3 Dye titration

The titration was performed with DAPI and Propidium Iodide (PI) to determine their optimal concentration. The risks of using inappropriate dye concentration are the increase of the unspecific staining, the decrease of signal/noise ratio, and the decrease in sensitivity. The optimal DAPI and PI concentration was defined as the lowest concentration, which gives 90% of the maximum signal. At this dye concentration, the staining is saturating and is most robust between experiential replicates. It was noticed that a DAPI concentration higher than 17 µM does not seem to increase the polyP staining significantly and can lead to the formation of yellow precipitates.
After the incubation in ethanol, the cell suspension was pelleted by centrifugation (5 min at 6'000 RCF, 4°C), the supernatant was discarded and replaced with ice-cold 10 mM HEPES buffer supplemented with 1% BSA (w/v). The sample was kept on ice for 15 min to allow the cells to rehydrate. Then another washing step was performed with 10 mM HEPES buffer. The cell suspension was incubated for 30 min at 4°C in 10 mM HEPES and 50 µg/mL RNAse A to remove the RNA interference on the polyP labeling. As the NaCl final concentration was lower than 0.3 M, the RNAse A cleaves

single-stranded and double-stranded RNA as well as the RNA strand in RNA-DNA hybrid (the commercial RNAse A solution contains: 15 mM NaCl, 0.1 M EDTA, 8 mM Sodium-Acetate, 45 mM Tris pH 7.5) Then the enzyme solution was replaced by 10 mM HEPES buffer after centrifugation.
The polyP and nucleic acids staining was performed using the defined optimal dye concentration for 1 h at 4°C incubation in 10 mM HEPES with 17 µM DAPI and 10 µM PI. The staining solution was removed after centrifugation (5 min at 6'000 RCF, 4°C) and replaced with 10 mM HEPES buffer supplemented with 1% BSA to wash the cells. The refractive index (RI) of the sheath fluid (FACS flow) was measured at 1.3354 at 21°C. The RI of the sorting buffer was matched to the RI of the sheath fluid using an aqueous solution containing 10 mM HEPES, 0.25% (w/v) BSA, and 0.1% (w/v) sodium-azide to avoid scattering noise. The cell suspension was then, after centrifugation, resuspended into the sorting buffer described above.

3.2.4 Gating strategy

The Median Fluorescence Intensity (MFI) is used to measure the central tendencies of the signal because the mean is heavily influenced by off-scale events and the mode by noise. As the FSC is measured here with a photodiode detector, the discrimination of the bacterial cells from the background is difficult using the FSC signal. Therefore, the PI fluorescence and the SSC are used as trigger parameters. The events must meet the value of both thresholds to be recognized by the flow cytometer. The thresholds are carefully set to prevent cells from being ignored, as they will not be included in the sorting decision process and can contaminate the sorted fraction. The fluorescent signal generated by the DAPI-polyP complexes after excitation at 407 nm is selected by a 530/30 nm band-pass filter before quantification. The fluorescent signal obtained by the PI-nucleic acids complexes after excitation at 561 nm is selected by a 610/20 nm band-pass filter before quantification. For the sake of reproducibility, gates are rectangular and, when possible, are not positioned in the overlap of the logarithmic and linear scale of the bi-exponential plot. The panel's evaluation was performed with an N by N bivariate plot presented in Figure 3.2.

3.2.5 Voltage optimization

The fluorescence signal was measured here by photomultiplier tubes (PMT). In the PMT, photons emitted by the fluorophore are converted into a photocurrent amplified based on the applied electric potential called gain. A linear relationship exists between the log(voltage) applied to the PMT and the log(signal intensity). The higher the measured fluorescent signal, the lower the electronic noise contribution. The background noise contribution can be correlated with the coefficient of variation (CV) of uniform fluorescent beads (Chase and Hoffman, 1998). A signal with a higher electronic noise will cause an increase in the CV, as presented in the supplementary Figure 3.1. At a specific voltage, the resolution of the fluorescent signal from the background noise will be plateaued, translating into CV stabilization. This voltage level is optimal because it enables a good resolution of the fluorescent signal and provides a linear range of detection of the brighter events. The optimal voltage was

further refined with unstained beads using the following indicators:
Staining Index (SI) = $\frac{MFI_{pos} - MFI_{neg}}{2 \times rSD_{neg}}$
Alternative Staining Index (AltSI) = $\frac{MFI_{pos}}{rSD_{neg}}$
Voltration Index (VI) = $\frac{AltSI}{\sqrt{Voltage}}$
A schematic representation of the resolution of the positive population from the negative population is presented in the supplementary Figure 3.2. The SD_{neg} is used to evaluate the spread of the negative peak. For a variable fitting a normal probability distribution, 68% of the values are within one standard deviation of the mean, and 95% of the values are within two standard deviations of the mean. The robust standard deviation (rSD) measures the dispersion from the median. For events normally distributed, the SD and the rSD are equal, and the rSD is less affected by outlying values than the SD.
The measures of the voltage optimization were performed using calibration beads containing a mixture of fluorophores (Sphero™, RCP-30-5A) and unstained beads (Sphero™, BCP-10-5). The acquisition was made at a flow rate of 10 µL/min using an FSC threshold. A gate was placed around the beads populations, and the area, height, and width parameters were collected for all gated events. The beads signal was recorded from 200 V to 1'000 V with 50 V increments for each detector. The SI, AltSI, and VI values were then calculated and plotted as a function of the PMT voltage setting. The experimental points were fitted with a linear plateau model (Mangiafico, 2016); the plateau value gives the minimum CV (CVmin). The optimal voltage was defined as the minimal voltage in which the electronic noise contributes to no more than 10% of the fluorescent signal CV. The obtained voltage was checked on the sample to ensure that the brightest fluorescent signals did not exceed the upper limit of the PMT detection range. Then the optimal voltage was evaluated on the resolution of the sample from unstained beads. Since PMT performances differ between flow cytometers, the optimal voltage values obtained here are unlikely relevant to other instruments.

3.2.6 Performance tracking

To consistently set voltages of the PMT detectors over time, fluorescent reference beads (Sphero™, RCP-30-5A) are used after the optimal voltage identification to generate target values. Between sorting performed on different days, the voltages are adjusted and monitored to reach the target values. Using the assumption that the cell count within a particular volume follows a Poisson distribution, the variance observed in a uniform positive population "A" is defined as:
CV = $Var(A)^{\frac{-1}{2}}$ (Poisson, 1837)
As good experimental practice suggests keeping the CV below 5%, the minimum number of events to record can be defined according to the proportion of target cells in a sample.

3.2.7 Sorting

In flow cytometers with sorting capabilities, the stream of fluid containing the cells is transformed into droplets that can be charged and deflected in an electric field to be directed into collection tubes. With a perfect monodisperse cell suspension, the cell number per drop follows a Poisson distribution (Cox et al., 1988) where the probability "p" of observing an event "n" times is given by:
p = $\frac{z^n e^{-z}}{n!}$ (Poisson, 1837)
where "z" is the average number of times the event occurs within the continuum.
During sorting, the flow cytometer's sorting system deflects drops containing the cell to be sorted depending on its location within a drop (measured by 1/32 increment) and whether the leading drop, the drop being interrogated, and the trailing drop are free of unwanted cells. Cell sorting can favor the yield or purity of the cells of interest based on the chosen parameters. Yield and purity depend on the event rate and the frequency of the cells of interest. The less abundant a cell population is, the lower needs to be the total event rate to ensure an acceptable yield and purity. The distance between the laser interrogation point and the point where the stream containing the sample breaks off into droplets is called the drop delay. The drop delay depends on constant parameters: the sheath pressure, the nozzle orifice size, the frequency, and the amplitude of its vibration. As the air pressure, humidity, and temperature affect the drop delay, it must be determined before every cell sorting to ensure that the correct droplet is being sorted.
The polyP positive cells were sorted using the purity precision mode of the BD FACSAria™ III Cell Sorter. The sorting rate used was about 7'000 events/sec with an efficiency higher than 80%. The sample was sorted till 2×10^7 polyP positive cells were collected.

3.2.8 DNA extraction

The volumes of the sample used for the DNA extraction were 200 µL and 1.5 mL for homogenized AGS and cell suspension, respectively. The cells were pelleted by centrifugation (5min at 12'000 RCF, 4°C), and the supernatant was removed. The sorted PAOs fraction was concentrated on a 0.2 µm filter (GPWP01300, Millipore). All the samples are then stored at -20°C for a maximum of 2 weeks. The DNA extraction was performed with the InstaGene™ Matrix (732-6030, Bio-Rad). A volume of InstaGene™ Matrix of 200 µL was added to the homogenized AGS and cell suspension pellets, and a 50 µL volume was added to the filter containing the sorted PAOs fraction. A first incubation was performed at 56°C for 30 min, followed by 1 min vortexing at max speed. The tubes were spined down before the second incubation at 100°C for 8 min, followed by 1 min vortexing at max speed. The samples were centrifuged (3 min at 12'000 RCF, 20°C), and the supernatant was transferred into a new tube.

3.2.9 Amplicon sequencing

After the DNA extraction, the samples were directly used to perform the first PCR of the amplicon sequencing of the V1–V2 region. The amplicon sequencing was

prepared based on the 16S Metagenomic Sequencing Library Preparation application note from Illumina (Illumina, 2013) using the forward primer and the reverse primer indicated in Table S3.6, which were fused with the required overhang nucleotide sequences. The modifications of the original protocol are specified hereafter. The amplicon PCR was performed with the commercial PCR mix Q5® High-Fidelity 2X Master Mix using 0.5 µM of each primer and 25 ng of template DNA. The PCR was performed with the following steps: initial denaturation (2 min, 98°C), followed by 30 amplification cycles (45 sec, 98°C; 45 sec, 50°C; 60 sec, 72°C), and a final extension step (5 min, 72°C). The size of the amplicons was verified by loading 5 µL of each amplified sample with a loading buffer on an agarose gel (1.5% agarose, 0.5x TAE buffer). After the amplicon PCR clean-up using the AMPure XP beads, the amplicon concentration is measured with the Qubit dsDNA HS assay kit. For the Index PCR, the amplicons were normalized at 5 ng/µL, the Q5® High-Fidelity 2X Master Mix replaced the 2x KAPA HiFi Hot Start Ready Mix, and the index primer sets B and C were used. The Lausanne Genomic Technologies Facility (GTF, University of Lausanne, Switzerland) performed the rest of the workflow after the Index PCR clean-up, and 96 samples were grouped and sequenced in paired-end mode with the MiSeq Reagent Kit v2 (2×250 bp) on an Illumina sequencing platform.

Reagents not referenced in (Illumina, 2013):

Name	Concentration / purity	Supplier	Reference
Lysozyme from chicken egg white	~100’000 U/mg	Sigma-Aldrich	62970-1G-F
Tris(hydroxymethyl)-aminomethane (Tris)	99%	ACROS Organics	140500025
Hydrochloric acid	25%	Merck Supelco	1.00316.1000
Ethylenediamine-tetraacetic acid (EDTA)	99%	ACROS Organics	118430010
Maxwell® 16 Tissue DNA Purification Kit	-	Promega Corporation	AS1030
Q5® High-Fidelity 2X Master Mix	-	New England Biolabs	M0492S
Primers	Desalted	Microsynth AG	-
Agarose	-	VWR Peqlab	35-1020
Tris-Acetate-EDTA, 50X Solution	-	Fisher BioReagents	BP13324
GelPilot DNA Loading Dye, 5x	-	QIAGEN	239901
Ethanol	99.8%	Fisher Chemical	E/0650DF/15
10 mM Tris-HCl, pH 8.5	-	QIAGEN	19086
Qubit™ dsDNA HS Assay Kit	-	Invitrogen	Q32854
Nextera XT Index Kit v2 Set B, C	-	Illumina Inc.	FC-131-2002, FC-131-2003

3.2.10 Analysis of the sequencing reads

The paired-end sequencing on the Illumina platform generates one R1 and one R2 FASTQ file per sample, which are grouped in a TAR archive to be treated by the FROGS pipeline (Escudié et al., 2018) as follows:

Preprocessing

Step 1: The reads R1 and R2 were merged with a maximum mismatch rate of 0.1 in the overlapped region (VSEARCH, Rognes et al., 2016). The maximum length of the reads allowed was 400 nucleotides to avoid too high stringency. Because the targeted amplicon size is short enough to induce an overlap between the reads, the non-merged reads were not considered for analysis.
Step 2: The primers used for sequencing were identified and removed from the sequences (cutadapt, Martin, 2011). The primer search accepted 10% of differences, and sequences without the two primers detected in the sequence were removed.
Step 3: The sequences with ambiguous nucleotides and lengths outside the range between '100 - primer length' and '800 - primer length' were filtered out. As the amplicon size in *E. coli* K-12 was 347bp, the filtering on the length was not meant to be stringent.
Step 4: The sequences were de-replicated: strictly identical sequences were represented only once, and the initial count was kept in the count file.
Note: A reduction of the dataset by the pre-processing step superior to 20% is highlighting a quality problem.

Clustering

Step 1: The sequences were sorted according to their abundance.
Step 2: The clustering of the reads is performed with Swarm (Mahé et al., 2014, Mahé et al., 2015) with a distance parameter of 1.

Chimera

Chimeras are sequences formed from two or more biological sequences joined together. Most of these abnormal sequences are created from an incomplete extension during a PCR cycle. A partially extended strand can bind to a template derived from a different but similar sequence during subsequent cycles. This phenomenon is widespread in amplicon sequencing, where closely related sequences are amplified. On the other hand, it is challenging to distinguish chimeras from correct sequences in the sequencing of the 16S genes (Edgar, 2016). If the chimeras are not removed, the number of OTUs and the observed diversity will artificially increase. This step was not performed as the diversity evaluation was not the aim here. When performed, the chimeras detected by VSEARCH ranged between 9% and 17% of the pre-processed reads.

Filtering

The OTUs were filtered according to their proportion of sequences. Because this study focused on the dominant OTUs, the threshold used ignores OTUs with an abundance below 0.5% of all sequences.

Affiliation

Step 1: The software blastn+ (Camacho et al., 2009) was used to create alignment between each filtered OTU and the MiDAS database (version 3.6) (Nierychlo et al., 2020), based on the Silva version 132 (Quast et al., 2013 Yilmaz et al., 2014). Only the best hits were reported. For each alignment result, several metrics were computed: identity percentage, coverage percentage, and alignment length.
Step 2: For each filtered OTU with several blastn+ alignment results, a consensus was determined at each taxonomic level. If all the taxa in a taxonomic rank were identical, the taxon name was reported; otherwise, a multi-affiliation was recorded.
Step 3: When the alignment of an OTU with the MiDas database gave a coverage or an identity below 95%, a manual alignment was performed with the database Silva version 138 and the EzBioCloud database (Yoon et al., 2017).
As exposed by Edgar, 2018 with a small fragment of the 16S rRNA gene, the accuracy of an OTU affiliation with an identity percentage below 100% is questionable. For our results, the uncertainty linked to the OTUs affiliation is represented in the supplementary Figure 3.5. The MiDAS database (version 3.6) was produced using the V1-3 variable regions of the bacterial 16S rRNA gene. Here the amplicons were generated using a different set of primers (supplementary Table 3.6) targeting the V1-2 variable regions. This primer choice affects the detection coverage of the bacterial OTUs in the database (the detailed coverage at the Phylum level is presented in the supplementary Figure 3.7).

3.2.11 Material and reagents

Name	Concentration / purity	Supplier	Reference
Potter-Elvehjem homogenizer	-	Roth	TT601.1, TT64.1
Stirrer	-	Heidolph	RZR 2051
Dounce homogenizer	-	Roth	CXE1.1
HEPES	99+%	Acros Organics	172571000
Potassium hydroxide	88.2%	Acros Organics	134060025
Sodium azide	99+%	Acros Organics	190381000
Conical Tubes 50 mL	-	Eppendorf	0030122178
Centrifuge 50 mL	-	Eppendorf	5804R
Filter, pore size 4-7 µm	-	Whatman	10311844
Spectrophotometer	-	Eppendorf	BioSpectromter
Formaldehyde 16% (w/v)	96.5%	Thermo Scientific	28908
2 mL tubes	-	Sarstedt	72.695.200
Centrifuge 2 mL	-	Eppendorf	5417R
BSA Fraction V	98+%	Acros Organics	240401000
Ethanol	99.8+%	Fisher Chemical	E/0650DF/15
Vortex-Genie 2	-	Scientific Industries	SI0276
RNase A Solution	4 mg/mL	Promega	A7973
DAPI	98+%	Applichem	A4099.0005
PI	98.2%	Acros Organics	440300250
5 mL PP Tubes	-	Falcon	352063

3.3 Results and discussion

3.3.1 Experimental strategy and challenges

The lab-scale AGS-EBPR bioreactor studied here was the one presented in Chapter 2 of this thesis. This bioreactor had a complete and stable phosphorus removal from a synthetic influent containing acetate and glucose as organic carbon sources.
The detection of PAOs with a DAPI and tetracycline labeling of the polyP was tested. The polyP labeling with tetracycline could not be achieved with the protocol of Günther et al., 2009. The inability to successfully reproduce the staining can be caused by production batch variation of the tetracycline, as reported by the authors, or due to the use of a different fixation method. The fixation was performed with formaldehyde instead of the protocol described in Günther et al., 2008 due to the potential risk of interference of heavy metals used in the latter fixation method with the amplicon sequencing of the cells sorted by FACS. Therefore, the detection of PAOs was achieved in this chapter by labeling intracellular polyP with the fluorescent dye DAPI.
DAPI binds to double-stranded DNA mainly at the minor groove in the presence of AT base pairs and emits a blue fluorescence with a maximum at 456 nm upon UV illumination (Williamson and Fennell, 1975). Other known DNA binding forms are intercalation (Wilson et al., 1989) and abduct formation (Beccia et al., 2012). The different binding types depend on experimental conditions such as the DAPI concentration, solvent type, or temperature. DAPI was described to interact with RNA as an intercalant with a maximum fluorescent emission at 468 nm (Tanious et al., 1992). Streichan et al., 1990 reported that lipid inclusion could have a weak yellow fluorescence upon DAPI labeling. When DAPI is used at a high dye/phosphate ratio, the DAPI bound to DNA forms dye-dye interactions leading to an enhanced fluorescence emission shifted to yellow (Cavatorta et al., 1985). DAPI also forms complexes with polyP, which exhibits a yellow fluorescence (Allan and Miller, 1980). The emission spectra of DAPI-DNA and DAPI-polyP complexes overlap. As the signal intensity of the DAPI-polyP fluorescence is more intense than DAPI-DNA fluorescence, it can not be compensated for the spillover measured by the DAPI detector using a spillover spreading matrix. For this reason, propidium iodide (PI) was selected as a second dye to stain the nucleic acids. PI is an intercalating dye binding to double-stranded nucleic acids with a stoichiometry of one dye per 4-5 base pairs with little or no sequence preference and emits a red fluorescence with a maximum at 617 nm upon green illumination (Waring, 1965).
The cells were detected based on their PI-nucleic acid fluorescence and the polyP positive cells were selected based on their DAPI-polyP fluorescence (Figure 3.1). The events considered meet a threshold value of 200 for the signal height of SSC and the nucleic acids labeling with PI. A first gate (displayed on the left plot representing the DAPI-DNA against the PI fluorescence) is applied to exclude cell aggregates. A second gate (displayed on the center plot representing the height against the width of the PI) is applied to filter out further the events created by two cells being analyzed simultaneously. The last gate (displayed on the right plot representing the PI against the polyP fluorescence) defines the polyP positive events.

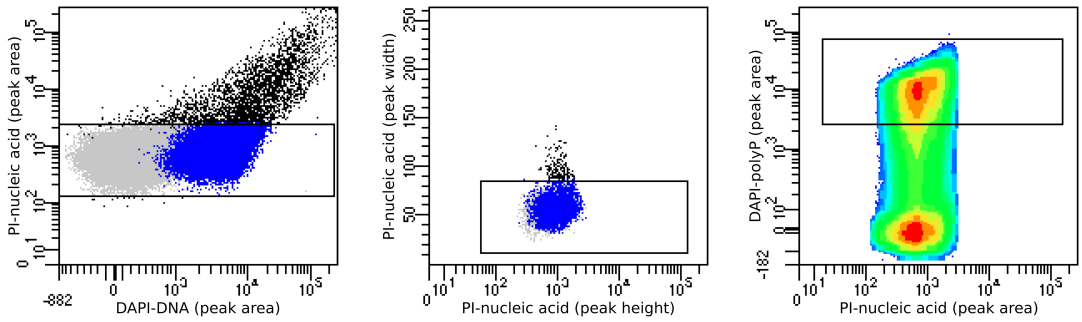

Figure 3.1: **Gating strategy of the AGS cell suspension analyzed by flow cytometry leading to the selection of polyP positive cells**
The left and center plots display 10’000 recorded events. Events defined as polyP positive are overlaid in blue. The right plot represents the density of the recorded events. The colors represent the accumulation of events with logarithmic spacing between contours. The innermost contour represents 50% of the events, and each successive contour line represents 50% of the preceding contour.

The spectral unmixing control was performed using the fully stained sample with an N by N bivariate plot (every parameter against every parameter) to check the gating strategy used in Figure 3.1 (Figure 3.2).

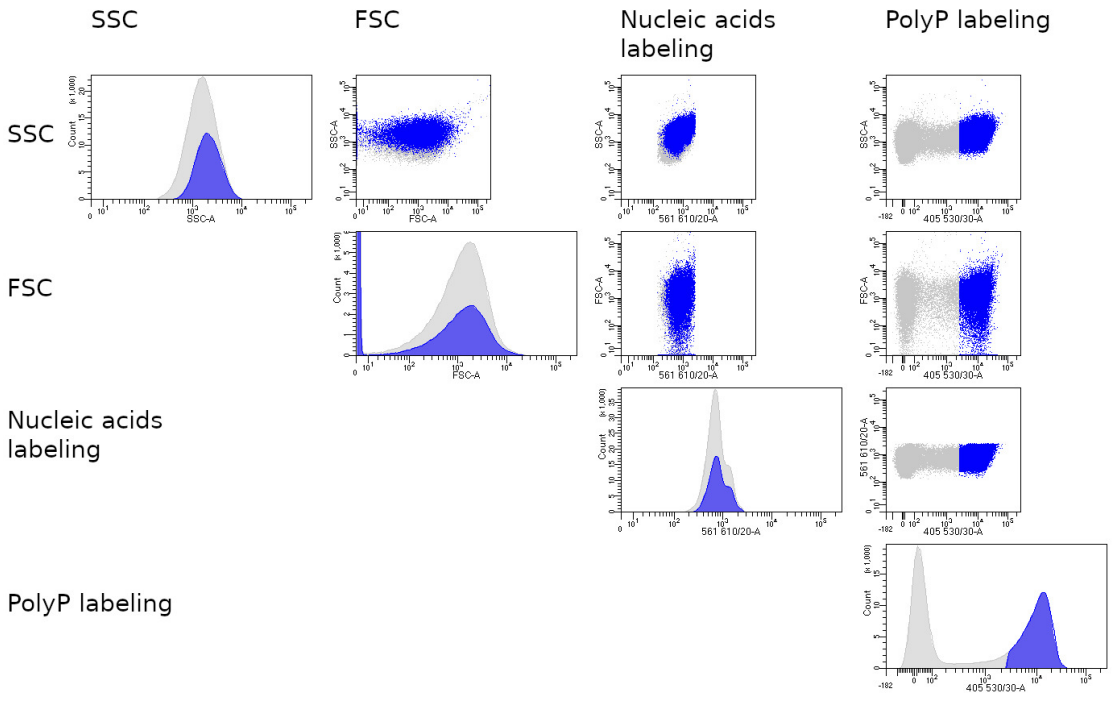

Figure 3.2: **Control of the gating strategy with an N by N bivariate plot of the sample’s fluorescence signal**
Every parameter is plotted against every other parameter to evaluate the panel. The plots display 10’000 recorded events. Events defined as polyP positive in Figure 3.1 are overlaid in blue.

3.3.2 PolyP positive cells detection in an AGS-EBPR bioreactor operated with a glucose-acetate influent

Figure 3.3 (A, left panel) shows the effect on the microbial community of the sample processing from the homogenized AGS (AGS) to the cell suspension (Cell) and then to the fixed and labeled cell suspension (Unsorted). Those samples were analyzed in duplicate by the 16S rRNA gene amplicon sequencing to evaluate the variability of this analysis. On the other hand, the sorted samples presented in Figure 3.3 (right panel) were only analyzed by amplicon sequencing once due to limitations of the amount of total DNA in these samples. The experimental procedure was repeated on three different days to evaluate the experimental variation (the replicates are named R1, R2, and R3).
A bias in the relative abundance of the different microbial community members was observed during the cell suspension preparation from the homogenized AGS. In the cell suspensions, several genera were underrepresented in the cell suspension compared to the homogenized AGS samples, such as *Runella*, an unknown genus of the family *Propionibacteriaceae*, *AAP99*, and *Ignavibacterium*. On the other hand, the microorganisms belonging to the genus *Ca.* Accumulibacter were more abundant in the cell suspensions than in the homogenized AGS. This bias observed for some genera is likely due to differences between microorganisms' adhesion strength, either to other microorganisms or the biofilm matrix, and/or their tendency to re-aggregate once they are in single-cell form. Differences of a lower extent were also observed in the relative abundance of some microbial community members between the cell suspensions before and after the fixation and labeling steps. This bias was observed for some groups of microorganisms, such as *AAP99* and *Ignavibacterium*, which can be due to the fixation procedure with formaldehyde known to impair DNA extraction and amplification (M. T. P. Gilbert et al., 2007, Dietrich et al., 2013).
The genus *Ca.* Accumulibacter was one of the dominant OTUs before sorting. Nevertheless, after sorting, this genus contributes to 50%, 60%, and 70% of the total analyzed reads in the triplicate experiments performed on different days. Consequently, it can be concluded that *Ca.* Accumulibacter is likely the main PAO in this lab-scale AGS-EBPR at the moment of the analysis. The OTU 14, OTU 46, and the OTU affiliated to an unknown genus of the family *Propionibacteriaceae* were also present in the sorted PAO fractions but were not enriched compared to the samples before sorting (OTU sequences accessible at https://github.com/ArnaudGelb/EPFL). This observation can be due to false positive cells sorted in the PAO fraction. Another explanation could be that these microorganisms belonging to the *Propionibacteriaceae* family could have some cells of their population with intracellular polyP and others without intracellular polyP. To conclude, if this microbial group behaves as PAO in EBPR conditions, the presence of polyP in their cells must be measured at different time points during the SBR cycle. The enrichment of microorganisms belonging to the genus *Ca.* Accumulibacter with an influent containing acetate was expected (Kong et al., 2004). In this lab-scale AGS-EBPR bioreactor, the presence of glucose in the influent did not promote other PAO, for example, microorganisms belonging to the genus *Tetrasphaera* (J. L. Nielsen et al., 2012, Kong et al., 2008). According to the model of Kristiansen et al., 2013, some microorganisms belonging to the *Tetrasphaera* genus are anaerobically taking up and fermenting glucose producing glycogen. The glycogen is catabolized to replenish polyP during the aerobic phase.

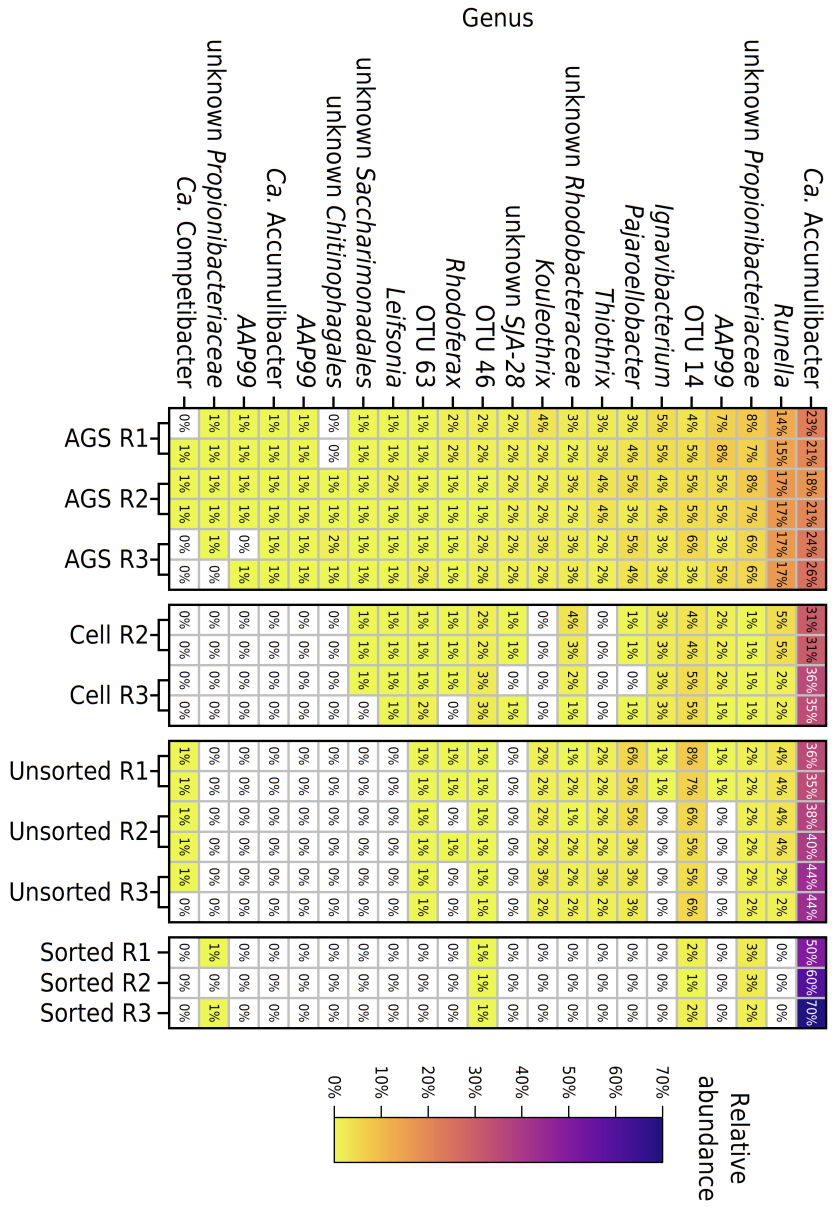

Figure 3.3: **Assessment of the microbial community throughout the experimental procedure leading to the sorting of the PAOs fraction**
Relative abundance of the OTUs compared to the sample's total number of preprocessed reads.
The left panel presents the samples sequenced in duplicates used to assess the variability of the sequencing. "AGS R1-3" are the experimental replicates of the homogenized AGS. "Cell R2-3" are the experimental replicates of the cell suspensions obtained from the homogenized AGS (the sample R1 was lost). "Unsorted R1-3" are the experimental replicates of the fixed and labeled cell suspensions.
The right panel presents the microbial composition of "Sorted R1-3", the experimental replicates of the FACS sorted polyP positive cells.
The OTUs analyzed had an abundance of at least 0.5% of the total number of preprocessed reads in one of the samples. The color scale displays the relative abundance; the table cells in white were below 0.5%. The overview of the processing of the sequencing reads is presented in the supplementary Figure 3.3.

3.3.3 PolyP positive cells detection in an AGS-EBPR bioreactor operated with an influent containing VFAs and fermentable mono- and polymeric substrates

The method developed here was applied on the lab-scale AGS-EBPR operated by Manuel Layer, treating artificial wastewater with a composition detailed in Layer, 2021 named "Complex synthetic wastewater" containing a mixture of acetate, propionate, glucose, starch, peptone, and amino acids together with a phosphate concentration of 5.4 mg/L. The microbial community composition harbored by this AGS-EBPR is presented in the supplementary Figure 3.4. Compared to the bioreactor described in Chapter 2, which is operated with an influent containing a phosphate concentration of 20 mgP/L, it is assumed that the PAOs will be less enriched in this microbial community. This is reflected by >50% of the sequencing reads affiliated to the *Ca.* Competibacter, *Nocardioides*, or *Amaricoccus* genera. A preliminary result obtained on one sample indicated that *Ca.* Accumulibacter was present in less than 1% of the sequencing reads and was not significantly enriched in the sorted polyP positive cells. On the other hand, *Microlunatus phosphovorus* (class of *Actinobacteria*) was present in higher abundance in the microbial community (>1% of the sequencing reads), experiencing a log enrichment in the sorted polyP positive cells, become the largest microbial group in the sequencing reads of the sorted fraction. The absence of experimental replicates does not allow the formulation of any strong conclusion. Still, it is an encouraging proof of concept regarding the capability of the protocol presented here to identify PAO in different EBPR systems. In this bioreactor, the observation that *Microlunatus* might be responsible for the biological phosphorus removal from wastewater instead of *Ca.* Accumulibacter can be due to the different carbon substrate selection pressure and lower influent phosphorus concentration creating a different environmental niche more adapted to *Microlunatus* metabolism. *Microlunatus phosphovorus* is a PAO isolated in pure culture from an EBPR sludge releasing phosphorus anaerobically and producing intracellular polyP aerobically (Nakamura et al., 1995, Zhong et al., 2018). In EBPR conditions, *Microlunatus phosphovorus* forms intracellular PHA anaerobically with glucose and acetate and consumes the stored PHA during aerobic phases (Akar et al., 2006).

3.4 General conclusions and perspectives

The obtained results demonstrate that PAOs sorting based on the staining of intracellular polyP is feasible with double DAPI/PI staining. In the lab-scale AGS-EBPR studied here, *Ca.* Accumulibacter is likely the main PAO. For the other groups identified in the sorted PAO fraction, the presence of intracellular polyP can be cross-checked. The presence of polyP in the microbial cells can be confirmed using fluorescent microscopy with DAPI labeling followed by the hybridization of specific Fluorescence *In situ* Hybridization (FISH) probes. It is also possible to use the single-cell sorting capability of the FACS to image the presence of polyP before the identification with 16S rRNA gene amplicon sequencing.
The method developed here offers promising possibilities to investigate the PAOs in different EBPR systems, as shown by the preliminary results leading to the detection of *Microlunatus* in a bioreactor operated with an influent containing VFAs and fermentable substrate.

3.5 Supplementary figures

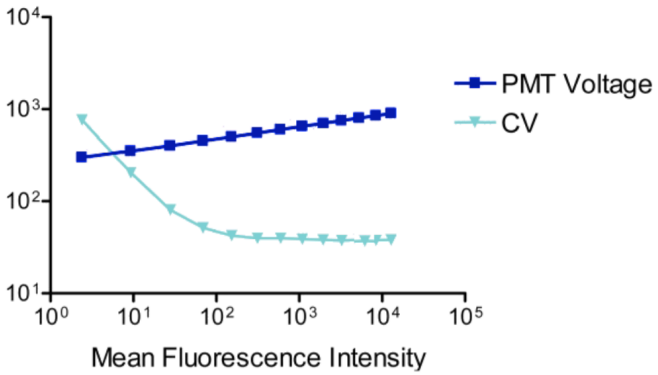

Supplementary Figure 3.1: **Characterization of a PMT detector at different voltages**
The voltage of a PMT detector measuring the signal of fluorescent beads is varied to define its optimal range of operation.
Adapted from Maecker and Trotter, 2006.

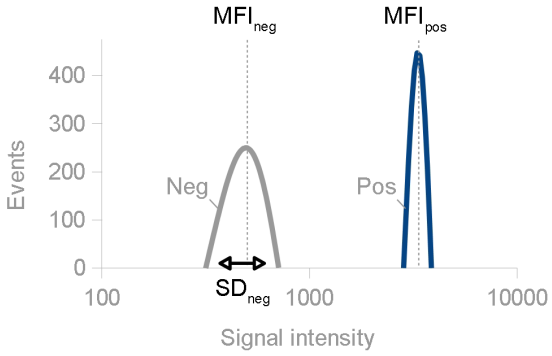

Supplementary Figure 3.2: **Illustration of the resolution of negative and positive populations**
This figure illustrates the fluorescence intensity distribution of negative and positive events obtained on a detector at a defined voltage.

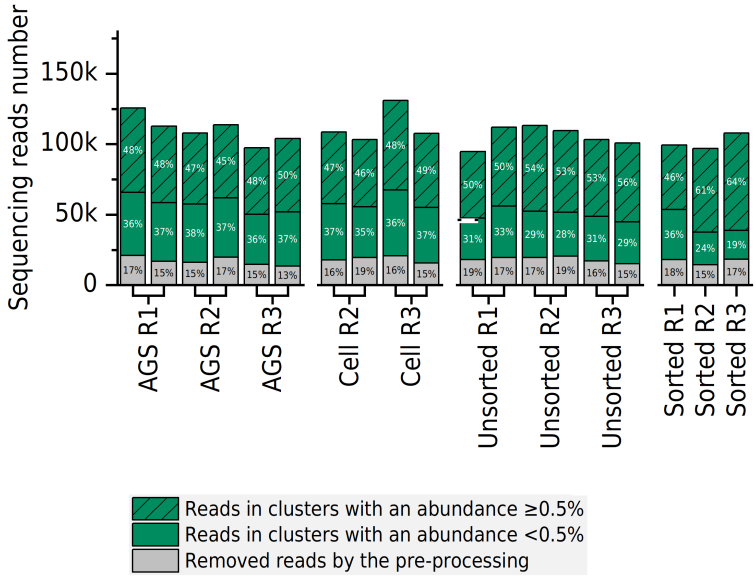

Supplementary Figure 3.3: **Overview of the processing of the sequencing reads of the PAOs sorting experiment**.
The hatched bars show the reads present in OTUs harboring an abundance higher than 0.5% of the total number of treated reads (displayed in dark green).
The gray bars show the reads not meeting the quality requirement set in the pre-processing.

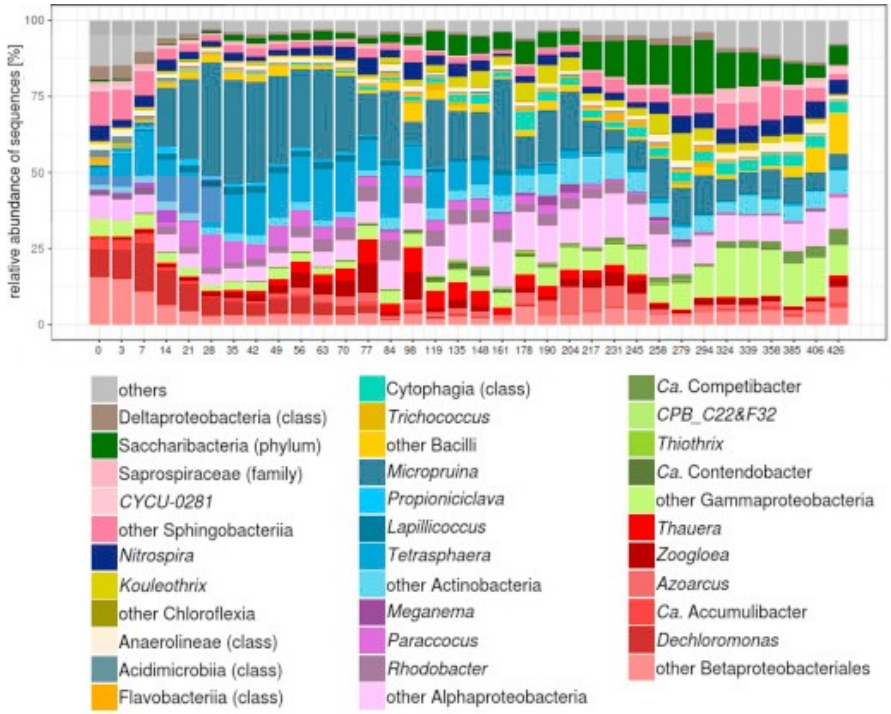

Supplementary Figure 3.4: **AGS-EBPR bacterial communities composition from inoculation to stable state.** Adapted from Layer et al., 2019.
The most abundant taxa are shown in colors depending on their class. One exception is the order of the *Betaproteobacteriales* (colored in red) that has recently been included in the class of the *Gammaproteobacteria* (Parks et al., 2018). The other taxa of the latter class are colored in green.

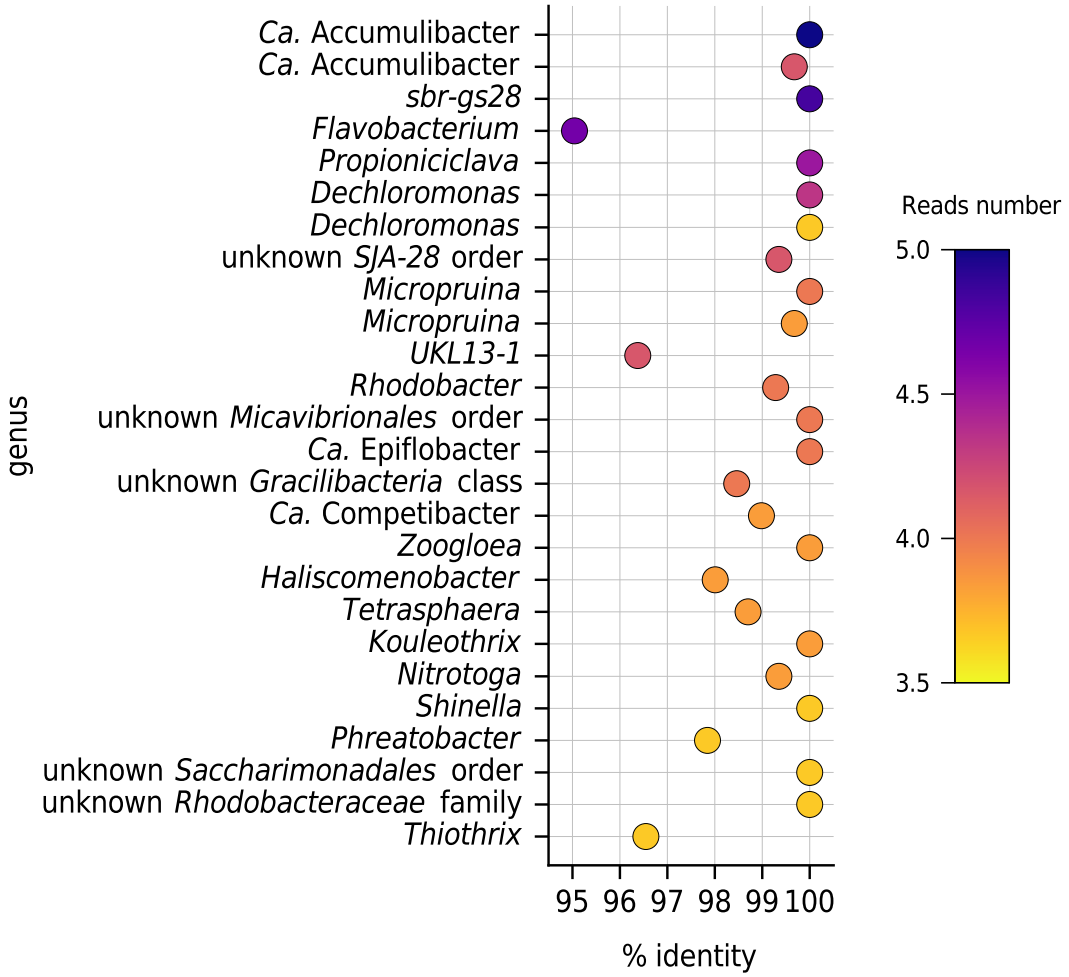

Supplementary Figure 3.5: **Visualization of the percentage of identity of the OTU affiliation to the MiDAS database (version 3.6)**
The coverage for all OTUs shown here is 100%.

Supplementary Figure 3.6: **Primers used for the amplicon sequencing**

	Forward primer	Reverse primer	Amplicon size in *E. coli* K-12
MiDAS	AGAGTTTGATCCTGGCTCAG	ATTACCGCGGCTGCTGG	526 bp
Used in this study	AGMGTTYGATYMTGGCTCAG	GCTGCCTCCCGTAGGAGT	347 bp

The primers used in this study were initially selected to analyze the mouse gut microbiome by Zaiss *et al.* Zaiss et al., 2015.

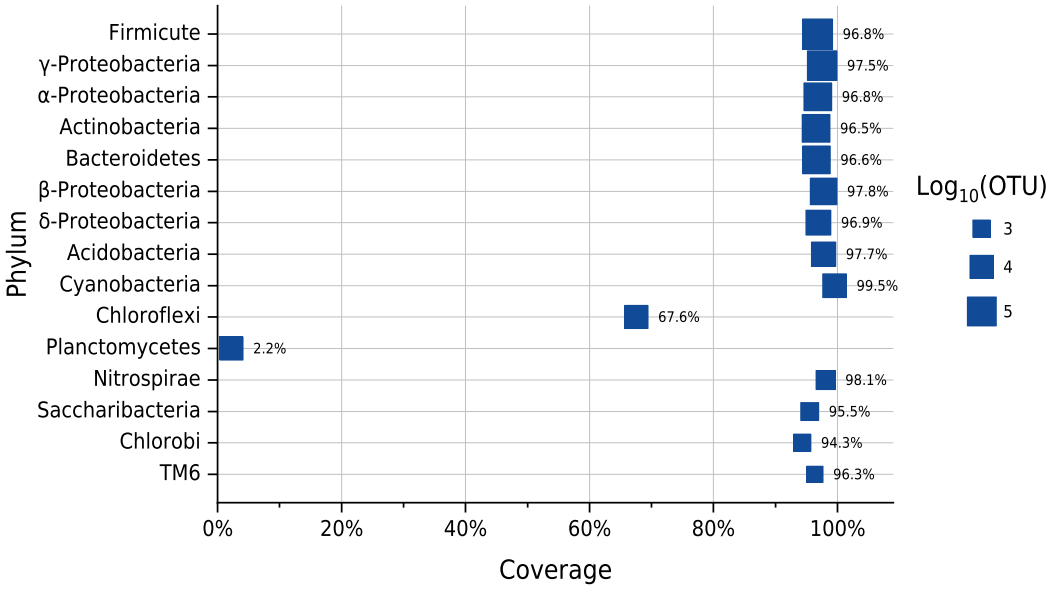

Supplementary Figure 3.7: **Coverage of the MiDAS database (version 3.6) with amplicon sequencing primers**.
The symbols' height represents the number of OTUs on a logarithmic scale.

4 Investigation of the AGS metabolic network using ^{13}C-enriched substrates

Author Contributions:
The conceptualization, methodology, and writing the original draft of this chapter were performed by Arnaud Gelb with the supervision of Christof Holliger.
The other individual contributions are listed below:
- Funding acquisition: Christof Holliger, Nicolas Derlon, and Eberhard Morgenroth.
- Investigation: Emmanuelle Rohrbach and Xenia Bender (16S rRNA gene sequencing library).
- Methodology: Stephanie A. Eichorst and Dagmar Woebken (DNA-SIP)
- Resources: "Genomics Technologies Facility" led by Julien Marquis at UNIL Lausanne (amplicon sequencing reads).
- Writing review: Julien Maillard and Laetitia Cardona.

4.1 Introduction

The lab-scale Sequencing Batch Reactor (SBR) presented in Chapter 2 is operated with Aerobic Granular Sludge (AGS) fed with an influent containing acetate and glucose as organic carbon sources. This lab-scale AGS bioreactor performs biological phosphorus removal from wastewater with the Enhanced Biological Phosphorus Removal (EBPR) process. This chapter aims to identify the subsets of microorganisms in the microbial community using these two carbon sources by Stable Isotope Probing (SIP). In addition, the overall goal was to identify secondary consumers feeding on the metabolites formed by the primary acetate and glucose consumers.
The SIP methodologies investigate microbial communities *in situ* using molecules enriched in heavy isotopes. Once the carbon of molecules containing the heavy isotopes is incorporated into the cells, various biomarkers (lipids, proteins, RNA, DNA) can be targeted, providing different levels of information. The DNA-SIP and RNA-SIP inform on the phylogenetic identity of the microorganisms. Using omics approaches, the DNA-SIP can reveal the microbial metabolic potential and the RNA-SIP the gene expression. The Protein-SIP and the Metabolite-SIP (including the Lipid-SIP) offer a limited phylogenetic identification but require a smaller isotope labeling than Nucleic acid-SIP. Using omics approaches, the Protein-SIP can provide insights into the micro-

bial activities and the Metabolite-SIP the metabolic fluxes.
This chapter aimed to phylogenetically identify the microorganisms consuming the labeled carbon substrates; therefore, the heavy isotope incorporation into nucleic acids was followed. Nucleic acid-SIP identifies microorganisms assimilating the isotopically labeled molecule into their DNA by measuring the difference in buoyant density of isotopically labeled nucleic acids ("heavy") relative to unlabeled nucleic acids ("light"). A DNA molecule with all the carbon positions substituted with ^{13}C will have an increased buoyant density of around 0.036 g/mL (Birnie and Rickwood, 1978). However, with a complex environmental community, it is unlikely to obtain a complete separation of labeled and unlabeled DNA. First, the incubation time with the labeled molecule must be sufficient to label all the cells of the assimilating population(s). Moreover, often other endogenous unlabeled substrates are simultaneously assimilated. In addition, the buoyancy of double-stranded DNA depends not only on its mass but also on its hydration state determined by the GC-content. GC-content variation within a single genome and between microbial genomes can produce buoyant density variation in the unlabeled DNA fragments of up to 0.03 g/mL and 0.05 g/mL, respectively (Youngblut and Buckley, 2014). Consequently, DNA should have incorporated a heavy isotope for at least 30% of its carbon atoms to be differentiated from unlabeled DNA (Jehmlich et al., 2008), and the buoyant density distributions of the labeled DNA should be carefully compared with an unlabeled control (Pepe-Ranney et al., 2016).
The growth of the microorganisms in the AGS-EBPR studied can be autotrophic or heterotrophic. The autotrophic organisms grow with CO_2 as a carbon source; the heterotrophic organisms use the organic carbon present in the artificial wastewater (acetate and/or glucose) or the organic products formed by the microbial community for their growth and for the extracellular polymeric substances (EPS) production. The microbial community supported by the artificial wastewater is more diverse than expected and suggests many microbial interactions. This coexistence of different organisms might be explained by a carbon food chain involving primary consumer(s) of the carbon source and cross-feeding interactions. In the work of Weissbrodt et al., 2014, it is hypothesized that some organisms produce cell and biofilm using the nutrients in the wastewater and that other microorganisms consume these molecules for growth. In Figure 4.1, predominant bacterial populations detected in an AGS-EBPR bioreactor have been represented according to their predicted metabolisms indicating which ones have the role of primary consumers of acetate and propionate and which ones function as secondary consumers.

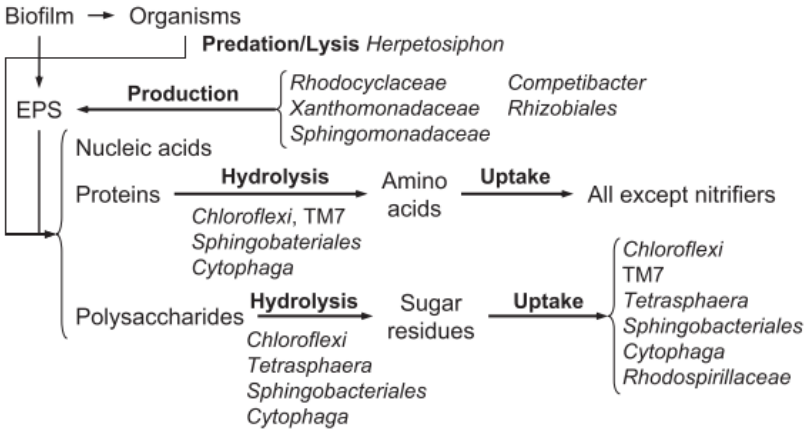

Figure 4.1: **Biofilm components (bacteria and EPS) as a source of nutrients for other bacteria not consuming VFAs during the anaerobic phase**
Adapted from Weissbrodt et al., 2014
Bacterial processes are displayed with thick arrows.
Legend: Extracellular polymeric substances (EPS)

In general, with DNA-SIP, a compromise must be defined between the amount of DNA labeling and the incubation time with the isotopically labeled carbon source to mitigate the labeling through nutrient transfer between cells. The trophic interactions between microbial community members cause cross-feeding. The externalized and transferred organic compounds that support a carbon food chain are diverse (e.g., metabolic waste products, biofilm matrix, cofactors) and shape different cross-feeding relationships. In the lab-scale bioreactor used here, acetate and glucose are replaced by ^{13}C-acetate and ^{13}C-glucose to identify the subsets of microorganisms in the microbial community using these carbon sources and the microorganisms sustained by cross-feeding interactions.

4.2 Material and methods

4.2.1 Sample preparation

The sampling for the DNA extraction and the PHA analysis was done using 15 mL of mixed sludge sampled at the middle height of the 0.4 L bioreactor, 5 min after the beginning of the aerobic phase of the SBR cycle. The samples were homogenized mechanically with an ice-cold Potter-Elvehjem homogenizer and a motor-driven PTFE pestle (pestle clearance 150-250 µm, three passages at 350 rpm). Two 0.75 mL aliquots of the homogenized AGS were flash-frozen in liquid nitrogen and stored at -80°C for three months to be later used for the DNA extraction. The volume of homogenized AGS left was flash-frozen in liquid nitrogen and stored at -80°C for one week to be later used for the PHA analysis.

4.2.2 DNA extraction and purification

Samples of 200 µL of homogenized AGS were enzymatically lysed with the addition of a 500 µL lysozyme solution (5 mg/mL lysozyme, 8 mM Tris-HCl pH 7.5, 0.08 mM EDTA) for 1 h at 37°C. Then the sample was further processed with the commercial kit Maxwell® 16 Tissue DNA Purification Kit to perform additional chemical lysis and DNA purification. The purified DNA was eluted in 300 µL of elution Buffer (10 mM Tris-HCl pH 7.5, 0.1 mM EDTA) and quantified by measuring the absorbance at 260 nm (NanoDrop, model: ND1000).

4.2.3 Amplicon sequencing

The protocol used was the same as the one described in Chapter 3.

4.2.4 PHA analysis

Sampling

The sampling from the bioreactor and the sample homogenization was performed as described above at the desired time points. Then, the supernatant was discarded after centrifugation (5 min at 8’000 RCF, 4°C), and the biomass pellet was flash-frozen in liquid nitrogen and stored at -20°C until the end of the sampling (3 weeks duration). Upon complete sample collection of the time series, the samples were lyophilized (Beta 2-8 LDplus, Martin Christ), homogenized manually with 2 mm glass beads, and stored at -20°C for one month.

Sample treatment

The protocol used is based on Oehmen, Keller-Lehmann, et al., 2005. Aliquots of 20 mg of lyophilized sludge and 0.4 mg of sodium benzoate (109169, Sigma-Aldrich), used as internal standard, were added to a solution composed of 2 mL of chloroform

(102445, Merck), 1.94 mL of methanol (A454SK-4, Fisher Scientific), and 60 µL of sulfuric acid (424520025, Acros Organics). The samples were digested in tightly sealed 11 mL glass vials with PTFE lined screw caps (982616, PYREX™) for 20 h at 100°C and cooled to room temperature. Distilled water (1 mL) was then added and mixed vigorously for 30 sec to separate the particulate debris from the chloroform phase. After the phase separation, the aqueous phase (top) was discarded. 1 mL of the chloroform phase was then diluted five times in chloroform in another vial. This diluted solution is initially turbid and turns clear over time. A volume of 200 µL of the dilution in chloroform was then transferred to another vial containing 800 µL of hexane and 500 mg of anhydrous sodium sulfate (used to capture water). The GC-MS analysis was done within the same day because degradation of the sample PHA monomers signals was observed over time.

Analysis of extracted PHA monomers with GC-MS

A Thermo Scientific™ TRACE™ 1310 Gas Chromatograph with auto-injector was operated with the Xcalibur™ software. Before each sample injection, three pre-washes and one rinsing step with the sample were performed. After the injection of 3 µL of the sample, five post-washes were performed. The separation column was a Zebron™ ZB-XLB (7FD-G019-08) with a coating thickness of 0.18 µm, an internal diameter of 0.18 mm, and a length of 20 m. The injection was performed in splitless mode with 30 mL/min of Helium 99.9999% as a carrier gas, a purge flow of 5 mL/min, and a pressure of 0.72 psi. The injector temperature was at 250°C, the oven temperature was set to 50°C for 2 min followed by an increase to 120°C at 10°C/min, and then to 270°C at 45°C/min to finish with a hold for 3 min. The mass spectrometer was a Thermo Scientific™ ISQ operated with the TraceFinder™ software to analyze the compounds separated by the GC. The ionization mode was EI with a positive-ion analysis, a vacuum pressure of 50 mTorr, and a source temperature of 250°C. The mass analyzer was a single quadrupole with acquisition mode SIM or scan. For the SIM mode, the dwell time was 0.1 sec; for the scan mode, the m/z scan range was 50-650 amu with a 0.404 sec scan interval. The standard curves were done using different solutions with different concentrations of 3-hydroxybutyrate (3-HB) and 3-hydroxyvalerate (3-HV) (403121, Sigma-Aldrich). The ^{13}C incorporation in 3-HB and 3-HV was measured with the 74.15 mass signal shift of a two carbon fragment. The negative control was obtained using a PHA extraction on a *Escherichia coli* strain BL21 cells sampled during the exponential growth phase in LB medium (10 g/L tryptone (211705, Gibco), 5 g/L yeast extract (212750, Gibco), 5 g/L NaCl (S7653, Sigma-Aldrich)). The compound used for m/z calibration was perfluorotributylamine (3132-2-04, SynQuest Laboratories) with a mass resolution of 0.5.

4.2.5 DNA-SIP

The DNA-SIP protocol used followed the procedure described by Dunford and Neufeld, 2010 with the following modification:

Sample Incubation

The influent used for the ^{13}C stable isotope labeling is the same as the regular influent described in Chapter 2, but with fully ^{13}C labeled acetate or glucose.
A 400 mL volume of the AGS of the lab-scale AGS-EBPR was transferred in a smaller lab-scale AGS-EBPR operated under the same conditions to perform the labeling with a reasonable amount of stable isotope.
The labeling strategy used was to feed the 400 mL lab-scale bioreactor for 4 days with an influent containing acetate-^{13}C2 (99%) or D-glucose-^{13}C6 (99%) (all the carbon positions containing ^{13}C) (Cambridge Isotope Laboratories). The labeled sample analyzed was sampled after 30 and 24 SBR cycles for the ^{13}C-acetate and ^{13}C-glucose labeling, respectively. After this pulse of feeding with a ^{13}C carbon source, the AGS-EBPR was fed with the regular influent without ^{13}C enriched substrate. This incubation time is short compared to the growth rate of the microorganisms studied. For this reason, all the buoyant density fractions were analyzed with 16S rRNA gene amplicon sequencing to resolve the heavy isotope incorporation in the labeled sample compared to the unlabeled control. The unlabeled control was obtained before the incubation with the ^{13}C carbon sources.

Ultracentrifugation

A total of 6 µg of DNA were combined with a buffer (10 mM Tris-HCl, 1 mM EDTA, pH 8) to obtain a final volume of 2.8 mL, which was added in 11.5 mL of 7.163 M CsCl to get a final density of 1.725 g/mL. The gradient was generated in 13.5 mL ultracentrifuge tubes (342413, Beckman Coulter) using ultracentrifugation at 177’000 RCF(av) in a vertical rotor (362755, Beckman Coulter) at 20°C for 40 h and deceleration without brake. Immediately upon completion of the ultracentrifugation, the gradient was fractionated in 500 µL fractions using a syringe pump (1 mL/min). Every fraction’s density was measured with a digital refractometer (Reichert AR200).

Fraction Characterization

After DNA recovery from the CsCl fraction through precipitation, the samples with a buoyant density ranging from 1.780 to 1.692 g/mL were analyzed by 16S rRNA gene amplicon sequencing. The relative microbial compositions of the samples before fractionation were used to select the OTUs with 0.5% of relative abundance in at least one sample. The heavy isotope incorporation by OTUs is measured by quantifying in the different density fractions the total DNA concentration by qPCR and the relative abundance of the OTUs by 16S rRNA gene amplicon sequencing. Then by using a linear interpolation of the values of the relative abundances of the OTUs normalized by the DNA concentrations across the buoyant gradient density range, the difference in the buoyant density between the isotopically labeled samples and unlabeled controls is calculated as suggested by (Hungate et al., 2015) using:
$\sum_i^n x_i m_{lab} - \sum_i^n x_i m_{unlab}$
Where x_i is the density of the gradient with i increments of 0.001 g/ml. And m_{lab} and m_{unlab} are the normalized OTU abundance of the labeled and unlabeled samples, respectively.

DNA quantification of the density fractions

The DNA recovered from the different CsCl fractions was compared to DNA concentration standards using qPCR with the primers 338f (ACTCCTACGGGAGGCAGCAG) (Jossi et al., 2006) and 518r (ATTACCGCGGCTGCTGG) (Muyzer et al., 1993). The PCR amplification was performed after a denaturation step at 95°C for 5 min, using 40 cycles (95°C for 30 sec, 62°C for 30 sec, and 72°C for 30 sec) on a thermocycler (MIC, Bio Molecular Systems). A standard curve was run in duplicate, and all samples were run in triplicate.

4.2.6 Nucleoside analysis

Nucleic acid digestion

Single nucleosides from DNA or RNA were generated using a commercial mixture of enzymes (M0649S, New England Biolabs) to digest 1 µg of the total nucleic acids obtained at different time points of the pulse-chase with the ^{13}C substrates.

LC-MS instrument description

The Agilent LC-MS 6530 QTOF liquid chromatography and mass spectrometer has an auto-injector at 4°C and a separation column Acquity Premier HSST3 2.1x100 mm (Waters) at 45°C. Nucleoside standards were used at 10 µM, and the samples from the nucleic acid digestion were diluted 1:1 in an aqueous 0.15% Formic Acid (v/v) before LCMS injection. 2 µL of samples were injected at a flow of 0.4 mL/min using as mobile phase A composed of 0.1% Formic Acid (v/v) in water, and B consisting of 0.1% Formic Acid (v/v) in acetonitrile. The gradient was formed using 1% B for 0.5 min, 1 to 30% B in 2.5 min, 30 to 95% B in 0.5 min, 95% B for 0.3 min, and 1% B for 0.2 min. The ionization mode is ESI with a positive-ion polarity, a fragmentor at 120V, and an MS full scan of 100-1000 m/z.

4.3 Results and discussion

When the excess sludge is removed selectively, AGS-EBPR commonly has biofilm aggregates of different sizes and settling speeds experiencing different Sludge Retention Times (SRTs) Ali et al., 2019. The operation of the AGS-EBPR studied here aimed to obtain an average SRT of 20 days, forming homogeneous biofilm aggregate with a non-selective excess sludge removal and a negligible biomass concentration in the treated effluent. Assuming that the microbial community is in a steady state, all the microorganisms have an average imposed generation time of 20 days. As DNA synthesis depends on cell replication, incorporating stable isotopes in the DNA is linked to the sludge age. Tests have been made to shorten the sludge age and obtain a faster isotope labeling of the DNA. However, shortening the sludge age led to the loss of the wastewater treatment performance using the microbial community and the operation condition of this lab-scale bioreactor. Therefore, the sludge age was kept at 20 days. To test if, with the growth dynamic of the AGS-EBPR bioreactor here tested, the turnover rate of RNA compared to DNA is leading to a faster and higher ^{13}C labeling, the ^{13}C incorporation in the nucleosides was measured at different time points during the labeling with ^{13}C-glucose (Figure 4.2). The ^{13}C-labeling kinetics of DNA and RNA are similar in this experimental setup. RNA-SIP can provide valuable transcriptomic data of the genes expressed by the microorganisms assimilating the labeled substrate. This chapter aims to use a biomarker to identify organisms consuming the labeled carbon source and cross-feeding interactions; therefore, DNA was used as a biomarker because less complex to analyze compared to RNA (no reverse transcription step).

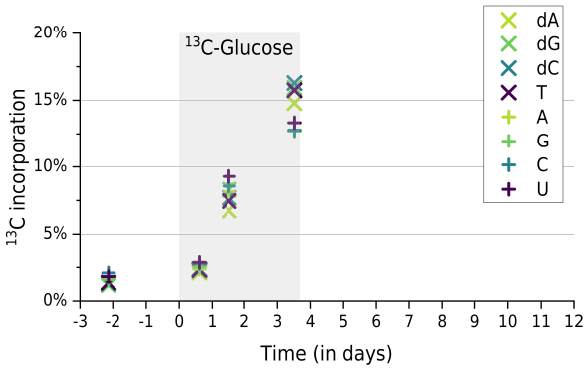

Figure 4.2: **Nucleosides labeling with ^{13}C-glucose**
^{13}C incorporation with ^{13}C-glucose labeling in dA, dG, dC, and T DNA nucleosides and A, G, C, and U RNA nucleosides.

Because the relative abundance of the microorganisms of a microbial community is affected by stochastic processes, the composition of the microbial community was controlled to ensure that a comparison between labeled and unlabeled samples was appropriate (Figure 4.3).
The incorporation of the ^{13}C labeling in the polyhydroxyalkanoates (PHA) monomers 3-hydroxybutyrate (3-HB) and 3-hydroxyvalerate (3-HV) was followed (Figure 4.4) to assess if Polyphosphate-Accumulating Organisms (PAOs) or Glycogen-Accumulating Organisms (GAOs) used the acetate and/or glucose to form PHA.

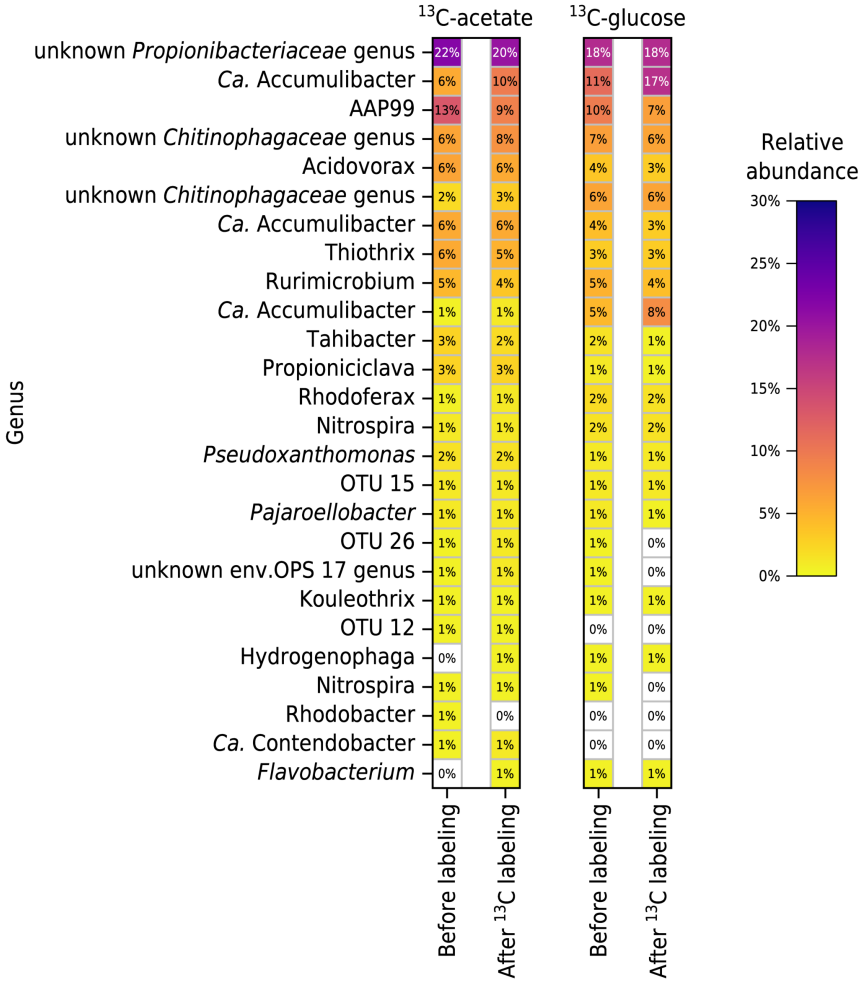

Figure 4.3: **Assessment of the microbial community before and after the DNA-SIP**
Relative abundance of the OTUs compared to the sample's total number of pre-processed reads.
The left panel presents the microbial composition before and after the ^{13}C-acetate labeling.
The right panel presents the microbial composition before and after the ^{13}C-glucose labeling.
The OTUs analyzed had an abundance of at least 0.5% of the total number of pre-processed reads in one of the samples. The color scale displays the relative abundance; the table cells in white were below 0.5%.

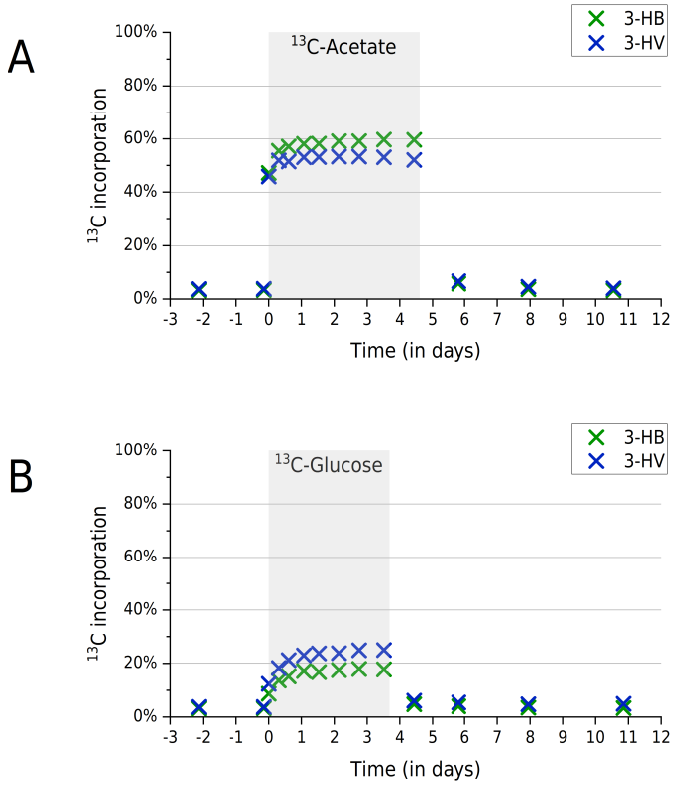

Figure 4.4: **^{13}C incorporation in PHA monomers]**
The pulse of labeling with the ^{13}C substrate is represented with the gray bar.
A: ^{13}C incorporation with ^{13}C-acetate labeling in the 3-HB and 3-HV PHA monomers
B: ^{13}C incorporation with ^{13}C-glucose labeling in the 3-HB and 3-HV PHA monomers

With ^{13}C-acetate, the formation of labeled PHA is observed from the first SBR cycle. The ^{13}C labeling in the PHA is plateauing after one day at around 50% of labeling in the PHA monomer measured. Approximately 40% of the monomers remain unlabeled at all the carbon positions (Figure 4.5). When the influent containing the labeled acetate is switched to the regular influent, the ^{13}C labeling in the PHA returns to ^{13}C incorporation values similar to those measured before labeling.
With ^{13}C-glucose, the observed trend is similar but with a lower ^{13}C labeling in the PHA (20%) and a higher proportion of monomers remaining unlabeled (70-80%) (Figure 4.5).
The incorporation of the ^{13}C labeling into PHA from the first SBR cycle suggests that acetate and glucose are directly used to form PHA by some microbial community members. The lower PHA labeling obtained with glucose compared to acetate indicates that a proportion of glucose is not used for the PHA formation in this AGS-EBPR. The ^{13}C labeling of the PHA is not reaching here 100% of the carbon positions of the monomers measured. This observation could be explained by a complete consumption of the PHA formed anaerobically during the aerobic phase. Another explanation is that some of the PHA monomers studied are not formed exclusively using acetate or glucose; for example, CO_2 can be incorporated by carboxylation (Erb, 2011). It should be noted that the use of substrates labeled with heavy isotopes might negatively affect the physiology and the PHA formation by the microorganisms due to

the "kinetic isotope effect" (Xie and Zubarev, 2015). Heavy isotopes form stronger molecular bonds slowing down the chemical reaction rate, which can interfere with metabolic fluxes and negatively impact growth (Millard et al., 2015, Filiou et al., 2012).

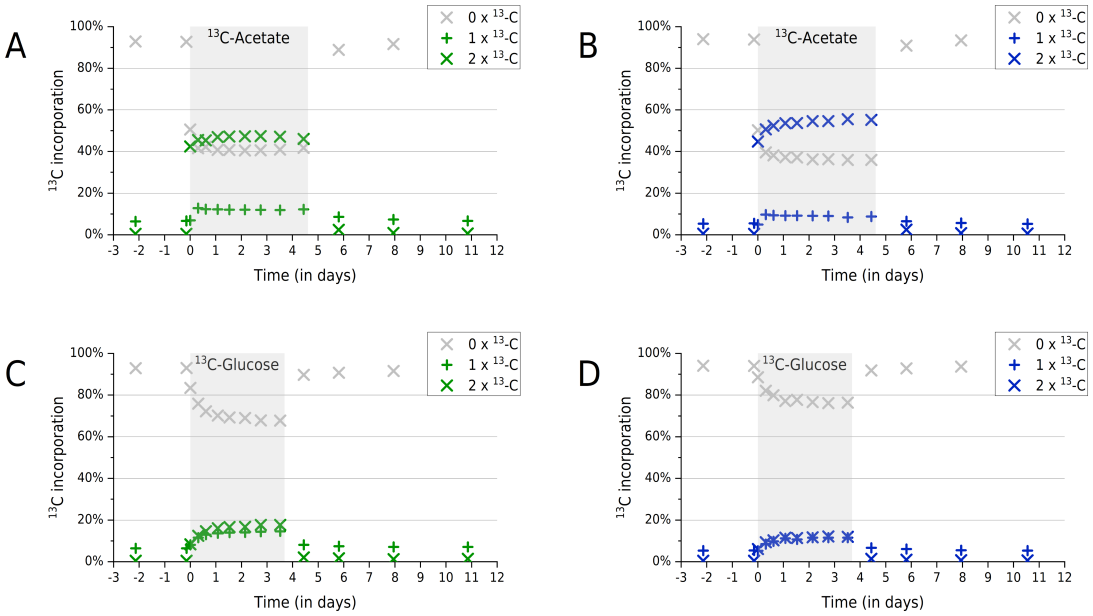

Figure 4.5: **^{13}C incorporation in PHA monomers**
The labeling of different carbon positions of the 3-HV and 3-HB PHA monomers is here analyzed by mass spectrometry with a molecule containing two carbons.
The legend indicates 0x13C for no ^{13}C substitution, 1x13C for one ^{13}C substitution, and 2x13C for two ^{13}C substitutions.
The pulse of labeling with the ^{13}C substrate is represented with the gray bar.
A: ^{13}C incorporation with ^{13}C-acetate labeling in the different carbon of the 3-HV PHA monomers
B: ^{13}C incorporation with ^{13}C-acetate labeling in the different carbon of the 3-HB PHA monomers
C: ^{13}C incorporation with ^{13}C-glucose labeling in the different carbon of the 3-HV PHA monomers
D: ^{13}C incorporation with ^{13}C-glucose labeling in the different carbon of the 3-HB PHA monomers

The DNA-SIP results presented in Figure 4.6 quantify the ^{13}C incorporation into DNA from the labeled organic carbon source of the influent in different groups of microorganisms. The calculated density shift compares the normalized distribution of the OTUs' DNA in the density gradient. As an example, the DNA density distribution of the unknown *Propionibacteriaceae* genus and *Ca.* Accumulibacter are presented before and after ^{13}C-acetate labeling in Figure 4.7.
The results show two different subgroups of microorganisms labeled with ^{13}C-acetate or ^{13}C-glucose except for two low abundance OTU belonging to the *Ca.* Accumulibacter and *Pajaroellobacter* genera labeled with both organic carbon sources.
The two most abundant genera in the sequencing reads of the subgroup labeled by ^{13}C-acetate are *Ca.* Accumulibacter and *Acidovorax*.

For the subgroup labeled by ^{13}C-glucose, the two most abundant genera in the sequencing reads are an unknown *Propionibacteriaceae* genus and *Sediminibacterium*. In the subgroup labeled by ^{13}C-acetate, it is not surprising to see organisms belonging to the genus *Ca.* Accumulibacter, known to have PAO metabolism using acetate. On the other hand, microorganisms belonging to the genus *Acidovorax* have not yet been described as belonging to PAOs or GAOs. Therefore *Acidovorax* might cross-feed on *Ca.* Accumulibacter metabolites. Interestingly, it has been shown that bacteria belonging to the genus *Acidovorax* can degrade PHA (Vigneswari et al., 2015).
In the experimental condition used here, microorganisms belonging to the *Nitrospira* genus are labeled with ^{13}C-acetate. If those bacteria can consume acetate, this would confirm that this group of microorganisms is not composed uniquely of strict autotrophs (Bayer et al., 2021).
Microorganisms belonging to the *Sediminibacterium* genus, the *Tahibacter* genus, and the *Pajaroellobacter* genus have not yet been described as belonging to PAOs or GAOs; therefore, in those conditions, they are most probably consuming glucose with fermentative metabolism. In Adler, 2019 and Layer et al., 2019, the fermentative bacteria *Propioniciclava* and *Propionicimonas* belonging to the family of *Propionibacteriaceae*, known to ferment glucose into propionate (L. Zhang et al., 2017, J. L. Nielsen et al., 2012) were shown to be abundant in AGS-EBPR bioreactors treating municipal wastewater and artificial wastewater containing glucose. If the *Propionibacteriaceae* unknown genus in this bioreactor can also ferment glucose into propionate, the propionate could be used for the PHA synthesis; this would explain the formation of ^{13}C-PHA with ^{13}C-glucose (Figure 4.4). Because some of the glucose is consumed anaerobically to form intracellular PHA (Figure 4.4), some *Ca.* Accumulibacter might be able to use this carbon source to produce PHA. *Ca.* Accumulibacter and *Pajaroellobacter* are the only genus detected here with a relative abundance >1% also present in the EBPR sampled in the "MiDAS field guide" at a percentage of read abundance >1% (Nierychlo et al., 2020). This difference in the relative abundance of the microbial community members in lab-scale AGS-EBPR compared to full-scale wastewater treatment plants is likely due to the different operation conditions.

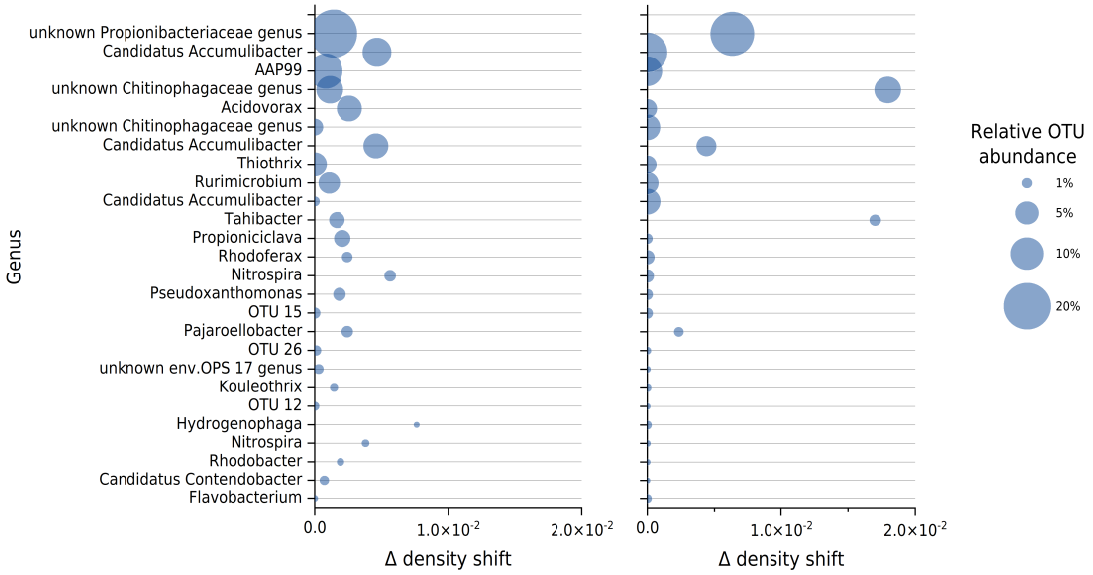

Figure 4.6: **^{13}C incorporation in the DNA of the microbial community**
The ^{13}C relative incorporation is visualized at the genus level for ^{13}C-acetate (left panel) and ^{13}C-glucose (right panel).
The corresponding relative abundance of the OTU in the pre-procced sequencing reads before and after the ^{13}C labeling pulse chase is represented in Figure 4.3.

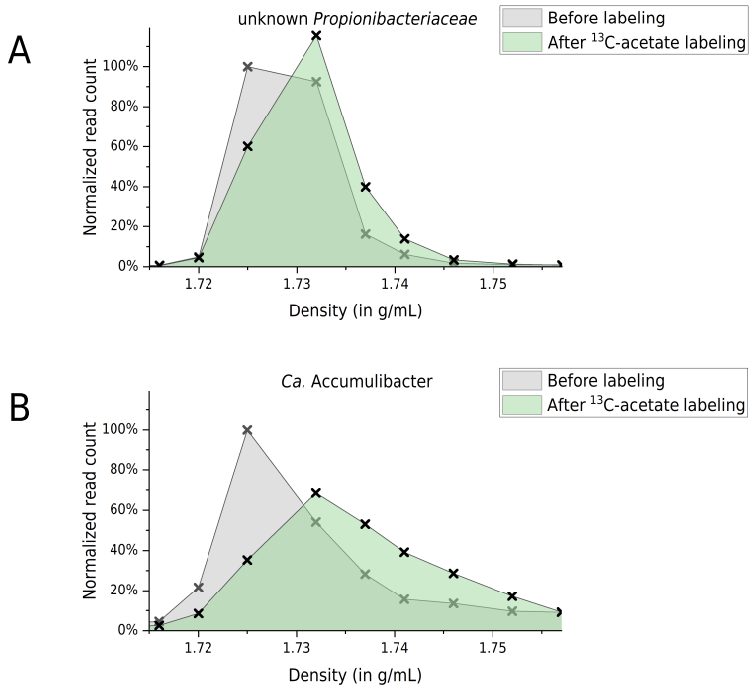

Figure 4.7: **DNA-SIP profiles of an unknown *Propionibacteriaceae* genus and *Ca.* Accumulibacter**
The normalized 16S rRNA gene reads of an unknown *Propionibacteriaceae* genus (panel A) and *Ca.* Accumulibacter (panel B) are shown distributed in the density gradient before and after ^{13}C-acetate labeling.

4.4 General conclusions and perspectives

Using two ^{13}C labeled carbon sources enabled the examination of the sub-groups of microorganisms sustained by those substrates. DNA-SIP experiments are costly and technically difficult; therefore, it is not practical to perform replicates. Fortunately, the buoyant density behavior of DNA fragments in CsCl gradients is highly reproducible (Meselson et al., 1957, Birnie and Rickwood, 1978). It revealed that acetate was used by PAOs belonging to the genus *Ca.* Accumulibacter. This finding is supported by the measure of significant ^{13}C PHA labeling when ^{13}C-acetate was added to the influent. On the other hand, compared with acetate, glucose leads to less significant ^{13}C labeling of the PHA, probably because this substrate is also consumed anaerobically by microorganisms not producing PHA in the conditions used here.

The results presented here reveal that different OTUs can consume acetate and/or glucose (*Sediminibacterium*, *Acidovorax*, *Sediminibacterium*, *Tahibacter*, and *Pajaroellobacter*). As those genera were not identified in Chapter 3 as PAO, they likely have a GAO phenotype in those conditions or feed on the organic compounds produced by the primary consumers of the carbon sources provided in the influent. The *Propionibacteriaceae* unknown genus was found in the polyP positive cell fraction at low abundance (Chapter 3), suggesting that part of this microbial population accumulates polyP in this AGS-EBPR bioreactor. Because this microbial group is labeled with ^{13}C-glucose and, to a lower extent with ^{13}C-acetate, it is a candidate for a not yet identified fermentative PAO.

To confirm the direct uptake of a carbon source (e.g., glucose) by PAOs, NanoSIMS measurement of the ratio ^{13}/^{12}C and ^{31}P/^{16}O could be done at the single-cell level.

The experimental conditions used here were not ideal for revealing a carbon food chain between primary consumers producing organic compounds used as a carbon source by other microbial community members. Nevertheless, because not all the microbial community members are labeled with the pulses of the ^{13}C-carbon sources, it suggests that the unlabeled heterotrophic microorganisms benefit from trophic interactions between the members of the microbial community.

5 Localization of polyphosphate-containing cells in the granular biofilm

Author Contributions:
The conceptualization, methodology, and writing the original draft of this chapter were performed by Arnaud Gelb with the supervision of Christof Holliger.
The other individual contributions are listed below:
- Formal analysis: Karen Gemayel (image processing).
- Funding acquisition: Christof Holliger, Nicolas Derlon, and Eberhard Morgenroth.
- Investigation: Benita Putlitz (X-ray micro-computed tomography).
- Resources: Olivier Burri, Romain Guiet, and José Artacho (microscopy). Karen Gemayel and Roland Dupuis (3D printing).
- Software: Olivier Burri (image processing).
- Writing review: Julien Maillard and Laetitia Cardona.

5.1 Introduction

Biofilms are the dominant form of microbial life in the environment. Biofilms are composed of microorganisms living in a matrix of extracellular polymeric substances (EPS) comprised of polysaccharides, proteins, lipids, and nucleic acids (Flemming and Wingender, 2010, Sutherland, 2001). Initially, biofilms were pictured as a homogeneous distribution of cells in a uniform exopolysaccharide matrix (Bakke and Olsson, 1986). The application of optical imaging techniques has demonstrated that mono- and multi-species biofilms have a variable distribution of cells and variable density of extracellular polymers, together with void spaces or water channels (Costerton et al., 1995, Wimpenny et al., 2000). The classic structural unit of the biofilm is the microcolony. It is presumed that the growth as microcolonies provides an ideal environment for the creation of gradients, exchange of genes, and quorum sensing (Shapiro, 1998).
Aerobic Granular Sludge (AGS) are quasi-spherical biofilm aggregates (X.-W. Liu et al., 2009). It is suggested that the aerobic granules are formed either by the aggregation of different microcolonies or by microcolony outgrowth into a dense biofilm aggregate (Barr et al., 2010); AGS formation is likely due to both of those mechanisms. Biofilm formation and colonization are extensively studied using defined mixed cultures in the

field of social microbiology (Mitri and Foster, 2013, Paula et al., 2020). Lemaire et al., 2008 have observed that the microcolonies in AGS present cauliflower-like outgrowths and voids connecting the interior to the outside of the biofilm aggregate. Gonzalez-Gil and Holliger, 2014 have further demonstrated a granule porosity of 35 to 40% at the center of the biofilm aggregate created by channels allowing for the growth of dense microcolonies also in the inner part of the biofilm. Contradicting observations were made by Winkler, Kleerebezem, Strous, et al., 2013, with the microbial cells being present only on the biofilm aggregate surface with an interior consisting mainly of EPS. AGS models commonly assume biofilm aggregates of a round sphere shape with stratification of the metabolic activities and microbial population. Those models are often based on limited data about the granule structure (de Kreuk, Picioreanu, et al., 2007, Su and Yu, 2006, L. Liu et al., 2010). Those simplified models ignore the structure and organization of the bacterial microcolonies, despite their effect on the metabolic activities responsible for wastewater treatment. The spatial organization of granular biofilms is shaped by environmental factors and by the interactions between the microbes of the community, which has a direct link to the biofilm function. The different microbial metabolic activities create nutrient and redox potential gradients across the outer and inner parts of the biofilm. Berg et al., 2020 have estimated the average diffusion coefficient of the penetrated volume to be 70% of the diffusion coefficient in water. Lemaire et al., 2008 hypothesized that a mass transfer limitation of nutrients at the core of a large granule would lead to its disintegration into smaller aggregates. The newly formed granules would then grow as larger ones that would break into smaller aggregates at their turn.

The functional characterization of the AGS microbial community requires understanding the spatial architecture and abundance of the different microorganisms harboring key metabolic activities for wastewater treatment.

This chapter describes the different approaches explored to investigate the microbial architecture in the granular biofilm aggregates of a lab-scale AGS with Enhanced Biological Phosphorus Removal (EBPR) to obtain quantitative experimental data on the 3D structures of aerobic granules. The techniques used include X-ray micro-computed tomography, confocal fluorescence microscopy, and Light-Sheet Fluorescence Microscopy (LSFM). The strength of LSFM in live imaging biological specimens with minimal light exposure was extensively used in the field of developmental biology to study the dynamic biological processes governing the development of multi-cellular organisms at the cellular, tissue, and whole-organism level (Huisken et al., 2004, Keller et al., 2008). LSFM is, at the moment, less commonly used to image microbial communities, but the work of Fuchs et al., 2002 showed how this technique could be used to investigate marine microbes. In 2018, the review article of Parthasarathy, 2018 highlighted recent applications and the potential of LSFM to study microbial systems. This work is, to our knowledge, the first application of Light-Sheet Fluorescence Microscopy (LSFM) on an AGS sample. Some of the structural features observed provided support to the hypotheses made previously by other researchers (Lemaire et al., 2008, Gonzalez-Gil and Holliger, 2014).

5.2 Material and methods

5.2.1 X-ray micro-computed tomography

Individual granular biofilm aggregates were placed into a 0.5 mL tube (0030121503, Eppendorf), fixed with adhesive putty on the rotating plate, and imaged with a 3D X-ray benchtop µCT (SKYSCAN 1173, Bruker) using 6 frames, a step size of 0.2°, and a pixel size of 5 µm. A voltage of 20 kV, a current source of 160 uA, and an exposure time of 5 sec were used for the hydrated biofilm samples. A voltage of 40 kV, a current source of 200 uA, and an exposure time of 1 sec were used for the biofilm soaked in a radiographic contrast medium (VISIPAQUE 320 mg I/mL, GE Healthcare).

5.2.2 PolyP labeling on thin cross-sections

The structural organization of granular biofilms is commonly studied with cross-sections (typically 10 µm) on a fixed sample. Then the slice is stained with dyes to highlight structures of interest and imaged with a widefield or a confocal microscope. As granular biofilms have a stiffness comparable to soft hydrogels, they must be embedded in a matrix before being sectioned on a microtome. Paraffin, a standard embedding matrix, requires dehydration of the sample. As granular biofilms are highly hydrated, the dehydration of the sample causes a significant shrinking of the structure. This shrinking can be avoided using a cryo-microtome and an embedding matrix that hardens with the sample while freezing. Aerobic granules were sampled at the end of the aerobic phase of the lab-scale bioreactor described in Chapter 2 to maximize polyP content. The fixation was performed with a 10 h incubation at 4°C in a 5 mL solution of 2% formaldehyde buffered with 10 mM HEPES, ph 7.4. Sucrose was used as a cryoprotectant by soaking the sample in two successive baths of 15% and 30% sucrose (22090-2500, Acros). The biofilm aggregates were placed individually in support (Tissue-Tek® Cryomold®, Sakura Finetek) and embedded with medium for cryotomy (Tissue-Tek® O.C.T. Compound, Sakura) and flash frozen at -70°C using a bath of isopentane (10542331, Acros) cooled with dry ice. Cross-sections of 10 µm thickness at the innermost of the biofilm aggregates were prepared on a cryostat (CM3050S, Leica) and placed on microscope glass slides. The DAPI staining was performed by covering the slice with 10 µM DAPI (A4099.0005, Applichem) in a 10 mM HEPES (172571000, Acros Organics) solution during a 30 min incubation at RT in the dark, followed by a wash with 10 mM HEPES solution before being mounted with CitiFluor™ AF1 (AF1-25, Electron Microscopy Sciences). The acquisition of the DAPI-stained AGS slices was performed on a Leica SP8 microscope with a 20x/0.75 objective using the following parameters. Laser: 405 nm, intensity: 30%, pinhole: 56.6 µm (1 AU based on a 580 nm emission wavelength), line average: 16 times, pixel dwell time: 0.3 µsec, DAPI-DNA HyD detector: 410 nm-485 nm, gain: 100, DAPI-polyP PMT detector: 486 nm-788 nm, gain: 535, pixel size: 0.3 µm, and 512x512 pixel tiles with a 30% overlap.

5.2.3 Light-Sheet Fluorescence Microscopy analysis

The investigation of the structural organization of granular biofilms with thin cross-sections has the inherent drawback caused by shearing artifacts which can occur during sectioning if the cutting blade encounters a stiffer zone inside the biofilm (e.g., inorganic precipitates). The structural artifacts due to the preparation of thin granules cross-sections can be circumvented using the possibility of fluorescent microscopy to perform optical sectioning. The optical sectioning is performed with confocal microscopes by selecting the fluorescent signal emitted from the focal plane. The fluorescent signal in focus is selected by coupling a point excitation to a point detection through a pinhole. This type of microscope is considered suited for acquiring up to 100 µm of depth. Indeed, more signal is lost at greater depth because the pinhole rejects the scattered fluorescence. For a sample of a millimeter scale, a more appropriate method of optical sectioning is performed by Light-Sheet Fluorescence Microscopy (LSFM, also called Selective plane illumination microscopy). LSFM does not suffer from scattering as much as confocal microscopes, thanks to its planar illumination. With the LSFM, a 2D optical planar section of the sample is formed by the selective illumination of the sample by an excitation laser beam shaped into a thin sheet. The fluorescent signal generated in the illumination plan is collected perpendicularly to the illumination axis (Figure 5.1).

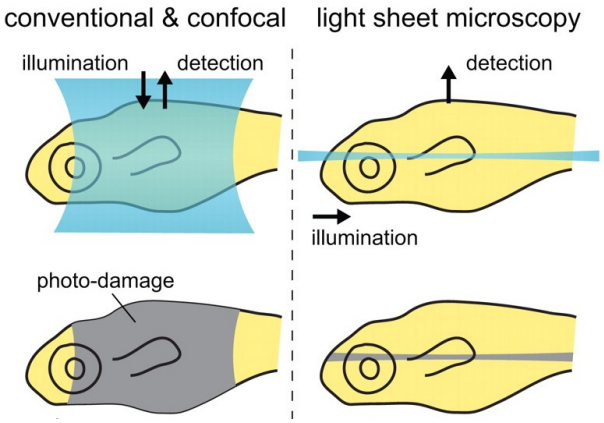

Figure 5.1: **Confocal fluorescence microscopy versus Light-Sheet Fluorescence Microscopy**
Figure from Keller and Stelzer, 2010 comparing the sample illumination and fluorescence detection in confocal microscopy (left) and LSFM (right).
In contrast to confocal microscopy, the selective illumination of LSFM does not inflict photodamage outside the imaged volume.

Additionally, the ability of some LSFM to acquire 3D volume from different angles enables the possibility of acquiring a large sample and reconstructing an isotropic dataset with an improved axial resolution. This fusion of the different stacks of images acquired from different angles requires an appropriate placement and number of reference points (e.g., fluorescent beads).
In LSFM, the higher the image resolution, the smaller the field of view and, consequently, the imaging depth. Therefore, to fully image a large sample at high resolution, multiple tiles are needed, which increases the risk of photo-bleaching.

Another challenge of imaging a large sample with the LSFM is the requirement for the sample to be held without interfering with the light path (e.g., agarose hydrogel). A limitation of LSFM imaging is the requirement to have a nearly transparent sample with low scattering. For this reason, AGS biofilm aggregates containing many inorganic particles and cellulosic fibers, as sometimes present in full-scale AGS-EBPR, are not suited for this imaging technique. Managing and analyzing large quantities of data generated by the LSFM can be complex; some light-sheet microscopes acquire up to 10 TB/h (Chhetri et al., 2015).

LSFM sample preparation

Biological samples are composed of high refractive index (RI) molecules (e.g., lipids, protein) present in a low RI medium (water). This RI mismatch leads to light scattering and causes the opacity of samples of millimeter size, limiting the image acquisition. Several published clearing methods describe protocols to render large biological samples translucent while keeping the internal 3D structure (Chung and Deisseroth, 2013, Rocha et al., 2019). Those methods contain two main groups: organic solvent-based clearing and aqueous-based clearing. They have in common a reduction of the sample opacity by dissolving lipids followed by matching the refraction indexes using a high RI medium. With a fixed granule sample, a satisfactory degree of translucency was obtained with a 1.45 RI Histodenz based solution, reducing the refractive index difference between the sample and the surrounding medium. The AGS was sampled at the end of the aerobic phase of the lab-scale bioreactor described in Chapter 2 to maximize polyP content. The granular biofilm was embedded in agarose (6351.1, Roth) to safely handle the sample throughout the staining process. A 2% (w/v) agarose preparation was melted at 70°C and then cooled above the gelling point at 30°C. The sample was warmed at 30°C and then mixed with one volume of agarose gel. The casting of the 1% (w/v) agarose gel containing the sample was performed into a square capillary (inner dimension 3 mm x 3 mm) with the inner wall per-covered with a layer of 1% (w/v) agarose gel to ease the position of the sample close to the middle. Then the gel was solidified at 4°C in the fridge for 5 min. The excess agarose was trimmed with a razor blade to leave 1 mm of agarose gel above and below the sample. The granule contained in the agarose gel was fixed with a 10 h incubation at 4°C in a 5 mL solution of 2% formaldehyde buffered with 10 mM HEPES, pH 7.4. The labeling was performed with a 10 h incubation at 4°C with 5 mL of 10 µM DAPI in a 10 mM HEPES solution. After a washing step in 10 mM HEPES solution, the stained sample was placed in the same square capillary used previously. Then a mixture of 1 µm fluorescent reference beads (URFP-10-5, Spherotech) mixed with 1% (w/v) agarose gel was added above and under the sample for the later 3D multi-view reconstruction. More agarose gel was added on one side to create an extremity to insert into the adapter (.stl file). Then the sample, casted in agarose gel, was submerged in a 10 mL 71% (w/v) Histodenz (D2158, Sigma-Aldrich) solution (RI= 1.45) at 4°C for 50 h to make the biofilm translucent.

LSFM image Acquisition

The ZEISS Lightsheet Z1 system used here is a three-lens microscope with the sample suspended in front of the detection objective. The illumination of the sample is performed by a laser sheet formed by a pair of opposing illumination lenses located on both sides. This dual illumination balances the attenuation of the excitation light by the sample occurring with the increased distance from the illumination source. Successive images are acquired at increasing depth by moving the sample through the excitation laser sheet to acquire a 3D volume. The multi-view imaging was performed by rotating the sample to acquire a different sample volume or the same volume with a different angle. The rotation prevents image quality degradation when acquiring the sample zone positioned at the greatest depth relative to the detection objective. This zone of the sample, which would have experienced the most absorption and scattering of the emitted fluorescence, is brought closer to the detection objective thanks to the rotation. The best features of the different views are combined thanks to the fusion of different views. When the acquisition volume has a penetration depth of at least half of the sample thinness, the fusion of the 3D datasets improves the axial resolution because it is compensated by the lateral resolution of the different views (Preibisch et al., 2008). The data processing steps used for the fusion of different views were described by Shaw et al., 1989. The initial step is aligning the different views to overlap the features visible in several 3D datasets. Then the fusion combines the different views in one image using the highest resolution information available in each view.
The working distance and the detection objective's magnification define the image's maximum thickness and width (about 5 mm penetration depth and 5 mm width using the 5x/0.16 EC Plan Neofluar, ZEISS). On the other hand, the maximum height is defined by the illumination objective capability to shape a homogeneous illumination (about 2.8 mm for the illumination optics 5x/0.1, ZEISS). As the illumination of the LSFM does not affect the lateral resolution, the resolution capability of the imaging system is dependent on the emission wavelength of the fluorophore and the NA of the detection objective:

$$d_{xy} = \frac{\lambda_{em}}{2 \times NA_{detect}}$$

In this experimental setup, the axial resolution of the detection objective is greater than the light-sheet thickness. Consequently, the axial resolution of the imaging system depends on the light sheet thickness. The illumination objective defines the bow-tie shape along the illumination axis of the laser sheet. The minimum thickness at the center is proportional to $\frac{1}{NA_{ill}}$, while its uniformity along the illumination axis, defining the field of view, is proportional to $\frac{1}{NA_{ill}^2}$. Consequently, the shape of the light sheet compromises between the optical sectioning and the field of view.
The Nyquist-Shannon sampling theorem defines the ideal Sampling density (Whittaker, 1915, Shannon, 1949). Images acquired at a Nyquist rate are sure to exploit the full resolution capability of the microscope. Here the aim was to measure the structures of the microcolonies of several µm; therefore, a concession was made on the resolution using a lateral sampling higher than the Nyquist rate to increase the field of view. For an application requiring a higher resolution, the field of view can be reduced, and the sample can be imaged in different tiles, which are later stitched to form a complete view.

The image acquisition was orthogonal to the four faces of the agarose cuboid. The four views were imaged with 20% overlap. The laser sheet thickness and z-step used were the ones defined by default by the software based on the 0.7x zoom factor. Experimental tests with smaller z-steps on a sample containing beads (URFP-10-5, Spherotech) did not show a significant improvement in the Point Spread Function (PSF) accuracy.

LSFM 3D image reconstruction

The multi-view alignment and fusion were done using the BigStitcher plugin of Fiji (Schindelin et al., 2012, Hörl et al., 2019). A first translation-invariant alignment was refined with an ICP alignment before the fusion of the different views. The details of the used parameters are presented in the following GitHub repository: https://github.com/ArnaudGelb/EPFL.

LSFM 3D image Processing

An initial denoising step is performed on the 3D stack using a Gaussian filter. Then, a "Li dark" auto-threshold is run on the stack to create a mask. The segmentation of the AGS biofilm boundary can be improved using the image's features with the Level-Sets function (Andrew, 2000). This approach was not used here due to the increased computational power required by this method. Empty images are added to both ends of the stacks, and the canvas is increased by 5 pixels in x and y to mitigate edge detection error if the image acquisition cropped the AGS biofilm. The obtained 3D mask is transformed into a Euclidean Distance Map (EDM), attributing to each pixel of the mask a gray value equal to that pixel's distance from the nearest edge. Using the original 3D stack and the 3D EDM, a Groovy script (accessible from the repository: https://github.com/ArnaudGelb/EPFL) was used to save the numerical results into a matrix containing the signal intensity and the distance from the nearest edge for every pixel of the object (Knig et al., 2015). This matrix is then used for data visualization to plot the pixel fluorescent intensity against the distance from the edge with one integer EDM values bins, as proposed by Gemayel, 2019.

5.3 Results and discussion

This study aimed to investigate the microbial architecture in the granular biofilm aggregates of a lab-scale AGS with Enhanced Biological Phosphorus Removal (EBPR), focusing on the "Polyphosphate Accumulating Organisms" (PAOs). The results presented here were obtained by testing different approaches; they all investigate the biofilm structure, revealing complementary findings. First, the macro-scale properties were investigated using X-ray micro-computed tomography; then, the micro-scale architecture was explored using confocal fluorescence microscopy and Light-Sheet Fluorescence Microscopy (LSFM).

5.3.1 Macro-scale properties of aerobic granular biofilm aggregates

The presence of a possible inert core (inorganic precipitates) in the granular biofilm aggregate was investigated by computed tomography imaging to test the proposed model by Winkler, Kleerebezem, Strous, et al., 2013.
The visible macro-scale shape and size of the granular biofilm aggregates were recorded using a digital camera. Figure 5.2 shows a macro-scale view of granular biofilm aggregates formed in the lab-scale AGS-EBPR bioreactor (see Chapter 2) after sieving on a 1 mm mesh size sieve. The majority of the biofilm aggregates have a size below 2 mm due to the low COD load and the turnover imposed by the sludge age of the bioreactor. In this picture, the AGS size fraction below 1 mm is not represented due to their negligible contribution to the overall AGS biomass volume, VSS, and TSS. The observed size distribution of the granular biofilm aggregates formed in this lab-scale AGS-EBPR bioreactor is smaller than other experimental setups (e.g., J.-h. Zhou et al., 2021) due to the use of a different COD load and sludge age.

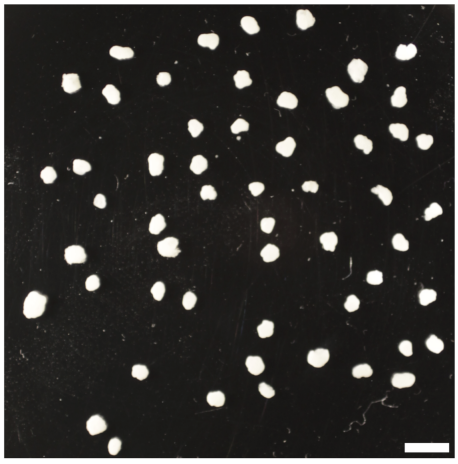

Figure 5.2: **AGS macroscopic properties**
Black and white picture of sieved AGS (> 1 mm) on a Petri dish showing bright AGS on a black background obtained with side illumination and out of focus background, scale bar: 2 mm.

In this lab-scale AGS-EBPR bioreactor, 4 out of the 11 tested biofilm aggregates had inorganic precipitates (Figure 5.3 and Supplementary Figure 5.1). Their presence was diffuse in the EPS matrix rather than forming a compact core. These inorganic precipitates are likely phosphate minerals, as they are commonly formed in EBPR due to the locally high phosphate concentrations caused by the PAOs' phosphate release during the anaerobic feeding phase (Arvin, 1983, Carlsson, 1997, Mañas et al., 2011). The presence of voids and channels in granular biofilm aggregate involved in the transport of substrates and waste products (Ivanov et al., 2005, Zheng and Yu, 2007) was investigated using a radiographic contrast medium for the computed tomography imaging (Figure 5.3D). Denser cell aggregation is observed at the edge of the microcolonies, as previously reported by Weissbrodt et al., 2013b. Biofilms with heterogeneous structures have been related to microbial growth under substrate limitation (Picioreanu et al., 2000, Alpkvist et al., 2006).
The instrument's pixel size was adapted to resolve structures bigger than 25 µm; therefore, it allowed to demonstrate the presence of different zones of the biofilm with different porosity but cannot capture channel-like structures smaller than 25 µm. Sub-micron X-ray computed tomography (Gelb et al., 2009) might be a promising non-destructive technique to visualize the internal 3D structure of granular biofilm aggregates worth exploring in future research.
The observations of granular biofilm aggregates made with X-ray micro-computed tomography show that models representing biofilm aggregates with defined concentric layers Wilén et al., 2018 and an inorganic core free of cells Winkler, Kleerebezem, Strous, et al., 2013 are an oversimplification representation of the granular biofilm aggregates studied here.

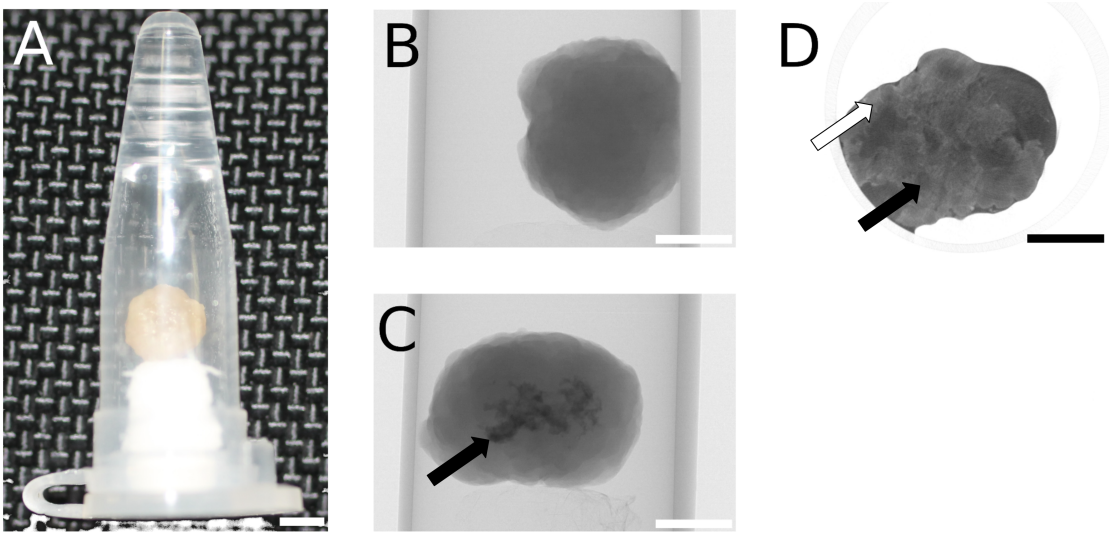

Figure 5.3: **X-ray micro-computed tomography**
(A) Example of the set-up used for the X-ray micro-computed tomography. The water in the tip of the tube maintains the moisture of the biofilm aggregate. The polypropylene 0.5 mL tube and white extruded polystyrene foam were used for their low X-ray absorption.
(B, C) Side view showing the inorganic precipitates X-ray attenuation at the center of some biofilm aggregates (black arrow).
(D) Slice on a 3D reconstructed volume obtained by the fusion of the different views showing the biofilm density in a biofilm aggregate soaked in radiographic contrast medium (white arrow: dense biofilm with low porosity, black arrow: biofilm with high porosity containing more radiographic contrast medium).
Scale bars: 2 mm

5.3.2 Micro-scale properties of granular biofilm aggregates and PAOs microcolonies

Confocal microscopy was employed to explore the AGS architecture at the micrometer scale with a targeted investigation of the PAOs' structure to understand their distribution and organization in granular biofilm aggregates (Figure 5.4).
The microscopic observations were in accordance with the X-ray micro-computed tomography observations that showed that the approximately spherical shape of the biofilm aggregates is composed of microcolonies of various sizes with cauliflower-like structures, confirming earlier results (Lemaire et al., 2008, Weissbrodt et al., 2013b, Gonzalez-Gil and Holliger, 2014). Additionally, the complexity of the biofilm structure suggests that the formation of the AGS studied here is unlikely caused by the scenario of a single microcolony outgrowth into a large biofilm aggregate suggested by Barr et al., 2010. The heterogeneous organization in microcolonies does not form defined concentric layers, and an inert core free of cells was not observed, contradicting the AGS representation in the models of Winkler, Bassin, et al., 2012, Winkler, Kleerebezem, Khunjar, et al., 2012, and Winkler, Kleerebezem, de Bruin, et al., 2013.
As shown in Chapter 3, the dominating PAO in this bioreactor belongs to the genus *Ca.* Accumulibacter. These aerobic bacteria need access to dissolved oxygen present in

the aerated wastewater. Consequently, the presence of metabolically active PAOs in the inner zones of the biofilm (Figure 5.4) indicates a contact of the aerated wastewater not only with the exterior of the biofilm aggregates but also with deeper zones in the structure via water channels. A similar observation on AGS cross-section was presented in Szabó et al., 2017b. Empty interstices are mainly located between the microcolonies' cauliflower-like outgrowths and are connected to the exterior of the biofilm. This introduces complexity in the distribution of the microbial metabolic niches as reflected by the localization of PAOs in the biofilm aggregate.
These observations highlight that with samples harboring a heterogeneous 3D organization like granular biofilm aggregates, analyzing a single cross-section might only partially represent the overall spatial organization. Therefore, if the aim is to draw conclusions at the scale of granular biofilm aggregates, it is recommended to analyze multiple slices to obtain representative results of the sample, for example, using a series of slices evenly spaced across the sample.

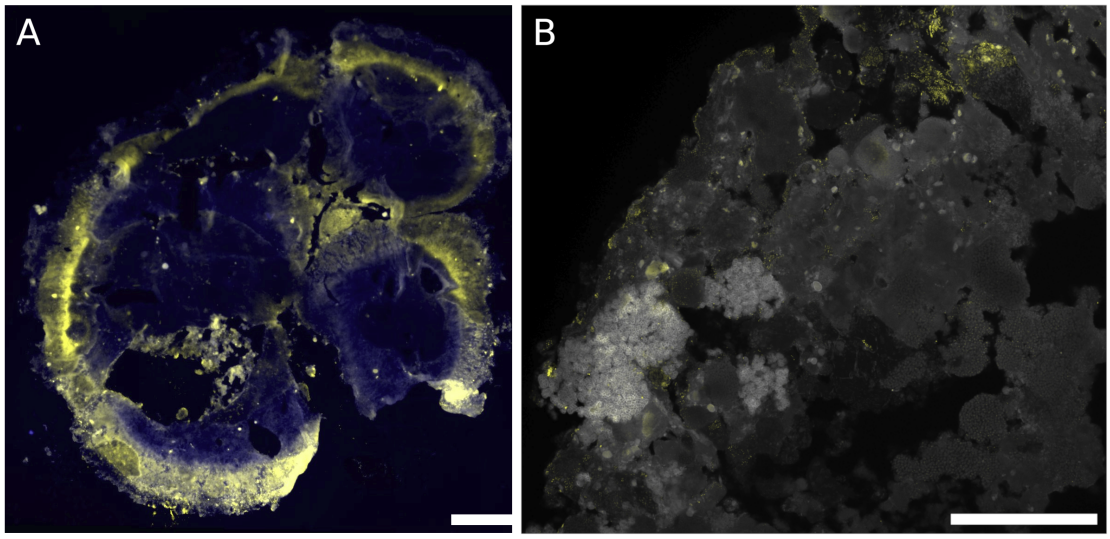

Figure 5.4: **2D AGS structure observation**
(A) Example of a 10 µm thin cross-section at the innermost of one biofilm aggregate (cells in blue, PAOs in yellow), scale bar: 500 µm.
(B) Close-up to highlight the biofilm porosity on another thin cross-section (cells in gray, PAOs in yellow), scale bar: 100 µm.

5.3.3 Micro-scale 3D structure of granular biofilm aggregates and PAOs distribution observed by LSFM

To overcome the limited representativity of thin cross-sections towards the investigation of the full heterogeneous granular biofilm aggregate structure, Light-Sheet Fluorescence Microscopy (LSFM), performing a non-destructive optical slicing, was used to image complete biofilm aggregates.
The localization of PAOs in the 3D biofilm aggregates structure at the single bacterium resolution showed a cell organization in microcolonies (Figure 5.5). In this lab-scale AGS-EBPR bioreactor, the organization of the cells in the biofilm aggregates of the different microbial populations appears to be mostly organized in microcolonies, as highlighted in Figure 5.6 representing a montage of the 3D dataset in 2D by projecting the average fluorescence intensity of the DNA fluorescence on the *z*-axis. The range of microcolonies' size is in accordance with previous observations made by Weissbrodt et al., 2013b.

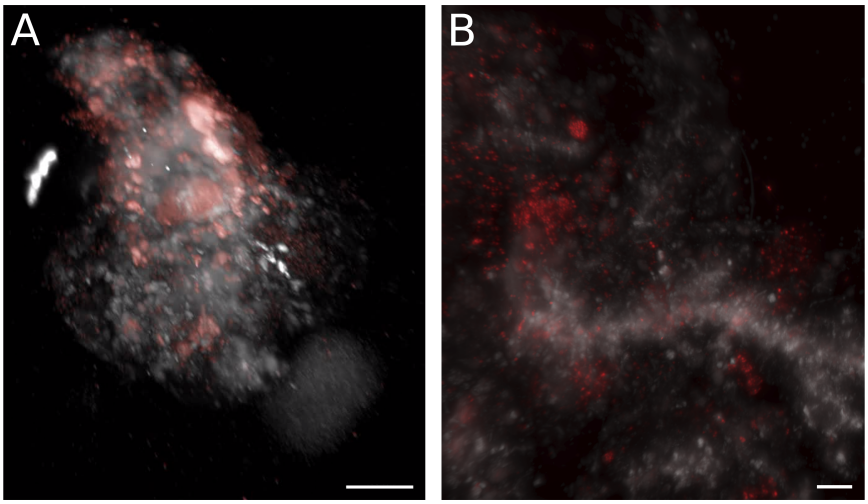

Figure 5.5: **3D AGS structure observation**
(A) 3D reconstructed biofilm aggregate stained with DAPI to localize PAOs (red) amongst the microbial cell (gray), scale bar 100 µm.
3D video is accessible at https://github.com/ArnaudGelb/EPFL.
(B) Close-up to visualize individual cells on the previous 3D reconstructed biofilm aggregate, scale bar 10 µm.

The 3D images of biofilm aggregates, compared to the thin section observation, allow a measure of the position of the microorganisms relative to the edge of the biofilm in the three axes. This benefit was exploited using image processing of the LSFM images in the Master Thesis of Gemayel, 2019. The image analysis workflow to obtain quantitative data on the localization of PAOs in the biofilm aggregates with respect to the distance to the edge is presented in Figure 5.7. In this dataset, the PAOs localization was observed mainly in the first 100 µm from the biofilm edge in contact with the wastewater. The reduction of the polyP signal after 100 µm of distance from the edge indicates that deeper zones in the biofilm aggregate are less favorable to the polyP accumulation, possibly due to the nutrient or redox gradients.

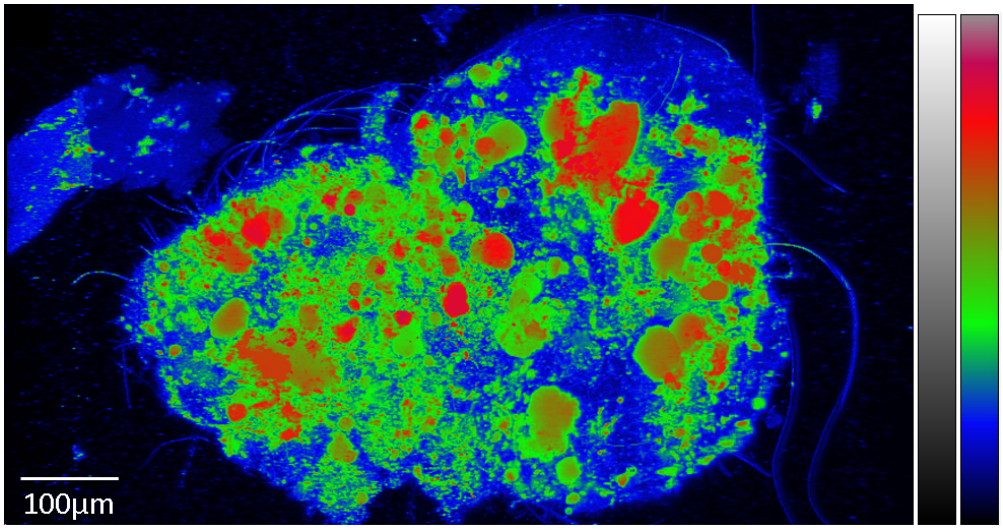

Figure 5.6: **Multi-view 3D reconstruction of an AGS biofilm aggregate**
Z-projection of 525 images of the DAPI/DNA fluorescence signal (420 nm to 470 nm) "flattening" the 3D reconstruction. The gray values are displayed with pseudo-color using the look-up table (LUT) "rainbow RGB" for visualization purposes (the equivalence of the two LUT is displayed on the right side of the figure; dim, medium, and high fluorescent signal intensities are represented in blue, green, and red, respectively).

This confirms the observation that PAOs tend to cluster in microcolonies (Weissbrodt et al., 2013b) and the visualization of large clusters of *Ca.* Accumulibacter at the edge of the biofilm aggregate (Gonzalez-Gil and Holliger, 2014).
In the different 3D datasets presented here, the bacterial density, measured by the DNA fluorescent signal, is not significantly less at the core, supporting the previous observations using X-ray micro-computed tomography and confocal fluorescent microscopy on thin cross-sections.
If the center of the granule did not contain microorganisms, a considerable drop in the DNA fluorescent intensity would be expected at a defined core region. This contradicts the complete lack of favorable conditions for microbial activity at the core, or the dominating presence of inhibitory metabolites or EPS, as hypothesized by Tay et al., 2003. In fact, the localization of the microorganisms at the center of the granule is in line with the observation of Matsumoto et al., 2010 that heterotrophic bacteria dominate the core. Furthermore, Szabó et al., 2017a postulate that an area dense in microbial cells is present at the center because protected from granule surface erosion. In the samples analyzed, cells furthest away from the biofilm aggregate edge are experiencing conditions favorable to their maintenance. This observation further substantiates the theory posed by Gonzalez-Gil and Holliger, 2014, stating that porosity in the granule leads to the formation of irrigation channels that transport nutrients to the inner part of the granule required for cell activity at the center. Earlier theories (Beun et al., 2002) presenting granules with a stable diameter and two or three internal layers of different microbial niches, have been shown to be too simplistic. The granules studied here have exhibited complex structures with wide ranges of cell densities showing that while there might be zones of increased cell activity in the granule, the modeled strict-layers approach does not correspond to

the quantitative data obtained here.
To draw general solid conclusions on the granule microbial architecture, a much larger number of granules should be analyzed with LSFM. But the promising result obtained in this chapter demonstrates the LSFM capability to investigate the complex microbial architecture in the granular biofilm aggregates.

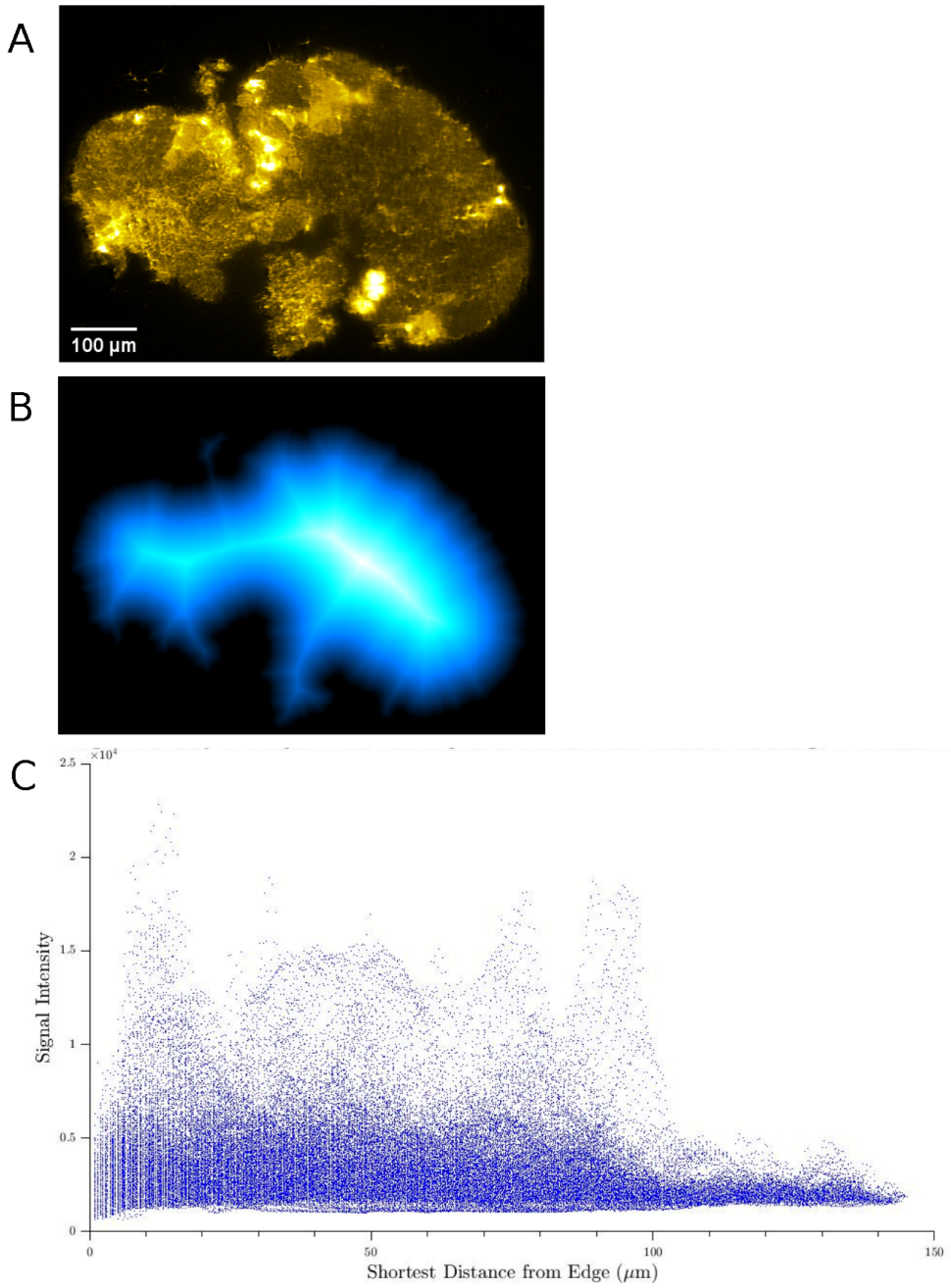

Figure 5.7: **Image analysis workflow**
(A) The original image was acquired on the LSFM using a band pass filter from 525 nm to 545 nm to record the DAPI/polyP fluorescence. In these experimental conditions, a background signal is caused by the DAPI/nucleic-acid fluorescence.
(B) After the edge detection of the granular biofilm aggregate, an Euclidean Distance Map (EDM) is generated to attribute to each pixel of the object a value based on the pixel's distance from the nearest edge.
(C) Plot representing the pixels polyP signal intensity expressed in function of the distance from the edge of the granular biofilm aggregate.

5.4 General conclusions and perspectives

The preliminary results obtained here indicate that a model of the microbial population organization in concentric layers is too simplistic to represent their organization in the granular biofilm aggregates studied here (Wilén et al., 2018). Microorganisms were distributed in the form of microcolonies throughout the biofilm thickness without the presence of an inert core empty of cells.
The observed complex architecture in the granular biofilm aggregates from this lab-scale AGS-EBPR bioreactor supports the previous observations of an intricate contact between the biofilm and the nutrients from the wastewater due to the structure irrigation by pores and channels (Lemaire et al., 2008, Gonzalez-Gil and Holliger, 2014, Quan et al., 2021).
Future LSFM acquisition of additional AGS biofilm aggregates should help characterize the variability across biofilm aggregates and lead to more robust conclusions on the biofilm from the AGS-EBPR bioreactor studied. It would be valuable to assess the effect of granular biofilm thickness on the microorganisms' structure with LSFM imaging of biofilm aggregates with different size categories since previous research has shown the significant contribution of microbial aggregated flocs in municipal wastewater treatment (Layer et al., 2022).
The PAOs detection using only polyP staining on fixed AGS samples cannot reveal if the observed intracellular polyP is experiencing cycling of hydrolysis or polymerization in EBPR condition. A possibility to follow the intracellular polyP fluctuations in PAO is to visualize the microorganisms described as PAO using specific Fluorescence *In situ* Hybridization (FISH) probes together with their polyP signal in samples obtained in the course of the different EBPR phases.
Using polyP measurements in biofilm aggregates by employing LSFM has proven to be a powerful tool for visualizing and quantifying PAOs in the biofilm structure. It was shown that the results are in agreement with confocal microscopy measurements with the advantage of overcoming the issue regarding the lack of representativity experienced with confocal microscopy regarding the entire biofilm aggregate structure.
The application of LSFM on AGS samples offers promising possibilities to asses the microbial structure in biofilm aggregates obtained in lab-scale AGS-EBPR reactors. The use of the protocol developed here on full-scale AGS-EBPR would need adjustments to cope with non-microbial particles present in the biofilm.

5.5 Supplementary figures

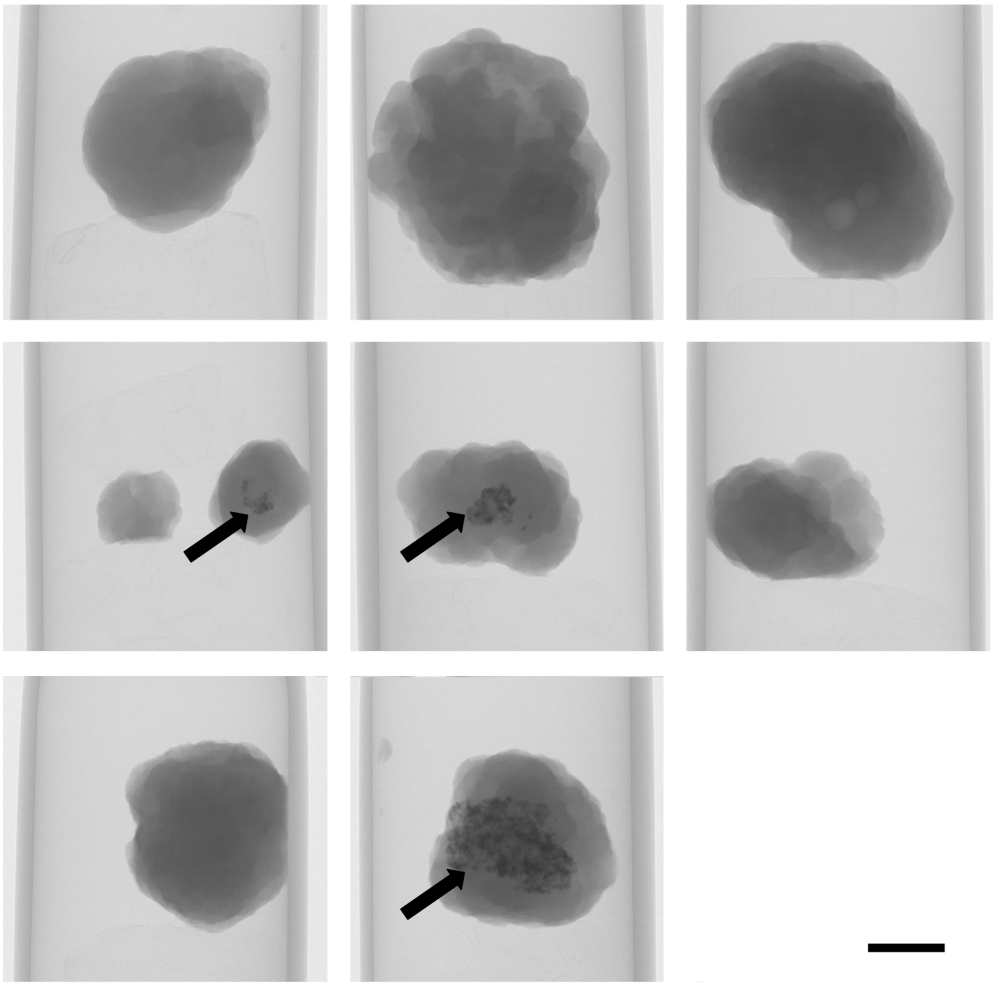

Supplementary Figure 5.1: **X-ray micro-computed tomography**
Side view showing the inorganic precipitates observed by the X-ray attenuation at the center of some biofilm aggregates (black arrows), scale bars: 2 mm.

6 Identification of substrates triggering anaerobic polyphosphate hydrolysis in AGS

Author Contributions:
The conceptualization, methodology, and writing the original draft of this chapter were performed by Arnaud Gelb with the supervision of Christof Holliger.
The other individual contributions are listed below:
- Funding acquisition: Christof Holliger, Nicolas Derlon, and Eberhard Morgenroth.
- Investigation: David Scheibler (carbon sources screening, effect of different glycine concentrations), Emmanuelle Rohrbach (16S rRNA gene sequencing library), Sylvain Coudret (ion chromatography), Dominique Grandjean (gas chromatography), Francesca Petriglieri and Jette Fischer Petersen from the "Center for Microbial Communities" led by Per Halkjær Nielsen at Aalborg University (Raman-FISH), Lee Kang Soo and Landry Zachary from the "Stocker lab" led by Roman Stocker at ETH Zürich (Raman-FISH), Laure Menin (liquid chromatography).
- Resources: "Genomics Technologies Facility" led by Julien Marquis at UNIL Lausanne (amplicon sequencing reads), "Central Environmental Laboratory" led by Florian Breider at EPFL Lausanne (analytical chemistry), "Crystal Growth and Characterization Plateform" led by Arnaud Magrez at EPFL Lausanne (Raman), "Mass Spectrometry – Elemental Analysis Plateform" led by Laure Menin at EPFL Lausanne (LC-MS).
- Writing review: Julien Maillard and Laetitia Cardona.

6.1 Introduction

This chapter aims to understand better the influence of organic carbon sources on the microorganisms involved in the biological phosphorus removal in the Enhanced Biological Phosphorus Removal (EBPR) bioreactor. This was done by applying the different organic carbon sources individually during the anaerobic feeding phase in two lab-scale reactors operated as EBPR with Aerobic Granular Sludge with two different carbon source mixtures (AGS) and following their consumption and the release of phosphate due to polyphosphate (polyP) hydrolysis.
It is known that polyphosphate-accumulating organisms (PAOs) can store anaerobically organic carbon present in wastewater. The energy required for this mechanism is obtained by the hydrolysis of intracellular polyP. The orthophosphate produced by the

polyP hydrolysis is released in the water. In aerobic conditions, PAOs use the stored carbon source to replenish intracellular polyP for maintenance and growth, thus creating a net phosphorus uptake from the water, thereby removing the phosphate from the wastewater. Depending on the ratio between phosphate and carbon source, the EBPR process can also select microorganisms known as glycogen-accumulating organisms (GAOs). GAOs share with PAOs the trait of storing organic carbon anaerobically but without accumulating phosphate, therefore not releasing phosphorus in EBPR conditions. It is hypothesized that GAOs use glycogen degradation to generate energy and reducing equivalents to support the organic carbon uptake storage during the anaerobic period. In EBPR conditions, if the PAOs/GAOs take up anaerobically completely an organic carbon source present in the influent, they will out-compete the organisms using this carbon source only in aerobic conditions (Comeau et al., 1986, Kuba et al., 1993, Satoh et al., 1996, M. C. M. van Loosdrecht, Hooijmans, et al., 1997, Lemos et al., 1998, Mino et al., 1998, Erdal et al., 2008, Y. Zhou et al., 2010, Oehmen et al., 2010, P. H. Nielsen et al., 2019).
Usually, microorganisms in wastewater treatment plants performing EBPR deal with a diverse range of substrates; therefore, there is probably a diversity of organisms involved in polyP accumulation with affinities for different carbon sources at different concentrations. Indeed, Barnard et al., 2017 suggest that conventional EBPR models using an anaerobic uptake of acetate and propionate may have unintentionally selected for less efficient PAOs. Cross-feeding caused by the trophic interactions between microorganisms is commonly observed in complex microbial communities. This phenomenon is illustrated for the carbon food chain in Figure 6.1 in the context of EBPR.

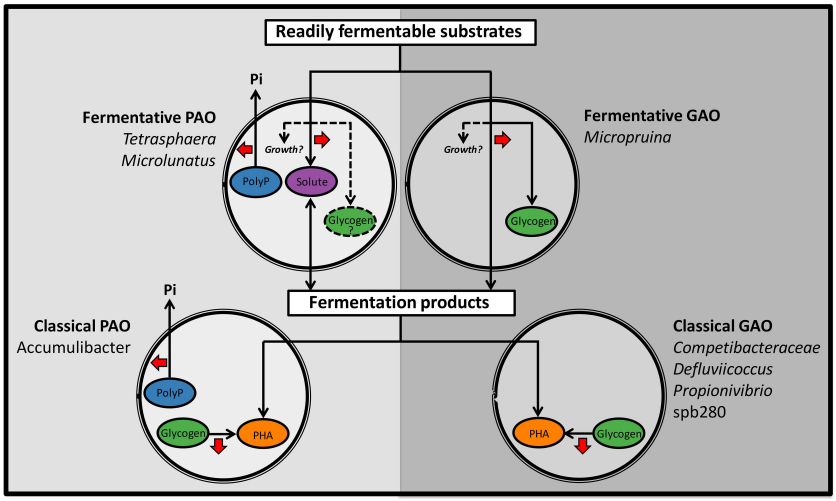

Figure 6.1: **Schematic diagram of metabolic cross-feeding in EBPR processes** (from McIlroy et al., 2018).
Representation of two types of PAO/GAO metabolism based on their usage of the carbon source. Proposed organisms involved in EBPR processes harboring a PAO phenotype are indicated on the left side and those with a GAO phenotype on the right side of the figure.
Red arrows indicate a contribution to energy conservation.

The ability of a carbon source to support EBPR depends on the metabolic capabilities of the microbial community present in and the operating conditions of the bioreactor. Even if the metabolic traits are not correlated with the phylogeny, a systematic analysis of microbial communities is recommended to compare results across studies, as suggested previously (R. J. Seviour et al., 2003). One should also remember that it is not because bioreactors are operated with similar conditions that they will necessarily harbor the same microbial community (Kaewpipat and Grady, 2002).
Consequently, divergent conclusions regarding the effects of a carbon source on the EBPR process can be drawn based on differences in the operating conditions (substrate concentration, sludge concentration, pH, ...) that affect the metabolic traits expressed by the microbial community, but also due to differences of metabolic capability present in different microbial community. The use of lab-scale AGS-EBPR bioreactors fed with synthetic wastewater helps controlling tight operation parameters. However, these bioreactors are experiencing different conditions than those encountered in the full-scale AGS-EBPR bioreactors, especially regarding the substrate selective pressure on the microorganisms.
In this chapter, the influence of different organic carbon sources (acetate, propionate, glucose, amino acids, starch, peptone) on biological phosphorus removal from wastewater was analyzed during one SBR cycle in parallel in two lab-scale AGS-EBPR bioreactors. These two bioreactors performed stable biological phosphorus removal of two synthetic influents with different compositions (Scheibler, 2018). The carbon sources tested can be classified as volatile fatty acids (VFA; acetate and propionate), and monomeric (glucose and amino acids), and polymeric (starch and peptone) substrates.

6.2 Material and methods

6.2.1 AGS-EBPR operation and influent composition

The characterization of AGS and the operation of the two AGS-EBPR bioreactors studied, referred to as RA and RB, is presented in Aline Adler's Ph.D. thesis in Chapter IV (Adler, 2019). The influent composition used to test the different organic carbon sources was modified as follows: the influent was prepared with 77.5% (v/v) of filtered water from Lake Geneva supplemented with 22.5% (v/v) of a concentrated aqueous solution containing 35.39 mM NH_4Cl, 4.19 mM K_2HPO_4, 2.10 mM KH_2PO_4, 0.72 mM $MgSO_4$, 1.12 mM KCl, and 4.80 mM $CaCl_2$. Then the influents containing the single organic carbon sources were obtained by adding the following carbon source to reach a theoretical COD concentration of 600 mg/L: 9.38 mM acetate, 5.36 mM propionate, 3.13 mM glucose, a combination of seven amino acids (0.89 mM alanine, 0.49 mM arginine, 0.89 mM aspartate, 0.60 mM glutamate,1.79 mM glycine, 0.36 mM leucine, and 0.49 mM proline), 507 mg/L starch, and 428 mg/L peptone. The influents containing single amino acids as organic carbon sources had their respective amino acid concentration indicated above multiplied by 7.

6.2.2 DNA extraction and amplicon sequencing

The microbial composition was assessed by amplicon sequencing during the experimental period (supplementary Figure 6.1). The protocol used for sampling to run amplicon sequencing is described in Adler, 2019 (Protocol n°2). The samplings for the DNA analysis of the microbial community were performed using 25 mL of mixed sludge sampled at the middle height of the 2.4 L bioreactor 5 min before the end of the aerobic phase of the SBR cycle.

6.2.3 PHA analysis

The PHA analysis was performed using the protocol described in Chapter 4.

6.2.4 Glycine analysis

Sampling

The sampling was performed using 25 mL of mixed sludge sampled at the middle height of the 2.4 L bioreactor at the desired time points. Then, the supernatant was collected after centrifugation (5 min at 8'000 RCF, 4°C), filtered with a 0.2 µm filter (83.1826.001, Sarstedt), and finally stored at 4°C before analysis for a maximum of three days.

LC-MS instrument description

A Waters Acquity LCMS XEVO TQ MS liquid chromatography and mass spectrometer with auto-injector were operated with the MassLynx software. Before each sample injection, four washes were performed: one wash with H_2O : Acetonitrile : Methanol : Isopropanol (1:1:1:1) and three washes with H_2O : Methanol (1:1). Volumes of 10 µL of samples were injected in 1 sec with one fill stroke. The separation column was a C18 silica reversed-phase column (186003539, Waters) with a pore size of 100 Å, a particle size of 1.8 µm, an inner diameter of 2.1 mm, and a length of 100 mm. The separation column was combined with an ACQUITY Column In-Line Filter (205000343, Waters). The column temperature was 30°C ±5°C with a running time of 5 min and an equilibration time of 0.1 min. The injection was performed using a mixture of 90.5% H_2O, 9.5% Methanol, and 0.1% ammonium formate as solvent at a flow of 0.4 mL/min with a seal wash of 2.5 min using H_2O : Methanol (80:20) and a high-pressure limit of 1034 bar. The ionization mode is ESI with a positive-ion analysis with a dwell time of 0.161 sec. The standard curve was done using different solutions with different concentrations of glycine (120070050, ACROS Organics). A mixture of sodium iodide and cesium iodide was used for m/z calibration (14379, Supelco).

6.2.5 Raman-FISH

The Raman-FISH was performed according to Fernando et al., 2019. The Fluorescence *In situ* Hybridization (FISH) staining of Daims et al., 2005 was adapted by removing the sodium dodecyl sulfate (SDS) in the final washing buffer to minimize the loss of intracellular storage compounds and biomass loss from the calcium fluoride microscope slides during the washing procedure. The FISH probe used is the *Candidatus* Accumulibacter phosphatis specific PAO651 with the 5’ end-labeled with 5(6)-carboxyfluorescein-N-hydroxysuccinimide ester (FLUOS). The FISH signal was observed without mounting media using the in-built fluorescence microscope of the Raman system.

6.3 Results and discussion

6.3.1 Influence of different carbon sources on both AGS-EBPR bioreactors

The influence of different organic carbon sources on the biological phosphorus removal from the wastewater was assessed on two AGS-EBPR bioreactors referred to as RB and RA (Figure 6.2 and Figure 6.3) using the influents described in Material and Methods during one SBR cycle.

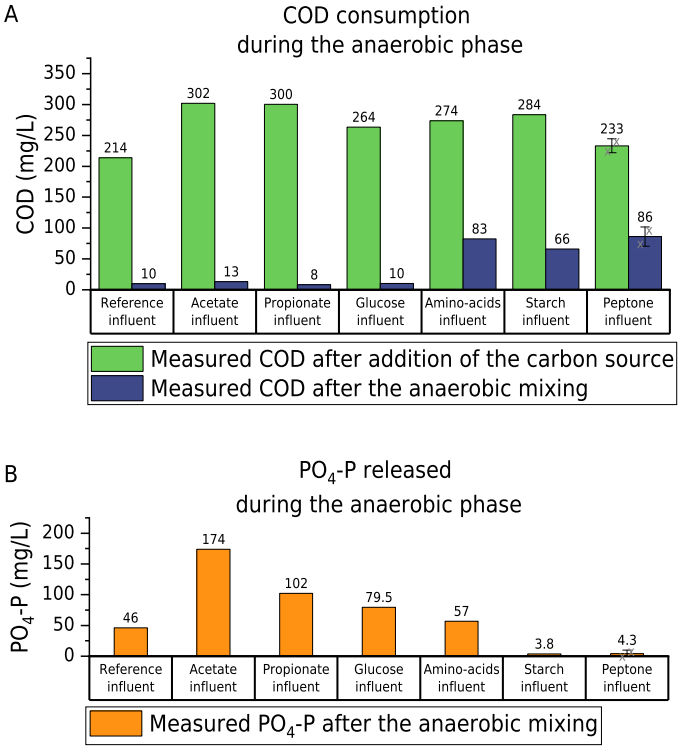

Figure 6.2: **Effect of different carbon sources on bioreactor RB**
RB's reference influent contains a mixture of acetate, propionate, glucose, a combination of seven amino acids, starch, and peptone as organic carbon sources. The different modified influents containing the carbon sources indicated in the figures were applied for one SBR cycle.
(A) Measure of the dissolved COD at the end of the feeding phase and the end of the subsequent anaerobic phase. A decrease between both values corresponds to a COD consumption during the anaerobic phase.
(B) Anaerobic PO_4-P release by PAOs measured as the dissolved PO_4-P concentration at the end of the anaerobic phase.
The targeted theoretical COD in the reference influent and the modified influent was 300 mg_{COD}/L. When replicate experiments were conducted, the bars represent the mean; the Y-error bars represent the standard deviation, and the cross-marks display individual data points.

In the AGS-EBPR bioreactor RB, the use of a feeding solution containing either acetate, propionate, or glucose led to a higher consumption of the carbon source and induced a higher phosphorus release in the water during the anaerobic phase as compared to the values obtained with the bioreactor RB reference influent (containing a mixture of all the carbon sources here tested). The feeding solution containing a mixture of amino acids led to a partial carbon source consumption and phosphorus release with levels comparable to that of the bioreactor RB reference influent. The feeding solutions containing either starch or peptone led to a partial carbon source consumption but did not induce any phosphorus release in the medium during the anaerobic phase.

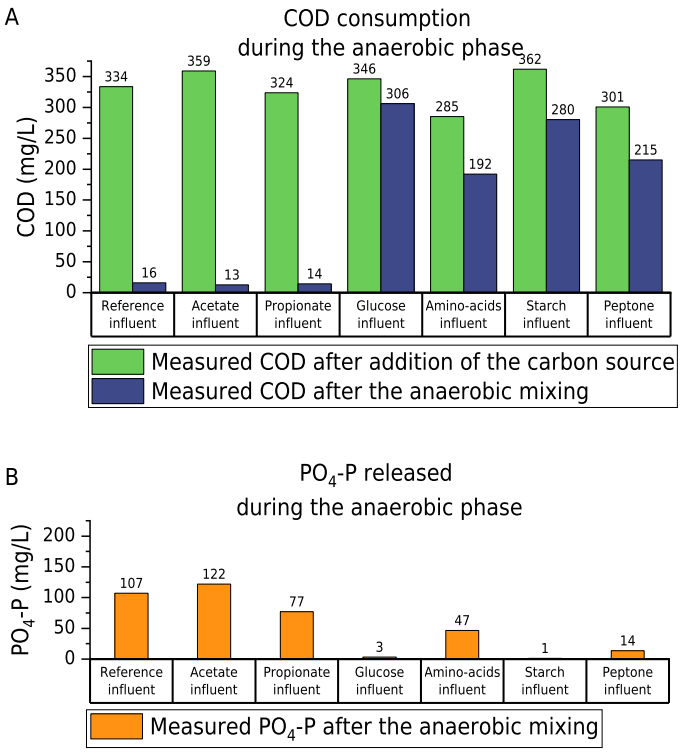

Figure 6.3: **Effect of different carbon sources on bioreactor RA**
RA's reference influent contains a mixture of acetate and propionate as organic carbon sources. The different modified influents containing the carbon sources indicated in the figure were applied for one SBR cycle.
(A) Measure of the dissolved COD at the end of the feeding phase and the end of the subsequent anaerobic phase. A decrease between both values corresponds to a COD consumption during the anaerobic phase.
(B) Anaerobic PO_4-P release by PAOs measured as the dissolved PO_4-P concentration at the end of the anaerobic phase.
The targeted theoretical COD in the reference influent and the modified influent was 300 mg_{COD}/L.

In bioreactor RA, the presence of acetate or propionate as a sole organic carbon source in the influent led to the consumption of the carbon source and the release of phosphorus during the anaerobic phase at a concentration comparable to the measure with the bioreactor RA reference influent (containing a mixture of acetate and propionate). The feeding solutions containing either glucose, starch, or peptone led to very low consumption of the carbon source and did not induce any significant release of phosphorus in the medium during the anaerobic phase. The feeding solution containing the mixture of amino acids led to a rather low carbon source consumption and to lower phosphorus release in the medium during the anaerobic phase compared to the values obtained with the bioreactor RA reference influent.
Some carbon sources used during the screening were not entirely consumed during the anaerobic phase for both lab-scale AGS-EBPR reactors. In bioreactor RB, the incomplete consumption of amino acids, starch, and peptone could be explained by the fact that in contrast to the other carbon sources tested, the microorganisms present in the AGS-EBPR were not able within 1 h in anaerobic conditions to fully use these particular carbon sources at a concentration six times higher than that present in the reference influent. Another possibility is that the higher concentration of these carbon sources could have induced some metabolic inhibition.
In bioreactor RA, the incomplete consumption of glucose, amino acids, starch, and peptone could be most probably explained by the fact that, since these substrates were not present in the bioreactor RA reference influent, the microbial community from this AGS-EBPR bioreactor was not adapted to the consumption of these specific substrates.
In bioreactors RB and RA, the acetate and propionate induced the release of orthophosphate, which was expected as those carbon sources were present in the reference influent and are known to be used by PAOs in EBPR conditions (Oehmen, Yuan, et al., 2005).
In bioreactor RB, the glucose and the mix of amino acids also induced an phosphate release. This observation can be explained by the anaerobic storage of those carbon sources by PAOs, and/or their transformation into products that PAOs can anaerobically store (e.g., acetate). Regarding starch and peptone, or their potential transformation products, they could not probably be stored in these two lab-scale AGS-EBPR reactors by PAOs.
In bioreactor RA, the amino acid mix induced an anaerobic phosphorus release which was not expected due to the absence of these carbon sources in the bioreactor RA reference influent. This observation led to additional experiments, as described in the next section.
The tests performed during one SBR cycle were distributed over 3 and 5 weeks for bioreactors RB and RA, respectively, to mitigate the microbial community's perturbation caused by the modified influents. The relative microbial composition during the experimental period was monitored by amplicon sequencing to asses the stability of the microbial community (Supplementary Figure 6.1). The sample taken from bioreactor RA in week 5 presents fewer OTUs harboring an abundance higher than 0.5%, possibly reflecting a quality issue in the 16S rRNA gene amplicon sequencing analysis with this sample.
A variation is observed in the relative composition of the microbial community throughout the experiment. On the other hand, these results clearly show differences in the microbial community composition between the two AGS-EBPR reactors operated with

different influents. However, the presence of some microorganisms does not necessarily imply the presence of a particular metabolic activity. Still, as these lab-scale EBPR bioreactors promote PAOs and GAOs, it was expected to find such organisms among the dominant OTUs detected by 16S rRNA gene amplicon sequencing. The *Dechloromonas* genus (Ginige et al., 2005) and the *Tetrasphaera* genus (Onda and Takii, 2002) have been described with a PAO phenotype and were more abundant in the bioreactor RB. In contrast, the *Ca.* Accumulibacter genus (Kong et al., 2004) described as PAO was more abundant in the bioreactor RA. The *Sbr-gs28* and the *Micropruina* genera (Kong et al., 2001) have been described with a GAO phenotype and were more abundant in the bioreactor RB. Finally, the *Ca.* Competibacter genus (McIlroy et al., 2014) has been described as GAO and was more abundant in the bioreactor RA. These differences in the distribution and abundance of putative PAO and GAO in the two AGS-EBPR bioreactors are not surprising as they were experiencing a different substrate selection pressure. The differences in the use of the organic carbon sources by the microbial communities in the two bioreactors are likely explained by functional differences in the respective microbial populations. Indeed, in the bioreactor RB regularly operated with an influent containing non-VFA carbon sources, the metabolic activities of hydrolysis and fermentation are expected to be present in opposition to the bioreactor RA.

6.3.2 Influence of different amino acids on the performances of bioreactor RA

As mentioned in the previous section, some phosphorus release was observed in the anaerobic phase in bioreactor RA operated with a reference influent containing VFA, was fed with a modified influent containing a mixture of amino acids as carbon sources. The individual contribution to the phosphorus release of the seven different amino acids in the mixture was analyzed (Figure 6.4).

In bioreactor RA, the presence of either alanine or arginine as a sole organic carbon source in the influent led to a partial consumption of the carbon source and an anaerobic release of phosphorus at a lower concentration compared to the influent containing the mixture of the seven amino acids. The feeding solution containing the acidic amino acids (aspartate or glutamate) led almost to the full consumption of the carbon source during the anaerobic phase with a simultaneous release of phosphorus at a concentration comparable to the mixed amino acids influent. The feeding solutions containing the hydrophobic amino acids (leucine or proline) led to a small consumption of the carbon source and did not induce any significant release of phosphorus in the medium during the anaerobic phase. The feeding solutions containing glycine led to a small carbon source decrease (approximately 10%) but a higher phosphorus release when compared to the mixed amino acids influent.
In bioreactor RA, it seems that aspartate and glutamate could be used as carbon sources for EBPR metabolism. Indeed, they are consumed during the anaerobic phase with a simultaneous phosphorus release. To confirm their ability to support the metabolism of PAOs, the phosphorus uptake during the aerobic phase should be investigated. These observations were not expected since aspartate and glutamate were absent in the reference influent composition feeding RA.
The role of alanine and arginine is unclear. However, the smaller COD consumption and anaerobic phosphorus release compared to the bioreactor RA reference influent indicate that they are likely not relevant substrates for PAOs within the microbial community studied here.
The influent containing glycine induced an anaerobic phosphorus release without any notable COD consumption. This effect was unexpected since glycine was also absent from the composition of the reference influent and mainly because the phosphorus release in the anaerobic phase is expected to support the uptake of organic carbon. In the hypothesis of a significant glycine import by the cells, the small decrease in soluble COD might be caused by a simultaneous export of the glycine or another carbon-containing metabolite. Excess glycine inhibits the growth of many bacteria and is used as a nonspecific antiseptic agent inhibiting cell wall synthesis (Hishinuma et al., 1969, Gillissen et al., 1991); therefore, glycine toxicity could interfere with the PAOs control of energy and metabolic homeostasis. Different glycine concentrations were applied, and the result is presented in the next section to understand glycine's effect better.

There are two notable limitations of the experimental approach of testing individual carbon sources one by one at a concentration higher than the one in the reference influent: (i) the potential co-metabolic effects induced by multiple carbon sources are lost, and (ii) the effect of a carbon source at a higher concentration might be

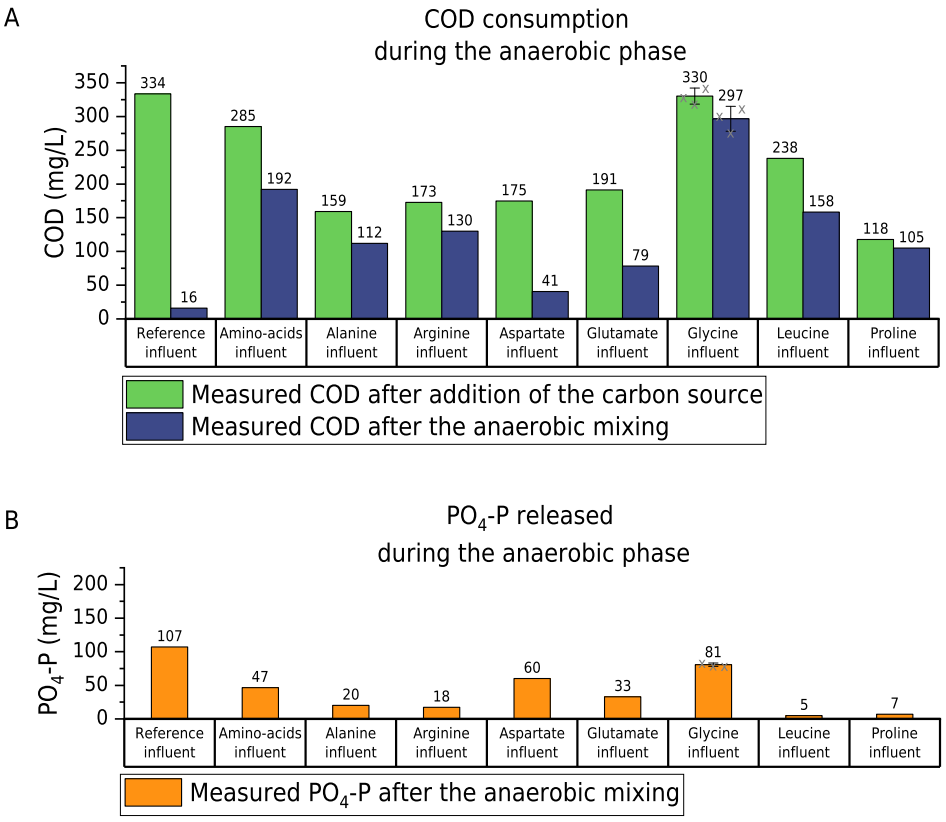

Figure 6.4: **Effect of individual amino acids on bioreactor RA**
RA's reference influent contains a mixture of acetate and propionate as organic carbon sources. The different modified influents containing the carbon source tested as a sole organic carbon source were used for one SBR cycle.
(A) Measure of the dissolved COD at the end of the feeding phase and the end of the subsequent anaerobic phase. A decrease between both values corresponds to a COD consumption during the anaerobic phase.
(B) Anaerobic PO_4-P release by PAOs measured as the dissolved PO_4-P concentration at the end of the anaerobic phase.
The targeted theoretical COD for the reference influent and the modified influent was 300 mg_{COD}/L.
When replicate experiments were conducted, the bars represent the mean; the Y-error bars represent the standard deviation, and the cross-marks display individual data points.

different in comparison to that at the concentration in the reference influent. An alternative screening of the contribution of the different substrates present in the reference influent could be performed by removing them one by one from the influent or by following a fractional factorial design 2^{6-3}_{III} (1/8 of a full factorial design). Also, the trace element solution was omitted in the influents used to screen the individual carbon sources, which might have had an effect.
A control experiment with inactivated AGS should be performed to measure the adsorption of the tested carbon sources on the biofilm, and thus to ensure that the COD decrease is due to the consumption of the substrate by the microorganisms. The results presented here with the different carbon sources were mainly obtained with a single measurement. In the absence of replicates, estimating the experimental and analytical variability is impossible. The discrepancies between the measured COD and the theoretical one (300 mg_{COD}/L), as discussed in Scheibler, 2018, can be, for example, due to a non-homogeneous mixing, adsorption on the AGS biofilm, or interference with the COD titrimetric measure.

6.3.3 Dose-dependent response of the glycine on the anaerobic phosphorus release in bioreactor RA

Influents with different glycine concentrations were applied to investigate if the effect of glycine observed during the anaerobic phase in bioreactor RA is correlated to its concentration (Figure 6.5).

For all the glycine concentrations tested, the dissolved COD only slightly decreased (around 10% to 20% of the initial COD in the influent). The higher the glycine concentration was, the higher the phosphorus was released during the anaerobic phase. It seems that the glycine effect displayed a fairly linear correlation from 37.5 to 150 mg_{COD}/L, while a response saturation might occur at 300 mg_{COD}/L. For some of the tests with influents containing glycine as a carbon source, the aerobic COD and the phosphorus uptake were monitored (Figure 6.6).

In the experiments with different glycine concentrations, the observed COD concentration decreased similarly during the anaerobic and aerobic phases. Glycine induced a phosphorus release during the anaerobic phase, and a phosphorous uptake during the aerobic phase was observed with all the different glycine concentrations tested. The results indicate that the effect of glycine on PAOs in this lab-scale AGS-EBPR bioreactor was dependent on the glycine concentration. These analyses need to be repeated with more replicates and additional glycine concentrations to validate the type of relationship between the glycine concentration and the anaerobic release of phosphorus. Nevertheless, these observations indicate that during the SBR cycles using an influent with glycine as a carbon source, phosphorus uptake occurs during the aerobic phase. If we assume that glycine is not used as an energy source, then the energy for glycine uptake might be driven from previously stored PHA in the cells. This hypothesis was further explored and is presented in the next section.

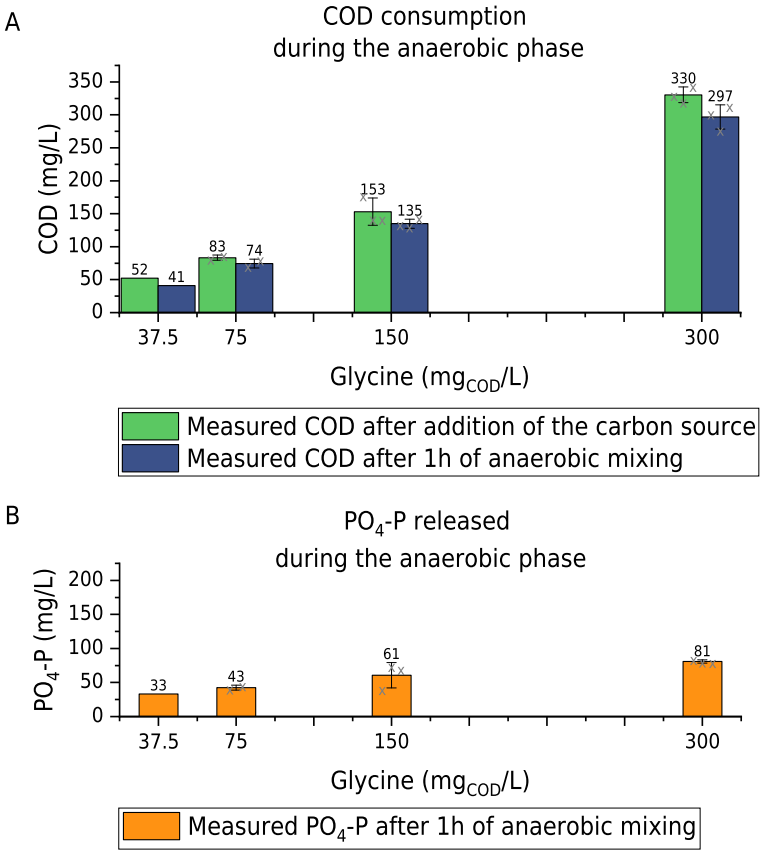

Figure 6.5: **Dose-dependent effect of glycine on bioreactor RA**
RA's reference influent contains a mixture of acetate and propionate as organic carbon sources. The different modified influents containing glycine as a sole organic carbon source were used for one SBR cycle.
(A) Evaluation of the anaerobic glycine consumption measured as the dissolved COD after the feeding phase and at the end of the subsequent anaerobic phase. The difference in COD likely represents the apparent consumption of glycine.
(B) Evaluation of the effect of glycine concentration on the phosphorus release by PAOs measured as the dissolved PO_4-P concentration at the end of the anaerobic phase.
When replicate experiments were conducted, the bars represent the mean; the Y-error bars represent the standard deviation, and the cross-marks display individual data points.

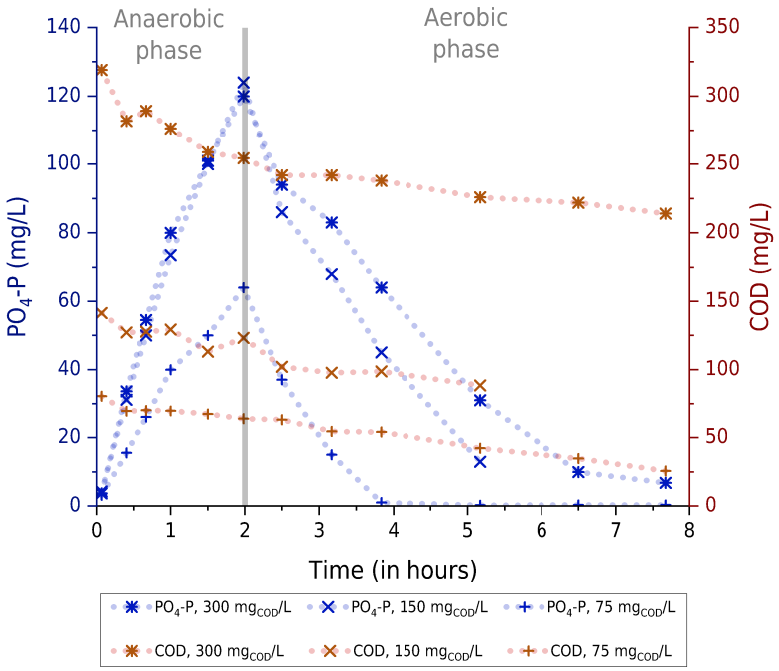

Figure 6.6: **COD and PO_4-P concentration during SBR cycles in bioreactor RA treating influents with different glycine concentrations**.
The modified influents containing different glycine concentrations as a sole organic carbon source were applied to one SBR cycle.
The glycine consumption was measured as the dissolved COD. The phosphorus release and uptake by PAOs were measured as the dissolved PO_4-P concentration.
The length of the aerobic phase was not constant due to the variable SBR operation parameters (Adler, 2019).

6.3.4 Addition of glycine in bioreactor RA at different SBR cycle phases

So far in this chapter, the glycine concentration was indirectly measured as the dissolved COD. In the presence of glycine in the influent, the COD showed a slight decrease compared to the reference influent containing acetate and propionate (Figure 6.4A). The drawback of the COD measurement is that it is impossible to ensure that the obtained values reflect the glycine concentration. The COD analysis may capture the contribution of a molecule resulting from the transformation of glycine or any other metabolite(s) formed. For this reason, glycine was specifically analyzed with Liquid Chromatography-Mass Spectrometry (LC-MS). The intracellular PHA storage was followed by the analysis of 3-hydroxybutyrate (3-HB) and 3-hydroxyvalerate (3-HV) to monitor the performance of PAOs.
To evaluate if the phosphorus release in the AGS-EBPR bioreactor RA upon the addition of glycine is dependent on the phase of the SBR cycle, glycine was added during the anaerobic and the aerobic phases in two different SBR cycles (Figure 6.7).

The results indicate that the COD and the glycine concentrations follow a similar trend. After adding glycine into the AGS-EBPR, the main fraction of the glycine is not consumed nor modified. Compared to an SBR cycle without glycine addition (right panels of Figure 6.8), the addition of glycine in the aerobic phase has a notable effect on the pH and the O_2 consumption by the microorganisms. After the addition of glycine in the aerobic phase, no phosphorus release was measured. On the other hand, when glycine was added in the anaerobic phase after feeding the reference influent, the phosphorus release in the anaerobic phase was higher than that in the other conditions tested. When added in the anaerobic phase, the glycine notably affected the pH and the O_2 consumption by the microorganisms. Additionally, the presence of glycine seemed to lower the PHA production and the nitrification compared to SBR cycles fed with the reference influent.
To measure the buffering effect of glycine molecule on the pH, 300 mg_{COD}/L of glycine were added in 0.2µm filtered effluent obtained at the end of an SBR cycle with the reference influent. The pH decreased from 8.4 to 8 after the addition of glycine.
To confirm the observations on the effect of glycine addition in the anaerobic and the aerobic phases of the SBR cycles, replicate experiments should be performed. The glycine analysis indicates that the main fraction of the glycine injected in the AGS-EBPR reactor was not modified by the microorganisms. This observation can result from the absence of active glycine metabolizing extracellular and intracellular enzymes (e.g., glycine cleavage GCV enzyme system) or the lack of cell import by the glycine transport system Cyc (Ghrist and Stauffer, 1995). As the acidification observed after adding glycine is greater than the buffering effect of this molecule, the glycine might have impacted the microorganisms by lowering the pH. The higher oxygen consumption after the addition of glycine can be explained by the antimicrobial activity of glycine (Hishinuma et al., 1969). Glycine was shown to inhibit growth and induce cell lysis in certain bacterial species.

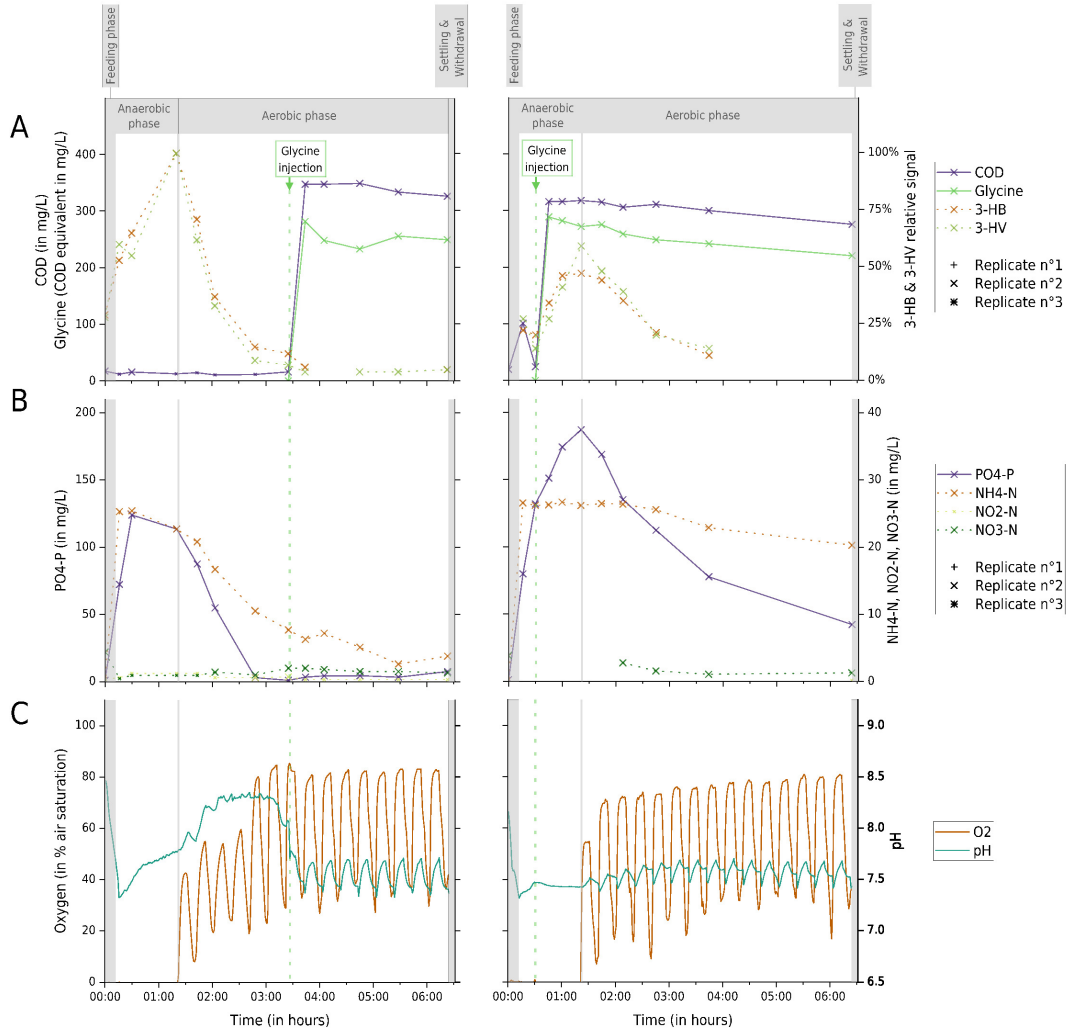

Figure 6.7: **Effect of a glycine addition in the anaerobic and aerobic phases during different SBR cycles of bioreactor RA**
The effects of glycine addition were monitored in the aerobic or anaerobic phases and presented on the left and right panels, respectively.
(A) Analysis of COD, glycine, and PHA.
The glycine concentration is expressed as mg_{COD}/L equivalent using the theoretical O_2 required to oxidize glycine into CO_2. The intracellular PHA was assessed by measuring the relative signal for the 3-hydroxybutyrate (3-HB) and 3-hydroxyvalerate (3-HV).
(B) Soluble orthophosphate (PO_4-P), ammonium (NH_4-N), nitrite (NO_2-N), and nitrate (NO_3-N) concentrations were measured in the aqueous phase of the AGS-EBPR reactor.
(C) Oxygen and pH signals were monitored by the lab-scale AGS-EBPR probes.
The pH was regulated to remain between 7.3 and 8.5, and the O_2 signal amplitude fluctuation was dependent on the height of the sludge bed (the O_2 probe was positioned at half the height of the AGS-EBPR reactor).
The data points with values below the detection limit are represented with a smaller point marker.

The observation of a higher phosphorus release when glycine is added in the anaerobic phase and the absence of phosphorus release when glycine was added in the aerobic phase indicate that the effect of glycine on PAOs differs depending on the presence of oxygen or the cells' metabolic states. To confirm this hypothesis, glycine should be injected at different time points of the different phases in individual SBR cycles. The lower PHA formation in the presence of glycine likely indicates a disturbance of the PAO metabolism. To understand the mechanism of action of glycine on PAOs, attempts to reverse the effect of glycine could be performed with the simultaneous addition of L-alanine, as suggested by Hishinuma et al., 1969.

6.3.5 Aerobic uptake of phosphorus in bioreactor RA after anaerobic exposure to glycine

Based on Figure 6.7, it was shown that after being exposed to glycine in the anaerobic phase, PAOs in the AGS-EBPR RA could perform an aerobic phosphorus uptake without significant glycine consumption. Therefore, it is hypothesized that the aerobic phosphorus uptake is supported by the hydrolysis of previously stored PHA formed with acetate and/or propionate. Therefore, SBR cycles were monitored in the next section with a glycine influent and compared with the bioreactor RA reference influent containing acetate and propionate.

The monitoring of the acetate and propionate present in the reference influent with the COD measurement shows a full consumption during the first 30 min of the anaerobic phase with a simultaneous formation of PHA (Figure 6.8 left panels). In comparison, with the glycine influent (right panels), only a small fraction of glycine was consumed in the anaerobic phase, and no PHA was formed.
In the SBR cycles fed with the reference influent, the aerobic phosphorus uptake can be considered complete after 3 h. On the other hand, the phosphorus uptake was either partial or absent in the SBR cycles fed with the glycine influent, depending on the replicates.
It can also be noted that the nitrification leading to the NO_3 formation was negatively affected in the SBR cycles with the glycine influent compared to the SBR cycles with the reference influent. The effect of glycine on the dissolved oxygen and pH in the lab-scale AGS-EBPR was similar to the behavior observed earlier in Figure 6.7.
In this lab-scale AGS-EBPR bioreactor, the glycine induced an anaerobic phosphorus release but did not support the PAO metabolism. Indeed glycine is not consumed nor supports the aerobic uptake of phosphorus. In Figure 6.6, the aerobic phosphorus uptake was probably supported by previous PHA storage, as shown in Figure 6.7 on the right panels.
To confirm these results, the aerobic phosphorus uptake should be monitored using AGS deprived of PHA by a long aerobic phase and then fed with different acetate and propionate concentrations to form different amounts of PHA before the anaerobic addition of glycine. A limitation of the PHA analysis used here was that only classical PHA composed of 3-HB and 3-HV subunits were targeted. Other forms of PHA might have a role in the PAO metabolism studied in the present AGS-EBPR bioreactor (Taguchi et al., 2002).

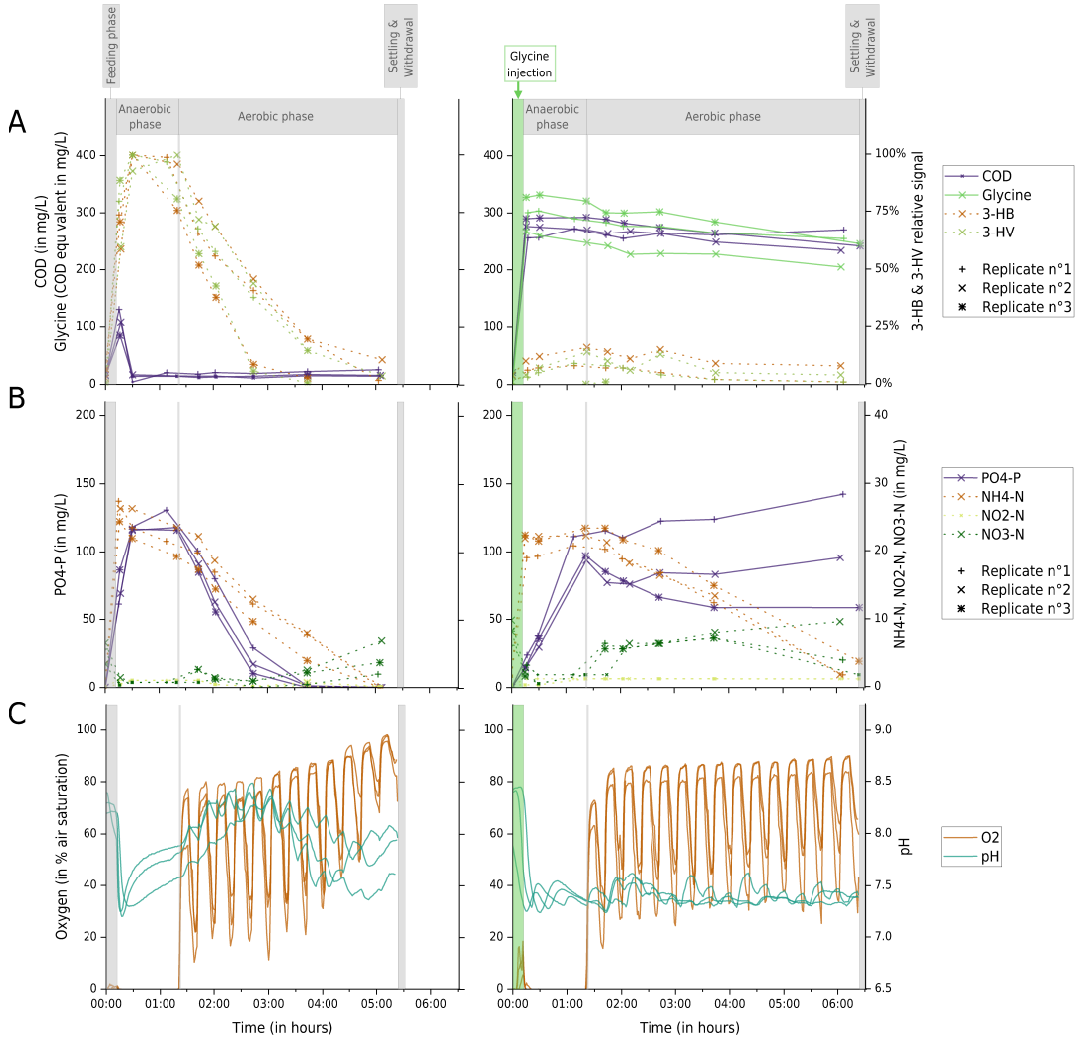

Figure 6.8: **Comparison between SBR cycles performed on bioreactor RA with the reference influent and with an influent containing glycine as sole organic carbon source**

The performances obtained with the reference influent and the glycine influent during one SBR cycle are presented on the left and right panels, respectively.

(A) Analysis of COD, glycine, and PHA.

The glycine concentration was expressed as mg_{COD}/L equivalent using the theoretical O_2 concentration required to oxidize glycine into CO_2. The intracellular PHA was assessed by measuring the relative signal for the 3-hydroxybutyrate (3-HB) and 3-hydroxyvalerate (3-HV).

(B) Soluble orthophosphate (PO_4-P), ammonium (NH_4-N), nitrite (NO_2-N), and nitrate (NO_3-N) concentrations were measured in the aqueous phase of the AGS-EBPR bioreactor.

(C) Oxygen and pH signals were analyzed by the lab-scale AGS-EBPR probes.

The pH was regulated to remain between 7.3 and 8.5. The O_2 signal amplitude fluctuation was dependent on the height of the sludge bed (the O_2 probe was positioned at half of the height in the AGS-EBPR bioreactor).

The data points with values below the detection limit are represented with a smaller point marker.

6.3.6 Following dynamics of intracellular storage polymers with Raman-FISH

The experiments performed so far in this chapter were performed on the AGS-EBPR level without distinction between the contribution of the different species of the microbial community. To assess the effect of glycine on defined phylogenetic groups, the Raman-FISH approach can be used (Fernando et al., 2019). The Raman-FISH approach combines phenotypic data from single-cell Raman microspectroscopy with the phylogenetic information using specific Fluorescence *In situ* Hybridization (FISH) probes (Huang et al., 2007). Furthermore, the Raman-FISH is an *in-situ* method providing information on the microscale structure of the biological sample (Ivleva et al., 2017). The bulk measurements indicated that glycine was not consumed during the anaerobic phase, but phosphate was released due to polyP hydrolysis. Raman microspectroscopy would allow quantifying the three intracellular polymers polyP, glycogen, and PHA and showing on a single cell level that glycine triggered polyP hydrolysis but did not lead to PHA formation.
Figure 6.9 presents the visualization of the *Ca.* Accumulibacter genus using the FISH probe PAO 651 and the Raman signal of a single cell. With this AGS sample, the microscopes used for the Raman-FISH did unfortunately not have sufficient sensitivity to acquire the fluorescence and Raman signals simultaneously. This issue can be solved using instruments equipped with different optical setups or by performing the Raman and FISH signal acquisition sequentially (e.g., using a calcium fluoride microscope slides with a gold grid deposition for single cells referencing purposes). With additional effort, one would be able to confirm our hypothesis at the single cell level that glycine triggers polyP hydrolysis in *Ca.* Accumulibacter but does not lead to PHA formation.

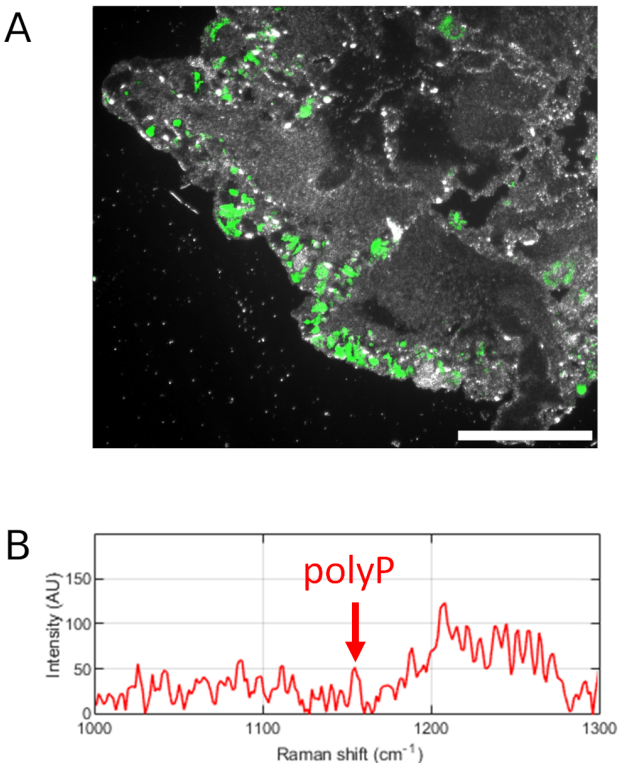

Figure 6.9: **FISH and Raman microspectroscopy**
(A) Example of FISH for *Candidatus* Accumulibacter phosphatis on a 10 µm thin cross-section at the innermost of one biofilm aggregate (brightfield in gray, PAOs in green), scale bar: 250 µm.
(B) Raman spectra of a single cell containing polyP (240 iterations and baseline subtraction). The arrow indicates the strongest Raman peak for polyP at 1170 cm^{-1} in the spectrum.

6.4 General conclusions and perspectives

In the lab-scale AGS-EBPRs studied here, the tests performed with modified influents containing different organic carbon sources during one SBR cycle showed that acetate, propionate, glucose, and probably some amino acids (like aspartate or glutamate) could support the PAO metabolism in contrast to starch and peptone. To know if these substrates are used directly by PAOs or if they need to be transformed (e.g., by glucose fermentation), isotopically labeled substrates could be used, and the labeling in the microbial metabolites followed.

The glycine did not support the PAO metabolism in the AGS-EBPR RA, even if it induced an anaerobic phosphorus release proportional to the glycine concentration of the influent. This observation might be explained by the antimicrobial effect of glycine, which induces active detoxification of the intracellular glycine with efflux pumps against the concentration gradient, causing the hydrolysis of polyP and phosphate release to generate energy during the anaerobic phase. The phosphorus uptake in the aerobic phase by PAOs when the AGS-EBPR RA was fed with glycine as a sole source of organic carbon was likely due to previous PHA storage since the microorganisms barely consumed glycine in this lab-scale AGS-EBPR. This observation indicates that carbon sources inducing an anaerobic phosphorus release must be further characterized before concluding on supporting the PAO metabolism (Oyserman et al., 2016).

In AGS-EBPR RA, the main active PAOs likely belong to *Ca.* Accumulibacter; thus, the results obtained here might agree with Kong et al., 2004. Using a MAR-FISH approach, they found that *Ca.* Accumulibacter phosphatis could assimilate acetate and propionate, but not glucose nor several amino acids, including glycine.

Nguyen et al., 2015 have shown, also using a MAR-FISH approach, that microorganisms belonging to the genus of *Tetrasphaera* were able to consume glycine. And in the microbial community they studied, those microorganisms might have had a PAO metabolism. Here, during the tests with glycine on the AGS-EBPR RA, *Tetrasphaera* was not significantly abundant in the microbial community (supplementary Figure 6.1).

To conclude on the assimilation of the different carbon sources used here, the MAR-FISH approach could be performed with FISH probes targeting the dominant OTUs identified in the 16S rRNA gene amplicon sequencing data.

6.5 Supplementary figures

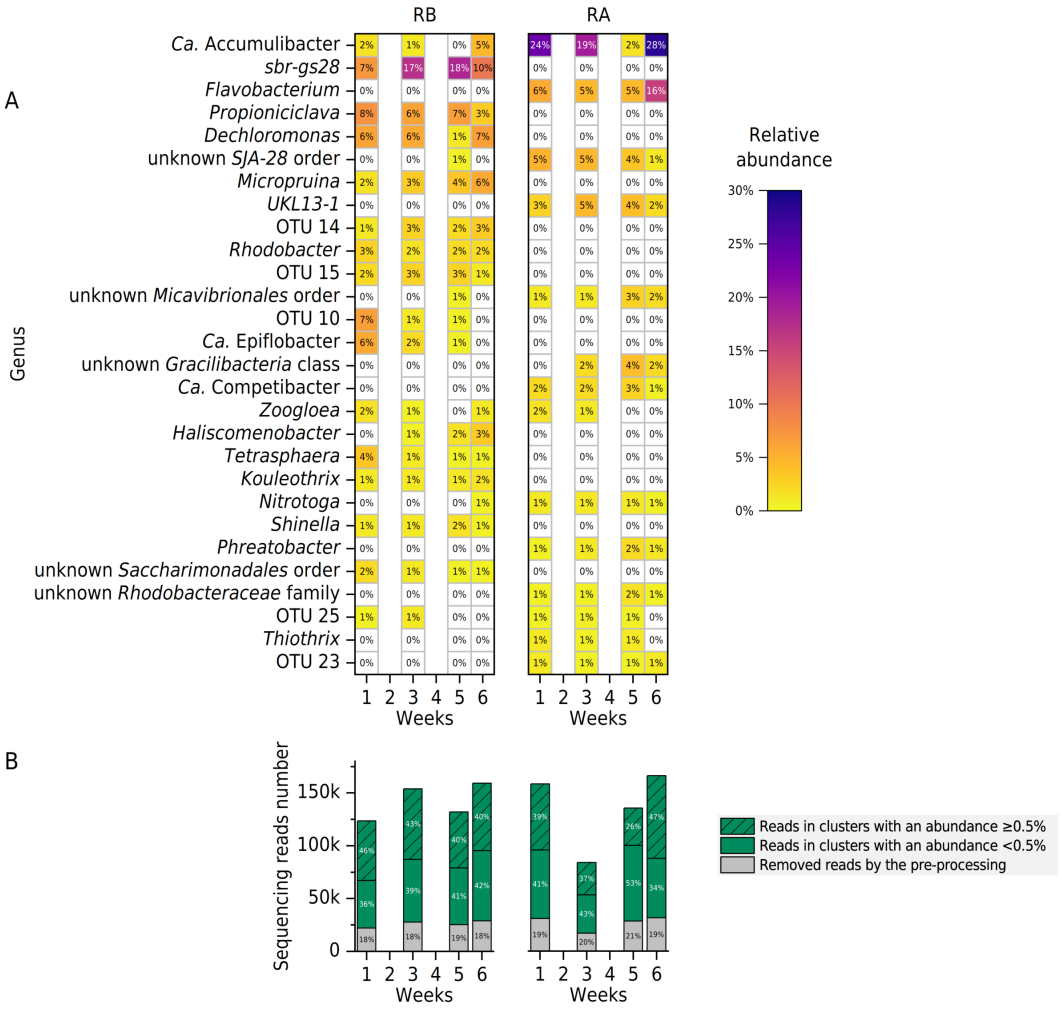

Supplementary Figure 6.1: **Assessment of the stability of the microbial community in bioreactors RB and RA**
The samples were collected to cover the period of the testing with modified influents which were interspersing SBR cycles treating the reference influent
(A) Relative abundance of the OTUs compared to the sample's total number of pre-processed reads.
The OTUs analyzed had an abundance of at least 0.5% of the total number of pre-processed reads in one of the samples. The color scale used displays the relative abundance; the cells in white are below 0.5%.
(B) Overview of the processing of the sequencing reads.
The hatched bars show the reads present in OTUs harboring an abundance higher than 0.5% of the total number of treated reads (displayed in dark green).
The gray bars show the reads not meeting the quality requirement set in the pre-processing.

7 Concluding remarks

The aim of the research work performed in the frame of this thesis was to improve the knowledge of microbial biological phosphorus removal from wastewater. This aim was pursued successfully in a model lab-scale bioreactor operated with Aerobic Granular Sludge (AGS) using different experimental approaches targeting Polyphosphate-Accumulating Organism (PAO) phenotype. In Chapters 3 and 5, the presence of intracellular polyphosphate was used to detect PAOs. In Chapter 6 used the metabolic activity characteristic of PAOs of the anaerobic organic carbon uptake and phosphate release. A complementary research hypothesis tested in Chapter 4 was that primary consumers of the organic carbon sources in the influent (e.g., PAOs) would produce microbial products used as nutrient sources by other microbial community members.

In Chapter 3, an identification of the PAOs responsible for the wastewater phosphorus treatment performances was successfully performed. The approach used was to reveal the presence of intracellular polyphosphate with the fluorescent dye DAPI and identify the labeled cells by 16S rRNA gene amplicon sequencing after sorting using a flow cytometer equipped with a sorting and collection system. In the lab-scale AGS bioreactor studied here, *Ca.* Accumulibacter is likely the main PAO. The method presented here opens the possibility of investigating the PAOs in different EBPR systems. The preliminary results suggest that bacteria from the *Microlunatus* genus might have a PAO metabolism in an AGS-EBPR bioreactor operated with a VFA and fermentable substrate influent.

In Chapter 4, two ^{13}C labeled carbon sources enabled the examination of the sub-groups of microorganisms sustained by those substrates by DNA-SIP. It revealed that acetate was used by PAO belonging to the genus *Ca.* Accumulibacter. This finding is supported by the measure of significant ^{13}C PHA labeling when ^{13}C-acetate was added to the influent. A strain of *Ca.* Accumulibacter present in lower abundance seems capable of using glucose as a carbon source. Glucose was mainly used by *Propionibacteriaceae* unknown genus. The smaller proportion of PHA labeled with ^{13}C-glucose can be explained by its anaerobic consumption by microorganisms not producing PHA in the conditions used here. It would be interesting to distinguish the direct use of glucose to form PHA from a carbon food chain, for example, using NanoSIMS.

In Chapter 5, the preliminary results obtained of the 3D microbial organization of the AGS biofilms indicate that a model of the microbial population organization in concentric layers is too simplistic. The distribution of PAOs microcolonies throughout the biofilm thickness can be explained by the flow of the nutrients from the medium into the biofilm structure irrigated by pores and channels. The proof of concept developed here offers promising possibilities to asses the microbial structure of AGS biofilms using different types of fluorescent staining.

In Chapter 6, the screening of different organic carbon sources showed that acetate, propionate, and probably some amino acids (aspartate and glutamate) could support the PAO metabolism in the conditions used here. Interestingly, it was demonstrated that glycine did not support the PAO metabolism, even if it induced an anaerobic phosphorus release proportional to the glycine concentrations tested in the lab-scale bioreactor studied here.

The panel of experimental approaches presented here can be seen as a toolset to characterize PAOs. For example, the bacteria belonging to the unknown *Propionibacteriaceae* genus detected by the flow cytometry approach as containing polyP were shown with DNA-SIP to use preferentially glucose over acetate. Then the abundance and structure in the AGS biofilm can be assessed with Light Sheet Microscopy, and the type of carbon sources capable of being stored anaerobically can be tested with Raman-FISH.

The results generated in this thesis aim to be helpful for the research community to build further knowledge on PAOs in AGS and EBPR bioreactors. The different approaches used in this thesis to study PAOs, some of them being applied for the first time in this field of research, offers promising possibilities to study these organisms in different wastewater treatment plants and ultimately improve the design and operation of the biological phosphorus removal from wastewater.

Bibliography

Acevedo, B., Oehmen, A., Carvalho, G., Seco, A., Borrás, L., & Barat, R. (2012). Metabolic shift of polyphosphate-accumulating organisms with different levels of polyphosphate storage. *Water Research*, *46*(6), 1889–1900. https://doi.org/10.1016/j.watres.2012.01.003

Achbergerová, L., & Nahálka, J. (2011). Polyphosphate–an ancient energy source and active metabolic regulator. https://doi.org/10.1186/1475-2859-10-63

Adler, A. S. (2019). *The effect of different organic substrates on the microbial communities of aerobic granular wastewater treatment sludge* (Doctoral dissertation). Lausanne, EPFL. https://doi.org/10.5075/epfl-thesis-9678

Akar, A., Akkaya, E. U., Yesiladali, S. K., Çelikyilmaz, G., Çokgor, E. U., Tamerler, C., Orhon, D., & Çakar, Z. P. (2006). Accumulation of polyhydroxyalkanoates by Microlunatus phosphovorus under various growth conditions. *Journal of Industrial Microbiology & Biotechnology*, *33*(3), 215–220. https://doi.org/10.1007/s10295-004-0201-2

Ali, M., Wang, Z., Salam, K. W., Hari, A. R., Pronk, M., van Loosdrecht, M. C. M., & Saikaly, P. E. (2019). Importance of Species Sorting and Immigration on the Bacterial Assembly of Different-Sized Aggregates in a Full-Scale Aerobic Granular Sludge Plant. *Environmental Science & Technology*, *53*(14), 8291–8301. https://doi.org/10.1021/acs.est.8b07303

Allan, R. A., & Miller, J. J. (1980). Influence of S -adenosylmethionine on DAPI-induced fluorescence of polyphosphate in the yeast vacuole. *Canadian Journal of Microbiology*, *26*(8), 912–920. https://doi.org/10.1139/m80-158

Alpkvist, E., Picioreanu, C., van Loosdrecht, M. C., & Heyden, A. (2006). Three-dimensional biofilm model with individual cells and continuum EPS matrix. *Biotechnology and Bioengineering*, *94*(5), 961–979. https://doi.org/10.1002/bit.20917

Alvarez, S., & Jerez, C. A. (2004). Copper Ions Stimulate Polyphosphate Degradation and Phosphate Efflux in Acidithiobacillus ferrooxidans. *Applied and Environmental Microbiology*, *70*(9), 5177–5182. https://doi.org/10.1128/AEM.70.9.5177-5182.2004

Andrew, A. M. (2000). Level Set Methods and Fast Marching Methods Evolving Interfaces in Computational Geometry, Fluid Mechanics, Computer Vision, and Materials Science. *Robotica*, *18*(1), 89–92. https://doi.org/10.1017/S0263574799212404

Angelova, P. R., Agrawalla, B. K., Elustondo, P. A., Gordon, J., Shiba, T., Abramov, A. Y., Chang, Y.-T., & Pavlov, E. V. (2014). In Situ Investigation of Mammalian Inorganic Polyphosphate Localization Using Novel Selective Fluorescent Probes JC-D7 and JC-D8. *ACS Chemical Biology*, *9*(9), 2101–2110. https://doi.org/10.1021/cb5000696

Ardern, E. (1927). The activated sludge process of sewage purification. *J. Soc. Chem. Ind.*, (36), 822–830.

Ardern, E., & Lockett, W. T. (1914). Experiments on the oxidation of sewage without the aid of filters. *Journal of the Society of Chemical Industry*, *33*(10), 523–539. https://doi.org/10.1002/jctb.5000331005

Arrojo, B., Mosquera-Corral, A., Garrido, J. M., & Méndez, R. (2004). Aerobic granulation with industrial wastewater in sequencing batch reactors. *Water Research*, *38*(14-15), 3389–3399. https://doi.org/10.1016/j.watres.2004.05.002

Arvin, E. (1983). Observations Supporting Phosphate Removal by Biologically Mediated Chemical Precipitation – A Review. *Water Science and Technology*, *15*(3-4), 43–63. https://doi.org/10.2166/wst.1983.0107

Bakke, R., & Olsson, P. (1986). Biofilm thickness measurements by light microscopy. *Journal of Microbiological Methods*, *5*(2), 93–98. https://doi.org/10.1016/0167-7012(86)90005-9

Bark, K., Sponner, A., Kämpfer, P., Grund, S., & Dott, W. (1992). Differences in polyphosphate accumulation and phosphate adsorption by Acinetobacter isolates from wastewater producing polyphosphate: AMP phosphotransferase. *Water Research*, *26*(10), 1379–1388. https://doi.org/10.1016/0043-1354(92)90131-M

Barnard, J. L., Dunlap, P., & Steichen, M. (2017). Rethinking the Mechanisms of Biological Phosphorus Removal. *Water Environment Research*, *89*(11), 2043–2054. https://doi.org/10.2175/106143017x15051465919010

Barr, J. J., Cook, A. E., & Bond, P. L. (2010). Granule Formation Mechanisms within an Aerobic Wastewater System for Phosphorus Removal. *Applied and Environmental Microbiology*, *76*(22), 7588–7597. https://doi.org/10.1128/AEM.00864-10

Bartholomew, J. W. (1981). *Stains for Microorganisms in Smears* (Clark, G). Williams; Wilkins.

Bassin, J., Tavares, D., Borges, R., & Dezotti, M. (2019). Development of aerobic granular sludge under tropical climate conditions: The key role of inoculum adaptation under reduced sludge washout for stable granulation. *Journal of Environmental Management*, *230*(April 2017), 168–182. https://doi.org/10.1016/J.JENVMAN.2018.09.072

Baxter, M., & Jensen, T. (1980). A study of methods for in situ X-ray energy dispersive analysis of polyphosphate bodies in Plectonema boryanum. *Archives of Microbiology*, *126*(3), 213–215. https://doi.org/10.1007/BF00409922

Bayer, B., Saito, M. A., McIlvin, M. R., Lücker, S., Moran, D. M., Lankiewicz, T. S., Dupont, C. L., & Santoro, A. E. (2021). Metabolic versatility of the nitrite-oxidizing bacterium Nitrospira marina and its proteomic response to oxygen-limited conditions. *The ISME Journal*, *15*(4), 1025–1039. https://doi.org/10.1038/s41396-020-00828-3

Beccia, M. R., Biver, T., Pardini, A., Spinelli, J., Secco, F., Venturini, M., Busto Vázquez, N., Lopez Cornejo, M. P., Martin Herrera, V. I., & Prado Gotor, R. (2012). The fluorophore 4',6-diamidino-2-phenylindole (DAPI) induces DNA folding in long

double-stranded DNA. *Chemistry - An Asian Journal*, *7*(8), 1803–1810. https://doi.org/10.1002/asia.201200177

Behrens, S., Lösekann, T., Pett-Ridge, J., Weber, P. K., Ng, W. O., Stevenson, B. S., Hutcheon, I. D., Relman, D. a., & Spormann, A. M. (2008). Linking microbial phylogeny to metabolic activity at the single-cell level by using enhanced element labeling-catalyzed reporter deposition fluorescence in situ hybridization (EL-FISH) and NanoSIMS. *Applied and Environmental Microbiology*, *74*(10), 3143–3150. https://doi.org/10.1128/AEM.00191-08

Berg, L., Kirkland, C. M., Seymour, J. D., Codd, S. L., Loosdrecht, M. C. M., & Kreuk, M. K. (2020). Heterogeneous diffusion in aerobic granular sludge. *Biotechnology and Bioengineering*, *117*(12), 3809–3819. https://doi.org/10.1002/bit.27522

Beun, J. J., Hendriks, A., van Loosdrecht, M., Morgenroth, E., Wilderer, P., & Heijnen, J. (1999). Aerobic granulation in a sequencing batch reactor. *Water Research*, *33*(10), 2283–2290. https://doi.org/10.1016/S0043-1354(98)00463-1

Beun, J. J., van Loosdrecht, M., & Heijnen, J. (2002). Aerobic granulation in a sequencing batch airlift reactor. *Water Research*, *36*(3), 702–712. https://doi.org/10.1016/S0043-1354(01)00250-0

Birnie, G., & Rickwood, D. (1978). *Centrifugal Separations in Molecular and Cell Biology* (G. Birnie & D. Rickwood, Eds.). Elsevier. https://doi.org/10.1016/C2013-0-11794-1

Blackall, L. L., Burrell, P. C., Gwilliam, H., Bradford, D., Bond, P. L., & Hugenholtz, P. (1998). The use of 16S rDNA clone libraries to describe the microbial diversity of activated sludge communities. *Water Science and Technology*, *37*(4-5), 451–454. https://doi.org/10.2166/wst.1998.0691

Bochner, B. R. (2009). Global phenotypic characterization of bacteria. *FEMS Microbiology Reviews*, *33*(1), 191–205. https://doi.org/10.1111/j.1574-6976.2008.00149.x

Boschker, H. T. S., Nold, S. C., Wellsbury, P., Bos, D., de Graaf, W., Pel, R., Parkes, R. J., & Cappenberg, T. E. (1998). Direct linking of microbial populations to specific biogeochemical processes by 13C-labelling of biomarkers. *Nature*, *392*(6678), 801–805. https://doi.org/10.1038/33900

Braun, F., Hamelin, J., Gèvaudan, G., & Patureau, D. (2011). Development and application of an enzymatic and cell flotation treatment for the recovery of viable microbial cells from environmental matrices such as anaerobic sludge. *Applied and Environmental Microbiology*, *77*(24), 8487–8493. https://doi.org/10.1128/AEM.05549-11

Brdjanovic, D., Slamet, A., van Loosdrecht, M., Hooijmans, C., Alaerts, G., & Heijnen, J. (1998). Impact of excessive aeration on biological phosphorus removal from wastewater. *Water Research*, *32*(1), 200–208. https://doi.org/10.1016/S0043-1354(97)00183-8

Buchan, L. (1983). Possible Biological Mechanism of Phosphorus Removal. *Water Science and Technology*, *15*(3-4), 87–103. https://doi.org/10.2166/wst.1983.0109

Camacho, C., Coulouris, G., Avagyan, V., Ma, N., Papadopoulos, J., Bealer, K., & Madden, T. L. (2009). BLAST+: Architecture and applications. *BMC Bioinformatics*, *10*, 1–9. https://doi.org/10.1186/1471-2105-10-421

Campo, R., Sguanci, S., Caffaz, S., Mazzoli, L., Ramazzotti, M., Lubello, C., & Lotti, T. (2020). Efficient carbon, nitrogen and phosphorus removal from low C/N real

domestic wastewater with aerobic granular sludge. *Bioresource Technology*, *305*(November 2019), 122961. https://doi.org/10.1016/j.biortech.2020.122961

Carlsson, H. (1997). Calcium phosphate precipitation in biological phosphorus removal systems. *Water Research*, *31*(5), 1047–1055. https://doi.org/10.1016/S0043-1354(96)00282-5

Cavatorta, P., Masotti, L., & Szabo, A. (1985). A time-resolved fluorescence study of 4',6'-diamidine-2-phenylindole dihydrochloride binding to polynucleotides. *Biophysical Chemistry*, *22*(1-2), 11–16. https://doi.org/10.1016/0301-4622(85)80021-1

Cech, J. S., & Hartman, P. (1993). Competition between polyphosphate and polysaccharide accumulating bacteria in enhanced biological phosphate removal systems. *Water Research*, *27*(7), 1219–1225. https://doi.org/10.1016/0043-1354(93)90014-9

Chase, E. S., & Hoffman, R. A. (1998). Resolution of dimly fluorescent particles: A practical measure of fluorescence sensitivity. *Cytometry*, *33*(2), 267–279. https://doi.org/10.1002/(SICI)1097-0320(19981001)33:2<267::AID-CYTO24>3.0.CO;2-R

Chhetri, R. K., Amat, F., Wan, Y., Höckendorf, B., Lemon, W. C., & Keller, P. J. (2015). Whole-animal functional and developmental imaging with isotropic spatial resolution. *Nature Methods*, *12*(12), 1171–1178. https://doi.org/10.1038/nmeth.3632

Chung, K., & Deisseroth, K. (2013). CLARITY for mapping the nervous system. *Nature Methods*, *10*(6), 508–513. https://doi.org/10.1038/nmeth.2481

Claudia R. Binder, Laura de Baan, & Dominic Wittmer. (2019). *Phosphorflüsse der Schweiz* (Bundesamt für Umwelt, Ed.; Bundesamt für Umwelt).

Coats, E. R., Brinkman, C. K., & Lee, S. (2017). Characterizing and contrasting the microbial ecology of laboratory and full-scale EBPR systems cultured on synthetic and real wastewaters. *Water Research*, *108*(208), 124–136. https://doi.org/10.1016/j.watres.2016.10.069

Colls, J. J. (1990). Exchange of trace gases between terrestrial ecosystems and the atmosphere. Edited by M. O. *Weather*, *45*(11), 416–416. https://doi.org/10.1002/j.1477-8696.1990.tb05572.x

Coma, M., Verawaty, M., Pijuan, M., Yuan, Z., & Bond, P. (2012). Enhancing aerobic granulation for biological nutrient removal from domestic wastewater. *Bioresource Technology*, *103*(1), 101–108. https://doi.org/10.1016/j.biortech.2011.10.014

Comeau, Y., Hall, K., Hancock, R., & Oldham, W. (1986). Biochemical model for enhanced biological phosphorus removal. *Water Research*, *20*(12), 1511–1521. https://doi.org/10.1016/0043-1354(86)90115-6

Comolli, L., Kundmann, M., & Downing, K. (2006). Characterization of intact subcellular bodies in whole bacteria by cryo-electron tomography and spectroscopic imaging. *Journal of Microscopy*, *223*(1), 40–52. https://doi.org/10.1111/j.1365-2818.2006.01597.x

Cossarizza, A., Chang, H.-D., Radbruch, A., Akdis, M., Andrä, I., Annunziato, F., Bacher, P., Barnaba, V., Battistini, L., Bauer, W. M., Baumgart, S., Becher, B., Beisker, W., Berek, C., Blanco, A., Borsellino, G., Boulais, P. E., Brinkman, R. R., Büscher, M., … Zimmermann, J. (2017). Guidelines for the use of flow cytometry and cell

sorting in immunological studies. *European Journal of Immunology*, *47*(10), 1584–1797. https://doi.org/10.1002/eji.201646632

Costerton, J. W., Lewandowski, Z., Caldwell, D. E., Korber, D. R., & Lappin-Scott, H. M. (1995). Microbial Biofilms. *Annual Review of Microbiology*, *49*(1), 711–745. https://doi.org/10.1146/annurev.mi.49.100195.003431

Cox, C., Reeder, J. E., Robinson, R. D., Suppes, S. B., & Wheeless, L. L. (1988). Comparison of frequency distributions in flow cytometry. *Cytometry*, *9*(4), 291–298. https://doi.org/10.1002/cyto.990090404

Crocetti, G. R., Banfield, J. F., Keller, J., Bond, P. L., & Blackall, L. L. (2002). Glycogen-accumulating organisms in laboratory-scale and full-scale wastewater treatment processes b bThe GenBank accession numbers for the sequences reported in this paper are given in Methods. *Microbiology*, *148*(11), 3353–3364. https://doi.org/10.1099/00221287-148-11-3353

Daims, H., Stoecker, K., & Wagner, M. (2005). Fluorescence in situ hybridization for the detection of prokaryotes. *Molecular microbial ecology* (1st Edition, p. 21). Taylor & Francis. https://doi.org/https://doi.org/10.4324/9780203503393

de Bruin, L., de Kreuk, M., van der Roest, H., Uijterlinde, C., & van Loosdrecht, M. (2004). Aerobic granular sludge technology: an alternative to activated sludge? *Water Science and Technology*, *49*(11-12), 1–7. https://doi.org/10.2166/wst.2004.0790

Deinema, M. H., van Loosdrecht, M., & Scholten, A. (1985). Some Physiological Characteristics of Acinetobacter spp. Accumulating Large Amounts of Phosphate. *Water Science and Technology*, *17*(11-12), 119–125. https://doi.org/10.2166/wst.1985.0226

de Kreuk, M. K., Heijnen, J., & van Loosdrecht, M. (2005). Simultaneous COD, nitrogen, and phosphate removal by aerobic granular sludge. *Biotechnology and Bioengineering*, *90*(6), 761–769. https://doi.org/10.1002/bit.20470

de Kreuk, M. K., Kishida, N., & van Loosdrecht, M. (2007). Aerobic granular sludge – state of the art. *Water Science & Technology*, *55*(8-9), 75–81. https://doi.org/10.2166/wst.2007.244

de Kreuk, M. K., Picioreanu, C., Hosseini, M., Xavier, J., & van Loosdrecht, M. (2007). Kinetic model of a granular sludge SBR: Influences on nutrient removal. *Biotechnology and Bioengineering*, *97*(4), 801–815. https://doi.org/10.1002/bit.21196

de Kreuk, M. K., & van Loosdrecht, M. (2004). Selection of slow growing organisms as a means for improving aerobic granular sludge stability. *Water Science and Technology*, *49*(11-12), 9–17. https://doi.org/10.2166/wst.2004.0792

de Kreuk, M. K., & van Loosdrecht, M. (2006). Formation of Aerobic Granules with Domestic Sewage. *Journal of Environmental Engineering*, *132*(June), 694–697. https://doi.org/10.1061/(ASCE)0733-9372(2006)132:6(694)

Derlon, N., Wagner, J., da Costa, R. H. R., & Morgenroth, E. (2016). Formation of aerobic granules for the treatment of real and low-strength municipal wastewater using a sequencing batch reactor operated at constant volume. *Water Research*, *105*, 341–350. https://doi.org/10.1016/j.watres.2016.09.007

Dietrich, D., Uhl, B., Sailer, V., Holmes, E. E., Jung, M., Meller, S., & Kristiansen, G. (2013). Improved PCR Performance Using Template DNA from Formalin-Fixed and Paraffin-Embedded Tissues by Overcoming PCR Inhibition. *PLoS ONE*, *8*(10), e77771. https://doi.org/10.1371/journal.pone.0077771

Docampo, R., de Souza, W., Miranda, K., Rohloff, P., & Moreno, S. N. (2005). Acidocalcisomes - Conserved from bacteria to man. *Nature Reviews Microbiology*, *3*(3), 251–261. https://doi.org/10.1038/nrmicro1097

Dolinšek, J., Lagkouvardos, I., Wanek, W., Wagner, M., & Daims, H. (2013). Interactions of nitrifying bacteria and heterotrophs: Identification of a Micavibrio-like putative predator of Nitrospira spp. *Applied and Environmental Microbiology*, *79*(6), 2027–2037. https://doi.org/10.1128/AEM.03408-12

Dreisbach, J. (1988). General Microbiology, Sixth Edition. *Biochemical Education*, *16*(2), 114. https://doi.org/10.1016/0307-4412(88)90095-7

Dunford, E. a., & Neufeld, J. D. (2010). DNA stable-isotope probing (DNA-SIP). *Journal of visualized experiments : JoVE*, (42), 1–7. https://doi.org/10.3791/2027

Edgar, R. (2016). UCHIME2: improved chimera prediction for amplicon sequencing. *bioRxiv*, 074252. https://doi.org/10.1101/074252

Edgar, R. (2018). Updating the 97% identity threshold for 16S ribosomal RNA OTUs. *Bioinformatics*, *34*(14), 2371–2375. https://doi.org/10.1093/bioinformatics/bty113

Eikelboom, D. H., & van Buijsen, H. (1983). *Microscopic sludge investigation manual*.

Eixler, S., Selig, U., & Karsten, U. (2005). Extraction and detection methods for polyphosphate storage in autotrophic planktonic organisms. *Hydrobiologia*, *533*(1-3), 135–143. https://doi.org/10.1007/s10750-004-2406-9

Eppendorf AG. (2015). OD600 Measurements Using Different Photometers. *White Pape*, *28*. https://www.eppendorf.com/product-media/doc/en/148370/Detection_White-Paper_028_BioPhotometer-D30_BioSpectrometer-family_OD600-Measurements-Different-Photometers.pdf

Erb, T. J. (2011). Carboxylases in Natural and Synthetic Microbial Pathways. *Applied and Environmental Microbiology*, *77*(24), 8466–8477. https://doi.org/10.1128/AEM.05702-11

Erdal, U. G., Erdal, Z. K., Daigger, G. T., & Randall, C. W. (2008). Is it PAO-GAO competition or metabolic shift in EBPR system? Evidence from an experimental study. *Water Science and Technology*, *58*(6), 1329–1334. https://doi.org/10.2166/wst.2008.734

Eschenhagen, M., Schuppler, M., & Roske, I. (2003). Molecular characterization of the microbial community structure in two activated sludge systems for the advanced treatment of domestic effluents. *Water Research*, *37*(13), 3224–3232. https://doi.org/10.1016/S0043-1354(03)00136-2

Escudié, F., Auer, L., Bernard, M., Mariadassou, M., Cauquil, L., Vidal, K., Maman, S., Hernandez-Raquet, G., Combes, S., & Pascal, G. (2018). FROGS: Find, Rapidly, OTUs with Galaxy Solution. *Bioinformatics*, *34*(8), 1287–1294. https://doi.org/10.1093/bioinformatics/btx791

Etterer, T., & Wilderer, P. A. (2001). Generation and properties of aerobic granular sludge. *Water Science and Technology*, *43*(3), 19–26. https://doi.org/10.2166/wst.2001.0114

Ezawa, T., Smith, S. E., & Smith, A., F. (2001). Differentiation of polyphosphate metabolism between the extra- and intraradical hyphae of arbuscular mycorrhizal fungi. *New Phytologist*, *149*(3), 555–563. https://doi.org/10.1046/j.1469-8137.2001.00040.x

Ferguson, S. J. (1994). Denitrification and its control. *Antonie van Leeuwenhoek*, *66*(1-3), 89–110. https://doi.org/10.1007/BF00871634

Fernando, E. Y., McIlroy, S. J., Nierychlo, M., Herbst, F. A., Petriglieri, F., Schmid, M. C., Wagner, M., Nielsen, J. L., & Nielsen, P. H. (2019). Resolving the individual contribution of key microbial populations to enhanced biological phosphorus removal with Raman–FISH. *ISME Journal*, *13*(8), 1933–1946. https://doi.org/10.1038/s41396-019-0399-7

Filiou, M. D., Varadarajulu, J., Teplytska, L., Reckow, S., Maccarrone, G., & Turck, C. W. (2012). The 15N isotope effect in Escherichia coli: A neutron can make the difference. *PROTEOMICS*, *12*(21), 3121–3128. https://doi.org/10.1002/pmic.201200209

Flemming, H.-C., & Wingender, J. (2010). The biofilm matrix. *Nature reviews. Microbiology*, *8*(9), 623–633. https://doi.org/10.1080/08927010310000721 90

Florentz, M., Granger, P., & Hartemann, P. (1984). Use of 31P nuclear magnetic resonance spectroscopy and electron microscopy to study phosphorus metabolism of microorganisms from wastewaters. *Applied and Environmental Microbiology*, *47*(3), 519–525. https://doi.org/10.1128/aem.47.3.519-525.1984

French, D., & Edsall, J. T. (1945). The Reactions of Formaldehyde with Amino Acids and Proteins. https://doi.org/10.1016/S0065-3233(08)60627-0

Fuchs, E., Jaffe, J., Long, R., & Azam, F. (2002). Thin laser light sheet microscope for microbial oceanography. *Optics Express*, *10*(2), 145. https://doi.org/10.1364/OE.10.000145

Gayon, U., & G. Dupetit. (1886). *Recherches sur la réduction des nitrates par les infiniment petits*.

Gelb, J., Feser, M., Tkachuk, A., Hsu, G., Chen, S., Chang, H., Fong, T., Hunter, L., Goldberger, I., Lau, S.-H., & Yun, W. (2009). Sub-micron X-ray Computed Tomography for Non-Destructive 3D Visualization and Analysis. *Microscopy and Microanalysis*, *15*(S2), 618–619. https://doi.org/10.1017/S1431927609093623

Gemayel, K. (2019). Quantifying bacterial structure of aerobic granular sludge using image analysis. *Infoscience*. https://infoscience.epfl.ch/record/281648?ln=fr

Ghrist, A. C., & Stauffer, G. V. (1995). The Escherichia coli glycine transport system and its role in the regulation of the glycine cleavage enzyme system. *Microbiology*, *141*(1), 133–140. https://doi.org/10.1099/00221287-141-1-133

Gilbert, M. T. P., Haselkorn, T., Bunce, M., Sanchez, J. J., Lucas, S. B., Jewell, L. D., Marck, E. V., & Worobey, M. (2007). The Isolation of Nucleic Acids from Fixed, Paraffin-Embedded Tissues–Which Methods Are Useful When? *PLoS ONE*, *2*(6), e537. https://doi.org/10.1371/journal.pone.0000537

Gilbert, N. (2009). Environment: The disappearing nutrient. *Nature*, *461*(7265), 716–718. https://doi.org/10.1038/461716a

Gillissen, G., Schumacher, M., & Breuer-Werle, M. (1991). Modulation of Antimicrobial Effects of Beta-Lactams by Amino Acids in vitro. *Zentralblatt für Bakteriologie*, *275*(2), 223–232. https://doi.org/10.1016/S0934-8840(11)80069-1

Ginige, M. P., Keller, J., & Blackall, L. L. (2005). Investigation of an acetate-fed denitrifying microbial community by stable isotope probing, full-cycle rRNA analysis, and fluorescent in situ hybridization-microautoradiography. *Applied and Environmental Microbiology*, *71*(12), 8683–8691. https://doi.org/10.1128/AEM.71.12.8683-8691.2005

Gleisberg, D., Kandler, J., Ulrich, H., & Hartz, P. (1976). Eutrophication and wastewater purification. *Angewandte Chemie (International ed. in English)*, *15*(6), 354–65. https://doi.org/10.1002/anie.197603541

Gonzalez-Gil, G., & Holliger, C. (2014). Aerobic Granules: Microbial Landscape and Architecture, Stages, and Practical Implications. *Applied and Environmental Microbiology*, *80*(11), 3433–3441. https://doi.org/10.1128/AEM.00250-14

Gujer, W. (2006). Activated sludge modelling: past, present and future. *Water Science and Technology*, *53*(3), 111–119. https://doi.org/10.2166/wst.2006.082

Günther, S., Hübschmann, T., Rudolf, M., Eschenhagen, M., Röske, I., Harms, H., & Müller, S. (2008). Fixation procedures for flow cytometric analysis of environmental bacteria. *Journal of microbiological methods*, *75*(1), 127–34. https://doi.org/10.1016/j.mimet.2008.05.017

Günther, S., Trutnau, M., Kleinsteuber, S., Hause, G., Bley, T., Röske, I., Harms, H., & Müller, S. (2009). Dynamics of polyphosphate-accumulating bacteria in wastewater treatment plant microbial communities detected via DAPI (4',6'-diamidino-2-phenylindole) and tetracycline labeling. *Applied and environmental microbiology*, *75*(7), 2111–21. https://doi.org/10.1128/AEM.01540-08

Hanada, S., Liu, W.-T., Shintani, T., Kamagata, Y., & Nakamura, K. (2002). Tetrasphaera elongata sp. nov., a polyphosphate-accumulating bacterium isolated from activated sludge. *International Journal of Systematic and Evolutionary Microbiology*, *52*(3), 883–887. https://doi.org/10.1099/00207713-52-3-883

He, S., Gu, A. Z., & McMahon, K. D. (2008). Progress Toward Understanding the Distribution of Accumulibacter Among Full-Scale Enhanced Biological Phosphorus Removal Systems. *Microbial Ecology*, *55*(2), 229–236. https://doi.org/10.1007/s00248-007-9270-x

Heffer, P., Prud'homme, M. P. R., Muirheid, B., & Isherwood, K. F. (2006). *Phosphorus Fertilisation: Issues and Outlook* (December 1, 2006, Vol. 586). International Fertiliser Society.

Helmer, C., & Kunst, S. (1998). Low temperature effects on phosphorus release and uptake by microorganisms in ebpr plants. *Water Science and Technology*, *37*(4-5). https://doi.org/10.1016/S0273-1223(98)00156-5

Hishinuma, F., Izaki, K., & Takahashi, H. (1969). Effects of glycine and d-amino acids on growth of various microorganisms. *Agricultural and Biological Chemistry*, *33*(11), 1577–1586. https://doi.org/10.1080/00021369.1969.10859511

Hörl, D., Rojas Rusak, F., Preusser, F., Tillberg, P., Randel, N., Chhetri, R. K., Cardona, A., Keller, P. J., Harz, H., Leonhardt, H., Treier, M., & Preibisch, S. (2019). BigStitcher: reconstructing high-resolution image datasets of cleared and expanded samples. *Nature Methods*, *16*(9), 870–874. https://doi.org/10.1038/s41592-019-0501-0

Huang, W. E., Stoecker, K., Griffiths, R., Newbold, L., Daims, H., Whiteley, A. S., & Wagner, M. (2007). Raman-FISH: combining stable-isotope Raman spectroscopy and fluorescence in situ hybridization for the single cell analysis of identity and function. *Environmental Microbiology*, *9*(8), 1878–1889. https://doi.org/10.1111/j.1462-2920.2007.01352.x

Huisken, J., Swoger, J., Del Bene, F., Wittbrodt, J., & Stelzer, E. H. K. (2004). Optical Sectioning Deep Inside Live Embryos by Selective Plane Illumination Microscopy. *Science*, *305*(5686), 1007–1009. https://doi.org/10.1126/science.1100035

Hungate, B. A., Mau, R. L., Schwartz, E., Caporaso, J. G., Dijkstra, P., van Gestel, N., Koch, B. J., Liu, C. M., McHugh, T. A., Marks, J. C., Morrissey, E. M., & Price, L. B. (2015). Quantitative Microbial Ecology through Stable Isotope

Probing. *Applied and Environmental Microbiology*, *81*(21), 7570–7581. https://doi.org/10.1128/AEM.02280-15

Hupfer, M., Glöss, S., Schmieder, P., & Grossart, H.-P. (2008). Methods for Detection and Quantification of Polyphosphate and Polyphosphate Accumulating Microorganisms in Aquatic Sediments. *International Review of Hydrobiology*, *93*(1), 1–30. https://doi.org/10.1002/iroh.200610935

Illumina. (2013). 16S Metagenomic Sequencing Library. *Illumina.com*, (B), 1–28. http://support.illumina.com/content/dam/illumina-support/documents/documentation/chemistry_documentation/16s/16s-metagenomic-library-prep-guide-15044223-b.pdf

Irvine, R. L., & Arthur W. Busch. (1979). Sequencing Batch Biological Reactors: An Overview. *Water Pollution Control Federation*, *51*(2), 235–243. https://www.jstor.org/stable/25039819

Ivanov, V., Tay, S.-L., Liu, Q.-S., Wang, X.-H., Wang, Z.-W., & Tay, J.-H. (2005). Formation and structure of granulated microbial aggregates used in aerobic wastewater treatment. *Water Science and Technology*, *52*(7), 13–19. https://doi.org/10.2166/wst.2005.0175

Ivanov, V., Wang, X.-H., Tay, S. T.-L., & Tay, J.-H. (2006). Bioaugmentation and enhanced formation of microbial granules used in aerobic wastewater treatment. *Applied Microbiology and Biotechnology*, *70*(3), 374–381. https://doi.org/10.1007/s00253-005-0088-5

Ivleva, N. P., Kubryk, P., & Niessner, R. (2017). Raman microspectroscopy, surface-enhanced Raman scattering microspectroscopy, and stable-isotope Raman microspectroscopy for biofilm characterization. *Analytical and Bioanalytical Chemistry*, *409*(18), 4353–4375. https://doi.org/10.1007/s00216-017-0303-0

James Barnard. (1976). A review of biological phosphorus removal in the activated sludge process. *Water S.A*, *2*(3), 136–144.

Jehmlich, N., Schmidt, F., von Bergen, M., Richnow, H.-H., & Vogt, C. (2008). Protein-based stable isotope probing (Protein-SIP) reveals active species within anoxic mixed cultures. *The ISME Journal*, *2*(11), 1122–1133. https://doi.org/10.1038/ismej.2008.64

Jing, S., Benefield, L., & Hill, W. (1992). Observations relating to enhanced phosphorus removal in biological systems. *Water Research*, *26*(2), 213–223. https://doi.org/10.1016/0043-1354(92)90221-O

Jossi, M., Fromin, N., Tarnawski, S., Kohler, F., Gillet, F., Aragno, M., & Hamelin, J. (2006). How elevated pCO2 modifies total and metabolically active bacterial communities in the rhizosphere of two perennial grasses grown under field conditions. *FEMS Microbiology Ecology*, *55*(3), 339–350. https://doi.org/10.1111/j.1574-6941.2005.00040.x

Kaewpipat, K., & Grady, C. P. (2002). Microbial population dynamics in laboratory-scale activated sludge reactors. *Water Science and Technology*, *46*(1-2), 19–27. https://doi.org/10.2166/wst.2002.0450

Kämpfer, P., Erhart, R., Beimfohr, C., Böhringer, J., Wagner, M., & Amann, R. (1996). Characterization of bacterial communities from activated sludge: Culture-dependent numerical identification versus in situ identification using group- and genus-specific rRNA-targeted oligonucleotide probes. *Microbial Ecology*, *32*(2). https://doi.org/10.1007/BF00185883

Kawaharasaki, M., Tanaka, H., Kanagawa, T., & Nakamura, K. (1999). In situ identification of polyphosphate-accumulating bacteria in activated sludge by dual staining with rRNA-targeted oligonucleotide probes and 4,6-diamidino-2-phenylindol (DAPI) at a polyphosphate-probing concentration. *Water Research*, *33*(1), 257–265. https://doi.org/10.1016/S0043-1354(98)00183-3

Keller, P. J., Schmidt, A. D., Wittbrodt, J., & Stelzer, E. H. (2008). Reconstruction of Zebrafish Early Embryonic Development by Scanned Light Sheet Microscopy. *Science*, *322*(5904), 1065–1069. https://doi.org/10.1126/science.1162493

Keller, P. J., & Stelzer, E. H. K. (2010). Digital Scanned Laser Light Sheet Fluorescence Microscopy. *Cold Spring Harbor Protocols*, *2010*(5), pdb.top78–pdb.top78. https://doi.org/10.1101/pdb.top78

Kim, J. M., Lee, H. J., Lee, D. S., & Jeon, C. O. (2013). Characterization of the Denitrification-Associated Phosphorus Uptake Properties of "Candidatus Accumulibacter phosphatis" Clades in Sludge Subjected to Enhanced Biological Phosphorus Removal. *Applied and Environmental Microbiology*, *79*(6), 1969–1979. https://doi.org/10.1128/AEM.03464-12

Knig, D., King, P., Laforge, G., D'Arcy, H., Champeau, C., Pragt, E., & Skeet, J. (2015). *Groovy in Action*. Manning Publications Co.

Kong, Y., Beer, M., Seviour, R. J., Lindrea, K. C., & Rees, G. N. (2001). Structure and Functional Analysis of the Microbial Community in an Aerobic: Anaerobic Sequencing Batch Reactor (SBR) with no Phosphorus Removal. *Systematic and Applied Microbiology*, *24*(4), 597–609. https://doi.org/10.1078/0723-2020-00075

Kong, Y., Nielsen, J. L., & Nielsen, P. H. (2004). Microautoradiographic Study of Rhodocyclus -Related Polyphosphate-Accumulating Bacteria in Full-Scale Enhanced Biological Phosphorus Removal Plants. *Applied and Environmental Microbiology*, *70*(9), 5383–5390. https://doi.org/10.1128/AEM.70.9.5383-5390.2004

Kong, Y., Nielsen, J. L., & Nielsen, P. H. (2005). Identity and ecophysiology of uncultured actinobacterial polyphosphate-accumulating organisms in full-scale enhanced biological phosphorus removal plants. *Applied and Environmental Microbiology*, *71*(7), 4076–4085. https://doi.org/10.1128/AEM.71.7.4076-4085.2005

Kong, Y., Xia, Y., & Nielsen, P. H. (2008). Activity and identity of fermenting microorganisms in full-scale biological nutrient removing wastewater treatment plants. *Environmental Microbiology*, *10*(8), 2008–2019. https://doi.org/10.1111/j.1462-2920.2008.01617.x

Kornberg, A., Rao, N. N., & Ault-Riché, D. (1999). Inorganic polyphosphate: a molecule of many functions. *Annual review of biochemistry*, *68*, 89–125. https://doi.org/10.1146/annurev.biochem.68.1.89

Kortstee, G. J., Appeldoorn, K. J., Bonting, C. F., Niel, E. W., & Veen, H. W. (1994). Biology of polyphosphate-accumulating bacteria involved in enhanced biological phosphorus removal. *FEMS Microbiology Reviews*, *15*(2-3), 137–153. https://doi.org/10.1111/j.1574-6976.1994.tb00131.x

Kristiansen, R., Nguyen, H. T. T., Saunders, A. M., Nielsen, J. L., Wimmer, R., Le, V. Q., McIlroy, S. J., Petrovski, S., Seviour, R. J., Calteau, A., Nielsen, K. L., & Nielsen, P. H. (2013). A metabolic model for members of the genus Tetrasphaera involved in enhanced biological phosphorus removal. *The ISME journal*, *7*(3), 543–54. https://doi.org/10.1038/ismej.2012.136

Kuba, T., Smolders, G., van Loosdrecht, M. C. M., & Heijnen, J. J. (1993). Biological Phosphorus Removal from Wastewater by Anaerobic-Anoxic Sequencing Batch Reactor. *Water Science and Technology*, *27*(5-6), 241–252. https://doi.org/10.2166/wst.1993.0504

Kwapinski, W., Kolinovic, I., & Leahy, J. J. (2021). Sewage Sludge Thermal Treatment Technologies with a Focus on Phosphorus Recovery: A Review. *Waste and Biomass Valorization*, *12*(11), 5837–5852. https://doi.org/10.1007/s12649-020-01280-2

Langer, S., Vogts, A., & Schulz-Vogt, H. N. (2018). Simultaneous Visualization of Enzymatic Activity in the Cytoplasm and at Polyphosphate Inclusions in Beggiatoa sp. Strain 35Flor Incubated with 18O-Labeled Water. *mSphere*, *3*(6). https://doi.org/10.1128/mSphere.00489-18

Layer, M. (2021). *The effect of particulate organic substrate on the formation, composition and performance of aerobic granular sludge* (Doctoral dissertation). ETH Zurich. https://doi.org/10.3929/ethz-b-000474564

Layer, M., Adler, A., Reynaert, E., Hernandez, A., Pagni, M., Morgenroth, E., Holliger, C., & Derlon, N. (2019). Organic substrate diffusibility governs microbial community composition, nutrient removal performance and kinetics of granulation of aerobic granular sludge. *Water Research X*, *4*, 100033. https://doi.org/10.1016/j.wroa.2019.100033

Layer, M., Brison, A., Villodres, M. G., Stähle, M., Házi, F., Takács, I., Morgenroth, E., & Derlon, N. (2022). Microbial conversion pathways of particulate organic substrate conversion in aerobic granular sludge systems: limited anaerobic conversion and the essential role of flocs. *Environmental Science: Water Research & Technology*, *8*(6), 1236–1251. https://doi.org/10.1039/D1EW00841B

Lee, N., Nielsen, P. H., Andreasen, K. H., Juretschko, S., Nielsen, J. L., Schleifer, K.-H., & Wagner, M. (1999). Combination of Fluorescent In Situ Hybridization and Microautoradiography—a New Tool for Structure-Function Analyses in Microbial Ecology. *Applied and Environmental Microbiology*, *65*(3), 1289–1297. https://doi.org/10.1128/AEM.65.3.1289-1297.1999

Lemaire, R., Webb, R. I., & Yuan, Z. (2008). Micro-scale observations of the structure of aerobic microbial granules used for the treatment of nutrient-rich industrial wastewater. *The ISME Journal*, *2*(5), 528–541. https://doi.org/10.1038/ismej.2008.12

Lemos, P., Viana, C., Salgueiro, E., Ramos, A., Crespo, J., & Reis, M. (1998). Effect of carbon source on the formation of polyhydroxyalkanoates (PHA) by a phosphate-accumulating mixed culture. *Enzyme and Microbial Technology*, *22*(8), 662–671. https://doi.org/10.1016/S0141-0229(97)00243-3

Leventhal, G. E., Boix, C., Kuechler, U., Enke, T. N., Sliwerska, E., Holliger, C., & Cordero, O. X. (2018). Strain-level diversity drives alternative community types in millimetre-scale granular biofilms. *Nature Microbiology*, *3*(11), 1295–1303. https://doi.org/10.1038/s41564-018-0242-3

Li, Z., Kuba, T., & Kusuda, T. (2006). Aerobic granular sludge: a promising technology for decentralised wastewater treatment. *Water Science & Technology*, *53*(9), 79–85. https://doi.org/10.2166/wst.2006.278

Lin, Y., de Kreuk, M., van Loosdrecht, M., & Adin, A. (2010). Characterization of alginate-like exopolysaccharides isolated from aerobic granular sludge in pilot-plant.

Water Research, *44*(11), 3355–3364. https://doi.org/10.1016/j.watres.2010.03.019

Liu, L., Sheng, G. P., Liu, Z. F., Li, W. W., Zeng, R. J., Lee, D. J., Liu, J. X., & Yu, H. Q. (2010). Characterization of multiporous structure and oxygen transfer inside aerobic granules with the percolation model. *Environmental Science and Technology*, *44*(22), 8535–8540. https://doi.org/10.1021/es102437a

Liu, W.-T., Nielsen, A. T., Wu, J.-H., Tsai, C.-S., Matsuo, Y., & Molin, S. (2001). In situ identification of polyphosphate- and polyhydroxyalkanoate-accumulating traits for microbial populations in a biological phosphorus removal process. *Environmental Microbiology*, *3*(2), 110–122. https://doi.org/10.1046/j.1462-2920.2001.00164.x

Liu, X.-W., Sheng, G.-P., & Yu, H.-Q. (2009). Physicochemical characteristics of microbial granules. *Biotechnology Advances*, *27*(6), 1061–1070. https://doi.org/10.1016/j.biotechadv.2009.05.020

Lochmatter, S., Gonzalez-Gil, G., & Holliger, C. (2013). Optimized aeration strategies for nitrogen and phosphorus removal with aerobic granular sludge. *Water Research*, *47*(16), 6187–6197. https://doi.org/10.1016/j.watres.2013.07.030

Lochmatter, S., & Holliger, C. (2014). Optimization of operation conditions for the startup of aerobic granular sludge reactors biologically removing carbon, nitrogen, and phosphorous. *Water research*, *59*, 58–70. https://doi.org/10.1016/j.watres.2014.04.011

Lochmatter, S., Maillard, J., & Holliger, C. (2014). Nitrogen removal over nitrite by aeration control in aerobic granular sludge sequencing batch reactors. *International journal of environmental research and public health*, *11*(7), 6955–78. https://doi.org/10.3390/ijerph110706955

Lopez-Vazquez, C. M., Oehmen, A., Hooijmans, C. M., Brdjanovic, D., Gijzen, H. J., Yuan, Z., & van Loosdrecht, M. C. M. (2009). Modeling the PAO-GAO competition: Effects of carbon source, pH and temperature. *Water Research*, *43*(2), 450–462. https://doi.org/10.1016/j.watres.2008.10.032

Lorenz, B., Münkner, J., & Oliveira, M. (1997). A novel method for determination of inorganic polyphosphates using the fluorescent dye Fura-2. *Analytical . . .*, *246*(2), 176–84. https://doi.org/10.1006/abio.1996.9998

Lu, H., Oehmen, A., Virdis, B., Keller, J., & Yuan, Z. (2006). Obtaining highly enriched cultures of Candidatus Accumulibacter phosphates through alternating carbon sources. *Water Research*, *40*(20), 3838–3848. https://doi.org/10.1016/j.watres.2006.09.004

Maecker, H. T., & Trotter, J. (2006). Flow cytometry controls, instrument setup, and the determination of positivity. *Cytometry Part A*, *69*(9), 1037–1042. https://doi.org/10.1002/cyto.a.20333

Mahé, F., Rognes, T., Quince, C., de Vargas, C., & Dunthorn, M. (2014). Swarm: Robust and fast clustering method for amplicon-based studies. *PeerJ*, *2014*(1), 1–13. https://doi.org/10.7717/peerj.593

Mahé, F., Rognes, T., Quince, C., de Vargas, C., & Dunthorn, M. (2015). Swarmv2: Highly-scalable and high-resolution amplicon clustering. *PeerJ*, *2015*(12), 1–12. https://doi.org/10.7717/peerj.1420

Maixner, F., Noguera, D. R., Anneser, B., Stoecker, K., Wegl, G., Wagner, M., & Daims, H. (2006). Nitrite concentration influences the population structure of Nitrospira-

like bacteria. *Environmental microbiology*, *8*(8), 1487–95. https://doi.org/10.1111/j.1462-2920.2006.01033.x

Majed, N., & Gu, A. Z. (2010). Application of Raman Microscopy for Simultaneous and Quantitative Evaluation of Multiple Intracellular Polymers Dynamics Functionally Relevant to Enhanced Biological Phosphorus Removal Processes. *Environmental Science & Technology*, *44*(22), 8601–8608. https://doi.org/10.1021/es1016526

Majed, N., Li, Y., & Gu, A. Z. (2012). Advances in techniques for phosphorus analysis in biological sources. *Current Opinion in Biotechnology*, *23*(6), 852–859. https://doi.org/10.1016/j.copbio.2012.06.002

Mañas, A., Biscans, B., & Spérandio, M. (2011). Biologically induced phosphorus precipitation in aerobic granular sludge process. *Water Research*, *45*(12), 3776–3786. https://doi.org/10.1016/j.watres.2011.04.031

Mangiafico, S. (2016). Summary and Analysis of Extension Program Evaluation in R, version 1.18.8. *Buildings*.

Martin, M. (2011). Cutadapt removes adapter sequences from high-throughput sequencing reads. *EMBnet.journal*, *17*(1), 10. https://doi.org/10.14806/ej.17.1.200

Maszenan, A. M., Seviour, R. J., Patel, B. K., Schumann, P., Burghardt, J., Tokiwa, Y., & Stratton, H. M. (2000). Three isolates of novel polyphosphate-accumulating gram-positive cocci, obtained from activated sludge, belong to a new genus, Tetrasphaera gen. nov., and description of two new species, Tetrasphaera japonica sp. nov. and Tetrasphaera australiensis sp. nov. *International Journal of Systematic and Evolutionary Microbiology*, *50*(2), 593–603. https://doi.org/10.1099/00207713-50-2-593

Matsumoto, S., Katoku, M., Saeki, G., Terada, A., Aoi, Y., Tsuneda, S., Picioreanu, C., & van Loosdrecht, M. C. M. (2010). Microbial community structure in autotrophic nitrifying granules characterized by experimental and simulation analyses. *Environmental Microbiology*, *12*(1), 192–206. https://doi.org/10.1111/j.1462-2920.2009.02060.x

McIlroy, S. J., Albertsen, M., Andresen, E. K., Saunders, A. M., Kristiansen, R., Stokholm-Bjerregaard, M., Nielsen, K. L., & Nielsen, P. H. (2014). Candidatus Competibacter-lineage genomes retrieved from metagenomes reveal functional metabolic diversity. *The ISME Journal*, *8*(3), 613–624. https://doi.org/10.1038/ismej.2013.162

McIlroy, S. J., Onetto, C. A., McIlroy, B., Herbst, F. A., Dueholm, M. S., Kirkegaard, R. H., Fernando, E., Karst, S. M., Nierychlo, M., Kristensen, J. M., Eales, K. L., Grbin, P. R., Wimmer, R., & Nielsen, P. H. (2018). Genomic and in Situ Analyses reveal the Micropruina spp. as Abundant fermentative glycogen accumulating organisms in enhanced biological phosphorus removal systems. *Frontiers in Microbiology*, *9*(MAY), 1–12. https://doi.org/10.3389/fmicb.2018.01004

McMahon, K. D., Yilmaz, S., He, S., Gall, D. L., Jenkins, D., & Keasling, J. D. (2007). Polyphosphate kinase genes from full-scale activated sludge plants. *Applied Microbiology and Biotechnology*, *77*(1), 167–173. https://doi.org/10.1007/s00253-007-1122-6

McSwain, B. S., Irvine, R. L., & Wilderer, P. a. (2004). The effect of intermittent feeding on aerobic granule structure. *Water Science and Technology*, *49*(11-12), 19–25.

Meselson, M., Stahl, F. W., & Vinograd, J. (1957). Equilibrium Sedimentation of Macromolecules in Density Gradients. *Proceedings of the National Academy of Sciences*, *43*(7), 581–588. https://doi.org/10.1073/pnas.43.7.581

Mielczarek, A. T., Nguyen, H. T. T., Nielsen, J. L., & Nielsen, P. H. (2013). Population dynamics of bacteria involved in enhanced biological phosphorus removal in Danish wastewater treatment plants. *Water Research*, *47*(4), 1529–1544. https://doi.org/10.1016/j.watres.2012.12.003

Millard, P., Portais, J.-C., & Mendes, P. (2015). Impact of kinetic isotope effects in isotopic studies of metabolic systems. *BMC Systems Biology*, *9*(1), 64. https://doi.org/10.1186/s12918-015-0213-8

Mino, T. (2000). Microbial selection of polyphosphate-accumulating bacteria in activated sludge wastewater treatment processes for enhanced biological phosphate removal. *Biochemistry. Biokhimiia*, *65*(3), 341–8. http://www.ncbi.nlm.nih.gov/pubmed/10739477

Mino, T., Van Loosdrecht, M. C. M., & Heijnen, J. J. (1998). Microbiology and biochemistry of the enhanced biological phosphate removal process. *Water Research*, *32*(11), 3193–3207. https://doi.org/10.1016/S0043-1354(98)00129-8

Mitri, S., & Foster, K. R. (2013). The genotypic view of social interactions in microbial communities. *Annual review of genetics*, *47*, 247–73. https://doi.org/10.1146/annurev-genet-111212-133307

Miyauchi, R., Oki, K., Aoi, Y., & Tsuneda, S. (2007). Diversity of Nitrite Reductase Genes in Candidatus Accumulibacter phosphatis-Dominated Cultures Enriched by Flow-Cytometric Sorting. *Applied and Environmental Microbiology*, *73*(16), 5331–5337. https://doi.org/10.1128/AEM.00175-07

Mohlman, F. M. (1934). The Sludge Index. *Sewage Works Journal*, *6*(1), 119–122.

Morgenroth, E., Sherden, T., Van Loosdrecht, M., Heijnen, J., & Wilderer, P. (1997). Aerobic granular sludge in a sequencing batch reactor. *Water Research*, *31*(12), 3191–3194. https://doi.org/10.1016/S0043-1354(97)00216-9

Mosqueracorral, a., Dekreuk, M., Heijnen, J., & Vanloosdrecht, M. (2005). Effects of oxygen concentration on N-removal in an aerobic granular sludge reactor. *Water Research*, *39*(12), 2676–2686. https://doi.org/10.1016/j.watres.2005.04.065

Mudaly, D. D., Atkinson, B. W., & Bux, F. (2001). 16S rRNA in situ probing for the determination of the family level community structure implicated in enhanced biological nutrient removal. *Water Science and Technology*, *43*(1), 91–98. https://doi.org/10.2166/wst.2001.0022

Murray, R. G., Doetsch, R. N., & Robinow, C. F. (1994). *Determinative and cytological light microscopy*.

Murray, R. G., & Stackebrandt, E. (1995). Taxonomic Note: Implementation of the Provisional Status Candidatus for Incompletely Described Procaryotes. *International Journal of Systematic Bacteriology*, *45*(1), 186–187. https://doi.org/10.1099/00207713-45-1-186

Muszynski, A., & Miłobedzka, A. (2015). The effects of carbon/phosphorus ratio on polyphosphate- and glycogen-accumulating organisms in aerobic granular sludge. *International Journal of Environmental Science and Technology*, *12*(9), 3053–3060. https://doi.org/10.1007/s13762-015-0828-8

Muyzer, G., de Waal, E. C., & Uitterlinden, A. G. (1993). Profiling of complex microbial populations by denaturing gradient gel electrophoresis analysis of polymerase

chain reaction-amplified genes coding for 16S rRNA. *Applied and Environmental Microbiology*, *59*(3), 695–700. https://doi.org/10.1128/aem.59.3.695-700.1993

Nakamura, K., Iizuka, R., Nishi, S., Yoshida, T., Hatada, Y., Takaki, Y., Iguchi, A., Yoon, D. H., Sekiguchi, T., Shoji, S., & Funatsu, T. (2016). Culture-independent method for identification of microbial enzyme-encoding genes by activity-based single-cell sequencing using a water-in-oil microdroplet platform. *Scientific Reports*, *6*(1), 22259. https://doi.org/10.1038/srep22259

Nakamura, K., Hiraishi, A., Yoshimi, Y., Kawaharasaki, M., Masuda, K., & Kamagata, Y. (1995). Microlunatus phosphovorus gen. nov., sp. nov., a New Gram-Positive Polyphosphate-Accumulating Bacterium Isolated from Activated Sludge. *International Journal of Systematic Bacteriology*, *45*(1), 17–22. https://doi.org/10.1099/00207713-45-1-17

Nguyen, H. T. T., Kristiansen, R., Vestergaard, M., Wimmer, R., & Nielsen, P. H. (2015). Intracellular accumulation of glycine in polyphosphate-accumulating organisms in activated sludge, a novel storage mechanism under dynamic anaerobic-aerobic conditions. *Applied and Environmental Microbiology*, *81*(14), 4809–4818. https://doi.org/10.1128/AEM.01012-15

Nguyen, H. T. T., Le, V. Q., Hansen, A. A., Nielsen, J. L., & Nielsen, P. H. (2011). High diversity and abundance of putative polyphosphate-accumulating Tetrasphaera-related bacteria in activated sludge systems. *FEMS microbiology ecology*, *76*(2), 256–67. https://doi.org/10.1111/j.1574-6941.2011.01049.x

Nguyen, H. T. T., Nielsen, J. L., & Nielsen, P. H. (2012). Candidatus Halomonas phosphatis', a novel polyphosphate-accumulating organism in full-scale enhanced biological phosphorus removal plants. *Environmental Microbiology*, *14*(10), 2826–2837. https://doi.org/10.1111/j.1462-2920.2012.02826.x

Nielsen, J. L., Nguyen, H., Meyer, R. L., & Nielsen, P. H. (2012). Identification of glucose-fermenting bacteria in a full-scale enhanced biological phosphorus removal plant by stable isotope probing. *Microbiology (United Kingdom)*, *158*(7), 1818–1825. https://doi.org/10.1099/mic.0.058818-0

Nielsen, P. H., McIlroy, S. J., Albertsen, M., & Nierychlo, M. (2019). Re-evaluating the microbiology of the enhanced biological phosphorus removal process. *Current Opinion in Biotechnology*, *57*, 111–118. https://doi.org/10.1016/j.copbio.2019.03.008

Nielsen, P. H., Mielczarek, A. T., Kragelund, C., Nielsen, J. L., Saunders, A. M., Kong, Y., Hansen, A. A., & Vollertsen, J. (2010). A conceptual ecosystem model of microbial communities in enhanced biological phosphorus removal plants. *Water Research*, *44*(17), 5070–5088. https://doi.org/10.1016/j.watres.2010.07.036

Nierychlo, M., Andersen, K. S., Xu, Y., Green, N., Jiang, C., Albertsen, M., Dueholm, M. S., & Nielsen, P. H. (2020). MiDAS 3: An ecosystem-specific reference database, taxonomy and knowledge platform for activated sludge and anaerobic digesters reveals species-level microbiome composition of activated sludge. *Water Research*, *182*, 115955. https://doi.org/10.1016/j.watres.2020.115955

Oehmen, A., Carvalho, G., Lopez-Vazquez, C., van Loosdrecht, M., & Reis, M. (2010). Incorporating microbial ecology into the metabolic modelling of polyphosphate accumulating organisms and glycogen accumulating organisms. *Water Research*, *44*(17), 4992–5004. https://doi.org/10.1016/j.watres.2010.06.071

Oehmen, A., Keller-Lehmann, B., Zeng, R. J., Yuan, Z., & Keller, J. (2005). Optimisation of poly-β-hydroxyalkanoate analysis using gas chromatography for enhanced biological phosphorus removal systems. *Journal of Chromatography A*, *1070*(1-2), 131–136. https://doi.org/10.1016/j.chroma.2005.02.020

Oehmen, A., Lemos, P. C., Carvalho, G., Yuan, Z., Keller, J., Blackall, L. L., & Reis, M. a. M. (2007). Advances in enhanced biological phosphorus removal: from micro to macro scale. *Water research*, *41*(11), 2271–300. https://doi.org/10.1016/j.watres.2007.02.030

Oehmen, A., Yuan, Z., Blackall, L. L., & Keller, J. (2005). Comparison of acetate and propionate uptake by polyphosphate accumulating organisms and glycogen accumulating organisms. *Biotechnology and Bioengineering*, *91*(2), 162–168. https://doi.org/10.1002/bit.20500

Oehmen, A., Zeng, R. J., Saunders, A. M., Blackall, L. L., Keller, J., & Yuan, Z. (2006). Anaerobic and aerobic metabolism of glycogen-accumulating organisms selected with propionate as the sole carbon source. *Microbiology*, *152*(9), 2767–2778. https://doi.org/10.1099/mic.0.28065-0

Ohtake, H., Takahashi, K., Tsuzuki, Y., & Toda, K. (1985). Uptake and release of phosphate by a pure culture of Acinetobacter calcoaceticus. *Water Research*, *19*(12), 1587–1594. https://doi.org/10.1016/0043-1354(85)90404-X

Onda, S., & Takii, S. (2002). Isolation and characterization of a Gram-positive polyphosphate-accumulating bacterium. *The Journal of general and applied microbiology*, *48*(3), 125–33. http://www.ncbi.nlm.nih.gov/pubmed/12469295

Oyserman, B. O., Noguera, D. R., Del Rio, T. G., Tringe, S. G., & McMahon, K. D. (2016). Metatranscriptomic insights on gene expression and regulatory controls in Candidatus Accumulibacter phosphatis. *ISME Journal*, *10*(4), 810–822. https://doi.org/10.1038/ismej.2015.155

Parks, D. H., Chuvochina, M., Waite, D. W., Rinke, C., Skarshewski, A., Chaumeil, P.-A., & Hugenholtz, P. (2018). A standardized bacterial taxonomy based on genome phylogeny substantially revises the tree of life. *Nature Biotechnology*, *36*(10), 996–1004. https://doi.org/10.1038/nbt.4229

Parthasarathy, R. (2018). Monitoring microbial communities using light sheet fluorescence microscopy. *Current Opinion in Microbiology*, *43*, 31–37. https://doi.org/10.1016/j.mib.2017.11.008

Paula, A. J., Hwang, G., & Koo, H. (2020). Dynamics of bacterial population growth in biofilms resemble spatial and structural aspects of urbanization. *Nature Communications*, *11*(1), 1354. https://doi.org/10.1038/s41467-020-15165-4

Pepe-Ranney, C., Campbell, A. N., Koechli, C. N., Berthrong, S., & Buckley, D. H. (2016). Unearthing the Ecology of Soil Microorganisms Using a High Resolution DNA-SIP Approach to Explore Cellulose and Xylose Metabolism in Soil. *Frontiers in Microbiology*, *7*. https://doi.org/10.3389/fmicb.2016.00703

Picioreanu, C., van Loosdrecht, M. C. M., & Heijnen, J. J. (2000). A theoretical study on the effect of surface roughness on mass transport and transformation in biofilms. *Biotechnology and Bioengineering*, *68*(4), 355–369. https://doi.org/10.1002/(SICI)1097-0290(20000520)68:4<355::AID-BIT1>3.0.CO;2-A

Poisson, S. D. (1837). *Recherches sur la probabilité des jugements en matière criminelle et en matière civile précédées des règles générales du calcul des probabilités* (Bachelier, Ed.). (Paris). https://gallica.bnf.fr/ark:/12148/bpt6k110193z

Preibisch, S., Rohlfing, T., Hasak, M. P., & Tomancak, P. (2008). Mosaicing of single plane illumination microscopy images using groupwise registration and fast content-based image fusion. In J. M. Reinhardt & J. P. W. Pluim (Eds.). https://doi.org/10.1117/12.770893

Qiu, G., Zuniga-Montanez, R., Law, Y., Thi, S. S., Nguyen, T. Q. N., Eganathan, K., Liu, X., Nielsen, P. H., Williams, R. B., & Wuertz, S. (2019). Polyphosphate-accumulating organisms in full-scale tropical wastewater treatment plants use diverse carbon sources. *Water Research*, *149*, 496–510. https://doi.org/10.1016/j.watres.2018.11.011

Quan, K., Hou, J., Zhang, Z., Ren, Y., Peterson, B. W., Flemming, H.-C., Mayer, C., Busscher, H. J., & van der Mei, H. C. (2021). Water in bacterial biofilms: pores and channels, storage and transport functions. *Critical Reviews in Microbiology*, 1–20. https://doi.org/10.1080/1040841X.2021.1962802

Quast, C., Pruesse, E., Yilmaz, P., Gerken, J., Schweer, T., Yarza, P., Peplies, J., & Glöckner, F. O. (2013). The SILVA ribosomal RNA gene database project: Improved data processing and web-based tools. *Nucleic Acids Research*, *41*(D1), 590–596. https://doi.org/10.1093/nar/gks1219

Radajewski, S., Ineson, P., Parekh, N. R., & Murrell, J. C. (2000). Stable-isotope probing as a tool in microbial ecology. *Nature*, *403*(6770), 646–649. https://doi.org/10.1038/35001054

Rao, N. N., Gómez-García, M. R., & Kornberg, A. (2009). Inorganic Polyphosphate: Essential for Growth and Survival. *Annual Review of Biochemistry*, *78*(1), 605–647. https://doi.org/10.1146/annurev.biochem.77.083007.093039

Ravishankara, A. R., Daniel, J. S., & Portmann, R. W. (2009). Nitrous Oxide (N2O): The Dominant Ozone-Depleting Substance Emitted in the 21st Century. *Science*, *326*(5949), 123–125. https://doi.org/10.1126/science.1176985

Richards, O. W., & Gurr, E. (1966). Rational Use of Dyes in Biology and General Staining Methods. *Transactions of the American Microscopical Society*, *85*(2), 326. https://doi.org/10.2307/3224655

Rocha, M. D., Düring, D. N., Bethge, P., Voigt, F. F., Hildebrand, S., Helmchen, F., Pfeifer, A., Hahnloser, R. H. R., & Gahr, M. (2019). Tissue Clearing and Light Sheet Microscopy: Imaging the Unsectioned Adult Zebra Finch Brain at Cellular Resolution. *Frontiers in Neuroanatomy*, *13*. https://doi.org/10.3389/fnana.2019.00013

Rognes, T., Flouri, T., Nichols, B., Quince, C., & Mahé, F. (2016). VSEARCH: A versatile open source tool for metagenomics. *PeerJ*, *2016*(10), 1–22. https://doi.org/10.7717/peerj.2584

Romero, D., Aguilar, C., Losick, R., & Kolter, R. (2010). Amyloid fibers provide structural integrity to Bacillus subtilis biofilms. *Proceedings of the National Academy of Sciences*, *107*(5), 2230–2234. https://doi.org/10.1073/pnas.0910560107

Röske, I., & Schönborn, C. (1994). Interactions between chemical and advanced biological phosphorus elimination. *Water Research*, *28*(5), 1103–1109. https://doi.org/10.1016/0043-1354(94)90196-1

Saito, K., Ohtomo, R., Kuga-Uetake, Y., Aono, T., & Saito, M. (2005). Direct labeling of polyphosphate at the ultrastructural level in Saccharomyces cerevisiae by using the affinity of the polyphosphate binding domain of Escherichia coli exopolyphosphatase. *Applied and Environmental Microbiology*, *71*(10), 5692–5701. https://doi.org/10.1128/AEM.71.10.5692-5701.2005

Satoh, H., Mino, T., & Matsuo, T. (1992). Uptake of organic substrates and accumulation of polyhydroxyalkanoates linked with glycolysis of intracellular carbohydrates under anaerobic conditions in the biological excess phosphate removal processes. *Water Science and Technology*, *26*(5-6), 933–942. https://doi.org/10.2166/wst.1992.0535

Satoh, H., Ramey, W. D., Koch, F. A., Oldham, W. K., Mino, T., & Matsuo, T. (1996). Anaerobic substrate uptake by the enhanced biological phosphorus removal activated sludge treating real sewage. *Water Science and Technology*, *34*(1-2). https://doi.org/10.1016/0273-1223(96)00489-1

Scheibler, D. (2018). Biological dephosphatation activity of aerobic granular sludge influenced by different substrates Master Thesis. https://github.com/ArnaudGelb/EPFL/blob/87b47a12b2467cfa7cb5cc8dc07aa279a25be937/MA_David_Scheibler_unsigned.pdf

Schindelin, J., Arganda-Carreras, I., Frise, E., Kaynig, V., Longair, M., Pietzsch, T., Preibisch, S., Rueden, C., Saalfeld, S., Schmid, B., Tinevez, J.-Y., White, D. J., Hartenstein, V., Eliceiri, K., Tomancak, P., & Cardona, A. (2012). Fiji: an open-source platform for biological-image analysis. *Nature Methods*, *9*(7), 676–682. https://doi.org/10.1038/nmeth.2019

Schindler, D. W. (1974). Eutrophication and Recovery in Experimental Lakes: Implications for Lake Management. *Science*, *184*(4139), 897–899. https://doi.org/10.1126/science.184.4139.897

Schroeder, S., Ahn, J., & Seviour, R. (2008). Ecophysiology of polyphosphate-accumulating organisms and glycogen-accumulating organisms in a continuously aerated enhanced biological phosphorus removal process. *Journal of Applied Microbiology*, *105*(5), 1412–1420. https://doi.org/10.1111/j.1365-2672.2008.03857.x

Serafim, L. S., Lemos, P. C., Levantesi, C., Tandoi, V., Santos, H., & Reis, M. a. (2002). Methods for detection and visualization of intracellular polymers stored by polyphosphate-accumulating microorganisms. *Journal of Microbiological Methods*, *51*(1), 1–18. https://doi.org/10.1016/S0167-7012(02)00056-8

Seviour, R. J., Mino, T., & Onuki, M. (2003). The microbiology of biological phosphorus removal in activated sludge systems. *FEMS Microbiology Reviews*, *27*(1), 99–127. https://doi.org/10.1016/S0168-6445(03)00021-4

Seviour, T. W., Lambert, L. K., Pijuan, M., & Yuan, Z. (2011). Selectively inducing the synthesis of a key structural exopolysaccharide in aerobic granules by enriching for Candidatus "competibacter phosphatis
. *Applied Microbiology and Biotechnology*, *92*(6), 1297–1305. https://doi.org/10.1007/s00253-011-3385-1

Seviour, T. W., Pijuan, M., Nicholson, T., Keller, J., & Yuan, Z. (2009). Understanding the properties of aerobic sludge granules as hydrogels. *Biotechnology and Bioengineering*, *102*(5), 1483–1493. https://doi.org/10.1002/bit.22164

Seviour, T. W., Yuan, Z., van Loosdrecht, M. C., & Lin, Y. (2012). Aerobic sludge granulation: A tale of two polysaccharides? *Water Research*, *46*(15), 4803–4813. https://doi.org/10.1016/j.watres.2012.06.018

Shannon, C. (1949). Communication in the Presence of Noise. *Proceedings of the IRE*, *37*(1), 10–21. https://doi.org/10.1109/JRPROC.1949.232969

Shapiro, J. A. (1998). Thinking about bacterial populations as multicellular organisms. *Annual Review of Microbiology*, *52*(1), 81–104. https://doi.org/10.1146/annurev.micro.52.1.81

Shaw, P., Agard, D., Hiraoka, Y., & Sedat, J. (1989). Tilted view reconstruction in optical microscopy. Three-dimensional reconstruction of Drosophila melanogaster embryo nuclei. *Biophysical Journal*, *55*(1), 101–110. https://doi.org/10.1016/S0006-3495(89)82783-3

Sicko-Goad, L., & Lazinsky, D. (1986). Quantitative ultrastructural changes associated with lead-coupled luxury phosphate uptake and polyphosphate utilization. *Archives of Environmental Contamination and Toxicology*, *15*(6), 617–627. https://doi.org/10.1007/BF01054908

Smolders, G. J. F., van der Meij, J., van Loosdrecht, M. C. M., & Heijnen, J. J. (1994a). Model of the anaerobic metabolism of the biological phosphorus removal process: Stoichiometry and pH influence. *Biotechnology and Bioengineering*, *43*(6), 461–470. https://doi.org/10.1002/bit.260430605

Smolders, G. J. F., van der Meij, J., van Loosdrecht, M. C. M., & Heijnen, J. J. (1994b). Stoichiometric model of the aerobic metabolism of the biological phosphorus removal process. *Biotechnology and Bioengineering*, *44*(7), 837–848. https://doi.org/10.1002/bit.260440709

Soo, R. M., Skennerton, C. T., Sekiguchi, Y., Imelfort, M., Paech, S. J., Dennis, P. G., Steen, J. A., Parks, D. H., Tyson, G. W., & Hugenholtz, P. (2014). An Expanded Genomic Representation of the Phylum Cyanobacteria. *Genome Biology and Evolution*, *6*(5), 1031–1045. https://doi.org/10.1093/gbe/evu073

Stefan Hartmann. (2019). *Valorisation du phosphore, de l'engrais issu des STEP* (Office fédéral de l'environnement (OFEV), Ed.).

Stokholm-bjerregaard, M., Mcilroy, S. J., Nierychlo, M., Karst, S. M., & Smith, C. J. (2017). A Critical Assessment of the Microorganisms Proposed to be Important to Enhanced Biological Phosphorus Removal in Full-Scale Wastewater Treatment Systems. *8*(April), 1–18. https://doi.org/10.3389/fmicb.2017.00718

Streichan, M., Golecki, J., & Schön, G. (1990). Polyphosphate accumulating bacteria from sewage plants with different proceses for biological phosphorus removal. *FEMS microbiology letters*, *73*, 113–124. http://onlinelibrary.wiley.com/doi/10.1111/j.1574-6968.1990.tb03931.x/full

Su, K.-Z., & Yu, H.-Q. (2006). A Generalized Model for Aerobic Granule-based Sequencing Batch Reactor. 2. Parametric Sensitivity and Model Verification. *Environmental Science & Technology*, *40*(15), 4709–4713. https://doi.org/10.1021/es060142e

Sutherland, I. W. (2001). Biofilm exopolysaccharides: A strong and sticky framework. *Microbiology*, *147*(1), 3–9. https://doi.org/10.1051/lait:2001108

Szabó, E., Liébana, R., Hermansson, M., Modin, O., Persson, F., & Wilén, B.-M. (2017a). Comparison of the bacterial community composition in the granular and the suspended phase of sequencing batch reactors. *AMB Express*, *7*(1), 168. https://doi.org/10.1186/s13568-017-0471-5

Szabó, E., Liébana, R., Hermansson, M., Modin, O., Persson, F., & Wilén, B.-M. (2017b). Microbial Population Dynamics and Ecosystem Functions of Anoxic/Aerobic Granular Sludge in Sequencing Batch Reactors Operated at Different Organic Loading Rates. *Frontiers in Microbiology*, *8*(May), 1–14. https://doi.org/10.3389/fmicb.2017.00770

Taguchi, K., Taguchi, S., Sudesh, K., Maehara, A., Tsuge, T., & Doi, Y. (2002). Metabolic Pathways and Engineering of Polyhydroxyalkanoate Biosynthesis. In Y. Doi

& A. Steinbüchel (Eds.), *Biopolymers online*. Wiley. https://doi.org/10.1002/3527600035.bpol3a07

Tan, C. H., Koh, K. S., Xie, C., Tay, M., Zhou, Y., Williams, R., Ng, W. J., Rice, S. a., & Kjelleberg, S. (2014). The role of quorum sensing signalling in EPS production and the assembly of a sludge community into aerobic granules. *The ISME Journal*, *8*(6), 1186–1197. https://doi.org/10.1038/ismej.2013.240

Tanaka, T., Kawasaki, K., Daimon, S., Kitagawa, W., Yamamoto, K., Tamaki, H., Tanaka, M., Nakatsu, C. H., & Kamagata, Y. (2014). A hidden pitfall in agar media preparation undermines cultivability of microorganisms. *Applied and environmental microbiology*, (October). https://doi.org/10.1128/AEM.02741-14

Tanious, F. A., Veal, J. M., Buczak, H., Ratmeyer, L. S., & Wilson, W. D. (1992). DAPI (4', 6-Diamidino-2-Phenylindóle) Binds Differently to DNA and RNA: Minor-Groove Binding at AT Sites and Intercalation at AU Sites. *Biochemistry*, *31*(12), 3103–3112. https://doi.org/10.1021/bi00127a010

Tatsuhiro, E., Sally E., S., & F., A. S. (2001). Differentiation of polyphosphate metabolism between the extra- and intraradical hyphae of arbuscular mycorrhizal fungi. *New Phytologist*, *149*(3), 555–563. https://doi.org/10.1046/j.1469-8137.2001.00040.x

Tay, J. H., Liu, Q. S., & Liu, Y. (2002). Characteristics of Aerobic Granules Grown on Glucose and Acetate in Sequential Aerobic Sludge Blanket Reactors. *Environmental Technology*, *23*(8), 931–936. https://doi.org/10.1080/09593332308618363

Tay, J. H., Liu, Q.-S., & Liu, Y. (2001). The effects of shear force on the formation, structure and metabolism of aerobic granules. *Applied Microbiology and Biotechnology*, *57*(1-2), 227–233. https://doi.org/10.1007/s002530100766

Tay, J. H., Tay, S. T. L., Ivanov, V., Pan, S., Jiang, H. L., & Liu, Q. S. (2003). Biomass and porosity profiles in microbial granules used for aerobic wastewater treatment. *Letters in Applied Microbiology*, *36*(5), 297–301. https://doi.org/10.1046/j.1472-765X.2003.01312.x

Terekhov, S. S., Smirnov, I. V., Stepanova, A. V., Bobik, T. V., Mokrushina, Y. A., Ponomarenko, N. A., Belogurov, A. A., Rubtsova, M. P., Kartseva, O. V., Gomzikova, M. O., Moskovtsev, A. A., Bukatin, A. S., Dubina, M. V., Kostryukova, E. S., Babenko, V. V., Vakhitova, M. T., Manolov, A. I., Malakhova, M. V., Kornienko, M. A., ... Altman, S. (2017). Microfluidic droplet platform for ultrahigh-throughput single-cell screening of biodiversity. *Proceedings of the National Academy of Sciences*, *114*(10), 2550–2555. https://doi.org/10.1073/pnas.1621226114

Thavarajah, R., Mudimbaimannar, V. K., Elizabeth, J., Rao, U. K., & Ranganathan, K. (2012). Chemical and physical basics of routine formaldehyde fixation. *Journal of Oral and Maxillofacial Pathology*, *16*(3), 400–405. https://doi.org/10.4103/0973-029X.102496

Tijssen, J., Beekes, H., & Van Steveninck, J. (1982). Localization of polyphosphates in Saccharomyces fragilis, as revealed by 4,6-diamidino-2-phenylindole fluorescence. *Biochimica et Biophysica Acta (BBA) - Molecular Cell Research*, *721*(4), 394–398. https://doi.org/10.1016/0167-4889(82)90094-5

Tsuneda, S., Ejiri, Y., Nagano, T., & Hirata, A. (2004). Formation mechanism of nitrifying granules observed in an aerobic upflow fluidized bed (AUFB) reactor. *Water Science and Technology*, *49*(11-12), 27–34. https://doi.org/10.2166/wst.2004.0796

Tumlirsch, T., Sznajder, A., & Jendrossek, D. (2015). Formation of Polyphosphate by Polyphosphate kinases and its Relationship to PHB Accumulation in Ralstonia eutropha H16. *Applied and Environmental Microbiology*, *81*(September), 02279–15. https://doi.org/10.1128/AEM.02279-15

Uhlmann, D., Röske, I., Hupfer, M., & Ohms, G. (1990). A simple method to distinguish between polyphosphate and other phosphate fractions of activated sludge. *Water Research*, *24*(11), 1355–1360. https://doi.org/10.1016/0043-1354(90)90153-W

Urbach, E., Vergin, K. L., & Giovannoni, S. J. (1999). Immunochemical Detection and Isolation of DNA from Metabolically Active Bacteria. *Applied and Environmental Microbiology*, *65*(3), 1207–1213. https://doi.org/10.1128/AEM.65.3.1207-1213.1999

van Groenestijn, J. W., Bentvelsen, M. M., Deinema, M. H., & Zehnder, A. J. (1989). Polyphosphate-degrading enzymes in Acinetobacter spp. and activated sludge. *Applied and Environmental Microbiology*, *55*(1), 219–223. https://doi.org/10.1128/aem.55.1.219-223.1989

van Loosdrecht, M. C. M., Hooijmans, C. M., Brdjanovic, D., & Heijnen, J. J. (1997). Biological phosphate removal processes. *Applied Microbiology and Biotechnology*, *48*(3), 289–296. https://doi.org/10.1007/s002530051052

van Loosdrecht, M. C. M., Nielsen, P. H., Lopez-Vazquez, C. M., & Brdjanovic, D. (2016). *Experimental Methods in Wastewater Treatment* (Vol. 15). https://doi.org/10.2166/9781780404752

van Loosdrecht, M. C. M., Smolders, G., Kuba, T., & Heijnen, J. (1997). Metabolism of micro-organisms responsible for enhanced biological phosphorus removal from wastewater. Use of dynamic enrichment cultures. *Antonie van Leeuwenhoek*, *71*(1/2), 109–116. https://doi.org/10.1023/A:1000150523030

Vigneswari, S., Lee, T. S., Bhubalan, K., & Amirul, A. A. (2015). Extracellular Polyhydroxyalkanoate Depolymerase by Acidovorax sp. DP5. *Enzyme Research*, *2015*, 1–8. https://doi.org/10.1155/2015/212159

Vishniac, W., & Santer, M. (1957). The thiobacilli. *Bacteriological reviews*, *21*(3), 195–213. https://doi.org/10.1128/br.21.3.195-213.1957

Wagner, M., Erhart, R., Manz, W., Amann, R., Lemmer, H., Wedi, D., & Schleifer, K. H. (1994). Development of an rRNA-targeted oligonucleotide probe specific for the genus Acinetobacter and its application for in situ monitoring in activated sludge. *Applied and Environmental Microbiology*, *60*(3), 792–800. https://doi.org/10.1128/aem.60.3.792-800.1994

Wang, X., Zhang, K., Ren, N., Li, N., & Ren, L. (2009). Monitoring microbial community structure and succession of an A/O SBR during start-up period using PCR-DGGE. *Journal of Environmental Sciences*, *21*(2), 223–228. https://doi.org/10.1016/S1001-0742(08)62255-X

Waring, M. J. (1965). Complex formation between ethidium bromide and nucleic acids. *Journal of Molecular Biology*, *13*(1), 269–282. https://doi.org/10.1016/S0022-2836(65)80096-1

Warington, R. (1878). Nitrification. *Nature*, *17*(436), 367–369. https://doi.org/10.1038/017367a0

Weissbrodt, D. G., Neu, T. R., Kuhlicke, U., Rappaz, Y., & Holliger, C. (2013a). Assessment of bacterial and structural dynamics in aerobic granular biofilms. *Frontiers in Microbiology*, *4*(JUL), 1–18. https://doi.org/10.3389/fmicb.2013.00175

Weissbrodt, D. G., Neu, T. R., Kuhlicke, U., Rappaz, Y., & Holliger, C. (2013b). Assessment of bacterial and structural dynamics in aerobic granular biofilms. *Frontiers in Microbiology*, *4*(July), 1–18. https://doi.org/10.3389/fmicb.2013.00175

Weissbrodt, D. G., Shani, N., & Holliger, C. (2014). Linking bacterial population dynamics and nutrient removal in the granular sludge biofilm ecosystem engineered for wastewater treatment. *FEMS Microbiology Ecology*, *88*(3), 579–595. https://doi.org/10.1111/1574-6941.12326

Welles, L., Tian, W. D., Saad, S., Abbas, B., Lopez-Vazquez, C. M., Hooijmans, C. M., van Loosdrecht, M. C. M., & Brdjanovic, D. (2015). Accumulibacter clades Type I and II performing kinetically different glycogen-accumulating organisms metabolisms for anaerobic substrate uptake. *Water Research*, *83*, 354–366. https://doi.org/10.1016/j.watres.2015.06.045

Wentzel, M. C., Dold, P. L., Ekama, G. A., & Marais, G. v. R. (1985). Kinetics of Biological Phosphorus Release. *Water Science and Technology*, *17*(11-12), 57–71. https://doi.org/10.2166/wst.1985.0221

Whiteley, A. S., Barer, M. R., & O'Donnell, A. G. (2000). Density gradient separation of active and non-active cells from natural environments. *Antonie van Leeuwenhoek*, *77*(2), 173–177. https://doi.org/10.1023/A:1002432010079

Whittaker, E. T. (1915). XVIII.—On the Functions which are represented by the Expansions of the Interpolation-Theory. *Proceedings of the Royal Society of Edinburgh*, *35*, 181–194. https://doi.org/10.1017/S0370164600017806

Wilén, B.-M., Liébana, R., Persson, F., Modin, O., & Hermansson, M. (2018). The mechanisms of granulation of activated sludge in wastewater treatment, its optimization, and impact on effluent quality. *Applied Microbiology and Biotechnology*, *102*(12), 5005–5020. https://doi.org/10.1007/s00253-018-8990-9

Williamson, D., & Fennell, D. (1975). Chapter 16 The Use of Fluorescent DNA-Binding Agent for Detecting and Separating Yeast Mitochondrial DNA. *Methods in cell biology* (pp. 335–351). https://doi.org/10.1016/S0091-679X(08)60963-2

Wilson, W. D., Tanious, F. A., Barton, H. J., Jones, R. L., Strekowski, L., & Boykin, D. W. (1989). Binding of 4',6-diamidino-2-phenylindole (DAPI) to GC and mixed sequences in DNA: intercalation of a classical groove-binding molecule. *Journal of the American Chemical Society*, *111*(13), 5008–5010. https://doi.org/10.1021/ja00195a080

Wimpenny, J., Manz, W., & Szewzyk, U. (2000). Heterogeneity in biofilms: Table 1. *FEMS Microbiology Reviews*, *24*(5), 661–671. https://doi.org/10.1111/j.1574-6976.2000.tb00565.x

Winkler, M. K. H., Bassin, J., Kleerebezem, R., Sorokin, D. Y., & van Loosdrecht, M. C. M. (2012). Unravelling the reasons for disproportion in the ratio of AOB and NOB in aerobic granular sludge. *Applied Microbiology and Biotechnology*, *94*(6), 1657–1666. https://doi.org/10.1007/s00253-012-4126-9

Winkler, M. K. H., Kleerebezem, R., de Bruin, L. M. M., Verheijen, P. J. T., Abbas, B., Habermacher, J., & van Loosdrecht, M. C. M. (2013). Microbial diversity differences within aerobic granular sludge and activated sludge flocs. *Applied Microbiology and Biotechnology*, *97*(16), 7447–7458. https://doi.org/10.1007/s00253-012-4472-7

Winkler, M. K. H., Kleerebezem, R., Strous, M., Chandran, K., & van Loosdrecht, M. C. M. (2013). Factors influencing the density of aerobic granular sludge. *Applied*

Microbiology and Biotechnology, *97*(16), 7459–7468. https://doi.org/10.1007/s00253-012-4459-4

Winkler, M. K. H., Kleerebezem, R., Khunjar, W. O., de Bruin, B., & van Loosdrecht, M. C. (2012). Evaluating the solid retention time of bacteria in flocculent and granular sludge. *Water Research*, *46*(16), 4973–4980. https://doi.org/10.1016/j.watres.2012.06.027

Winkler, M. K. H., Meunier, C., Henriet, O., Mahillon, J., Suárez-Ojeda, M. E., Del Moro, G., De Sanctis, M., Di Iaconi, C., & Weissbrodt, D. G. (2018). An integrative review of granular sludge for the biological removal of nutrients and recalcitrant organic matter from wastewater. *Chemical Engineering Journal*, *336*(July 2017), 489–502. https://doi.org/10.1016/j.cej.2017.12.026

Wu, L., Ning, D., Zhang, B., Li, Y., Zhang, P., Shan, X., Zhang, Q., Brown, M., Li, Z., Van Nostrand, J. D., Ling, F., Xiao, N., Zhang, Y., Vierheilig, J., Wells, G. F., Yang, Y., Deng, Y., Tu, Q., Wang, A., … Zhou, H. (2019). Global diversity and biogeography of bacterial communities in wastewater treatment plants. *Nature Microbiology*, *4*(7), 1183–1195. https://doi.org/10.1038/s41564-019-0426-5

Xie, X., & Zubarev, R. A. (2015). Isotopic Resonance Hypothesis: Experimental Verification by Escherichia coli Growth Measurements. *Scientific Reports*, *5*(1), 9215. https://doi.org/10.1038/srep09215

Yi, S., Tay, J.-H., Maszenan, A., & Tay, S.-L. (2003). A culture-independent approach for studying microbial diversity in aerobic granules. *Water Science and Technology*, *47*(1), 283–290. https://doi.org/10.2166/wst.2003.0068

Yilmaz, P., Parfrey, L. W., Yarza, P., Gerken, J., Pruesse, E., Quast, C., Schweer, T., Peplies, J., Ludwig, W., & Glöckner, F. O. (2014). The SILVA and "all-species Living Tree Project (LTP)"taxonomic frameworks. *Nucleic Acids Research*, *42*(D1), 643–648. https://doi.org/10.1093/nar/gkt1209

Yoon, S. H., Ha, S. M., Kwon, S., Lim, J., Kim, Y., Seo, H., & Chun, J. (2017). Introducing EzBioCloud: A taxonomically united database of 16S rRNA gene sequences and whole-genome assemblies. *International Journal of Systematic and Evolutionary Microbiology*, *67*(5), 1613–1617. https://doi.org/10.1099/ijsem.0.001755

Youngblut, N. D., & Buckley, D. H. (2014). Intra-genomic variation in G+C content and its implications for DNA stable isotope probing. *Environmental Microbiology Reports*, *6*(6), 767–775. https://doi.org/10.1111/1758-2229.12201

Yuan, Z., Pratt, S., & Batstone, D. J. (2012). Phosphorus recovery from wastewater through microbial processes. *Current Opinion in Biotechnology*, *23*(6), 878–883. https://doi.org/10.1016/j.copbio.2012.08.001

Zaiss, M. M., Rapin, A., Lebon, L., Dubey, L. K., Mosconi, I., Sarter, K., Piersigilli, A., Menin, L., Walker, A. W., Rougemont, J., Paerewijck, O., Geldhof, P., McCoy, K. D., Macpherson, A. J., Croese, J., Giacomin, P. R., Loukas, A., Junt, T., Marsland, B. J., & Harris, N. L. (2015). The Intestinal Microbiota Contributes to the Ability of Helminths to Modulate Allergic Inflammation. *Immunity*, *43*(5), 998–1010. https://doi.org/10.1016/j.immuni.2015.09.012

Zarlenga, D. S., & Gamble, H. (1987). Simultaneous isolation of preparative amounts of RNA and DNA from Trichinella spiralis by cesium trifluoroacetate isopycnic centrifugation. *Analytical Biochemistry*, *162*(2), 569–574. https://doi.org/10.1016/0003-2697(87)90435-0

Zeng, R. J., Lemaire, R., Yuan, Z., & Keller, J. (2003). Simultaneous nitrification, denitrification, and phosphorus removal in a lab-scale sequencing batch reactor. *Biotechnology and bioengineering*, *84*(2), 170–8. https://doi.org/10.1002/bit.10744

Zeng, R. J., Yuan, Z., & Keller, J. (2003). Model-based analysis of anaerobic acetate uptake by a mixed culture of polyphosphate-accumulating and glycogen-accumulating organisms. *Biotechnology and Bioengineering*, *83*(3), 293–302. https://doi.org/10.1002/bit.10671

Zhang, H., Sekiguchi, Y., Hanada, S., Hugenholtz, P., Kim, H., Kamagata, Y., & Nakamura, K. (2003). Gemmatimonas aurantiaca gen. nov., sp. nov., a Gram-negative, aerobic, polyphosphate-accumulating micro-organism, the first cultured representative of the new bacterial phylum Gemmatimonadetes phyl. nov. *International Journal of Systematic and Evolutionary Microbiology*, *53*(4), 1155–1163. https://doi.org/10.1099/ijs.0.02520-0

Zhang, L., Li, Q., Chen, C., Li, X., Li, M., Hu, J., & Shen, X. (2017). Propioniciclava sinopodophylli sp. nov., isolated from leaves of Sinopodophyllum hexandrum (Royle) Ying. *International Journal of Systematic and Evolutionary Microbiology*, *67*(10), 4111–4115. https://doi.org/10.1099/ijsem.0.002265

Zheng, Y.-M., & Yu, H.-Q. (2007). Determination of the pore size distribution and porosity of aerobic granules using size-exclusion chromatography. *Water research*, *41*(1), 39–46. https://doi.org/10.1016/j.watres.2006.09.015

Zhong, C., Fu, J., Jiang, T., Zhang, C., & Cao, G. (2018). Polyphosphate metabolic gene expression analyses reveal mechanisms of phosphorus accumulation and release in Microlunatus phosphovorus strain JN459. *FEMS Microbiology Letters*, *365*(6), 1–8. https://doi.org/10.1093/femsle/fny034

Zhou, J.-h., Ren, Q., Xu, X.-l., Fang, J.-y., Wang, T., Wang, K.-m., & Wang, H.-y. (2021). Enhancing stability of aerobic granules by microbial selection pressure using height-adjustable influent strategy. *Water Research*, *201*, 117356. https://doi.org/10.1016/j.watres.2021.117356

Zhou, J.-h., Zhao, H., Hu, M., Yu, H.-t., Xu, X.-y., Vidonish, J., Alvarez, P. J., & Zhu, L. (2015). Granular activated carbon as nucleating agent for aerobic sludge granulation: Effect of GAC size on velocity field differences (GAC versus flocs) and aggregation behavior. *Bioresource Technology*, *198*, 358–363. https://doi.org/10.1016/j.biortech.2015.08.155

Zhou, Y., Pijuan, M., Oehmen, A., & Yuan, Z. (2010). The source of reducing power in the anaerobic metabolism of polyphosphate accumulating organisms (PAOs) - a mini-review. *Water science and technology : a journal of the International Association on Water Pollution Research*, *61*(7), 1653–62. https://doi.org/10.2166/wst.2010.983

Arnaud Gelb

linkedin.com/in/gelbarnaud

Proactive and curious with an Environmental Engineering & Biotechnology background.

Education

Swiss Federal Institute of Technology - Lausanne *Lausanne, CH*

PhD in Environmental Engineering *2023*

- This research in Environmental biotechnology uses the potential of microorganisms to preserve the environment.

University of Strasbourg *Strasbourg, FR*

MS in Biology of microorganisms *2014*

- This Master's program provides multidisciplinary training to research and a thorough grounding in cell and molecular biology.

University of Strasbourg *Strasbourg, FR*

BS in Cell biology & physiology *2012*

- This Bachelor's program allows students to gain insight into the functioning of a living organism (animal, plant, or microorganism).

Research Projects

PhD Candidate *Lausanne, CH*

Swiss Federal Institute of Technology - Lausanne *2015 - 2022*

- Characterization of the biological phosphorus removal in biofilm-bioreactors used in wastewater treatment (Aerobic granular sludge)

Scientific Assistant *Lausanne, CH*

Swiss Federal Institute of Technology - Lausanne *2014*

- Removal of micropollutants from wastewater using phenol-oxidase enzymes produced by bacteria

Assistant Research Engineer *Molsheim, FR*

Merck Millipore *2013*

- Rapid detection of foodborne pathogens by using molecular-biology techniques

Languages

English	Professional proficiency
French	Native proficiency
German	Elementary proficiency